ISTANBUL TECHNICAL UNIVERSITY ★ GRADUATE SCHOOL

SYNTHESIS, TEMPERATURE SENSİNG AND WHITE LIGHT PRODUCTION PROPERTIES OF THE LITHIUMNIOBATE AND TUNGSTENOXIDE MODIFED TeO_2+Yb_2O_3+Er_2O_3 OPTICAL GLASSES

M.Sc. THESIS

Güliz KONCA

Department of Physics Engineering

Physics Engineering Programme

JULY 2022

ISTANBUL TECHNICAL UNIVERSITY ★ GRADUATE SCHOOL

SYNTHESIS, TEMPERATURE SENSİNG AND WHITE LIGHT PRODUCTION PROPERTIES OF THE LITHIUMNIOBATE AND TUNGSTENOXIDE MODIFED TeO_2+Yb_2O_3+Er_2O_3 OPTICAL GLASSES

M.Sc. THESIS

Güliz KONCA
(509181109)

Department of Physics Engineering

Physics Engineering Programme

Thesis Advisor: Prof. Dr. Gönül ERYÜREK

JULY 2022

ISTANBUL TEKNİK ÜNİVERSİTESİ ★ LİSANSÜSTÜ EĞİTİM ENSTİTÜSÜ

LİTYUMNİOBAT VE TUNGSTENOKSİT KATKILI TeO_2+Yb_2O_3+Er_2O_3 OPTİK CAMLARIN SENTEZ, SICAKLIK ALGILAMA VE BEYAZ IŞIK ÜRETİMİ ÖZELLİKLERİ

YÜKSEK LİSANS TEZİ

Güliz KONCA
(509181109)

Fizik Mühendisliği Anabilim Dalı

Fizik Mühendisliği Programı

Tez Danışmanı: Prof. Dr. Gönül ERYÜREK

TEMMUZ 2022

Güliz KONCA, a M.Sc. student of İTU Graduate School student ID 509181109, successfully defended the thesis entitled "SYNTHESIS, TEMPERATURE SENSİNG AND WHITE LIGHT PRODUCTION PROPERTIES OF THE LITHIUMNIOBATE AND TUNGSTENOXIDE MODIFED TeO_2+Yb_2O_3+Er_2O_3 OPTICAL GLASSES", which she prepared after fulfilling the requirements specified in the associated legislations, before the jury whose signatures are below.

Thesis Advisor :	**Prof. Dr. Gönül ERYÜREK** İstanbul Technical University	.....
Jury Members :	**Assoc. Prof. Demet AKTAŞ** Istanbul Technical University	.....
	Assoc. Prof. Murat ERDEM Marmara University	.....

Date of Submission : 24 June 2022
Date of Defense : 07 July 2022

FOREWORD

The main acknowledgement is to my dear thesis advisor, Prof. Dr. Gönül ÖZEN ERYÜREK, for always supporting me on this long journey, with her loving and tolerant attitude, and her knowledge and experience.

I would like to thank my dear lecturer Assoc. Prof. Murat ERDEM, whom I knew during my undergraduate years, who has signed into all my academic achievements so far, and who taught me how to be a real scientist, for his contribution to my thesis and his belief in me.

To my dear Tonties Hande KORDON and Handan YILMAZ, who have always given me strength with their unconditional support and love all the way; To Işık SÜMER, who happily and tirelessly came to ITU Laser laboratory during the experimental process of my thesis and had a great time; To Anıl DOĞAN for keeping me alive with his patience and support during my thesis process; To my family of Turkish Basketball Federation Referees, whom I have enjoyed being a part of since my undergraduate years; To Dear head of department Prof. Dr. Adnan KAYPMAZ, Dr. Dilek KUZALİÇ BÜRÜCÜ, Ezgi ÖZTÜRK YILMAZ and Onur ÜNVER, who created a happy working environment with their trust and love for me; I would like to thank Dinçer ADİLLER, who is always by my side with his unconditional love.

To my brother Kerem KONCA, whom I love more than anyone else in my life, To my dear mother Güler KONCA who made me who I am, and to my dear father Cengiz KONCA; I would like to thank my dear aunt Gülsen ÇAKAN and my dear uncle Saim ÇAKAN for their love and compassion.

June 2022 Güliz.

TABLE OF CONTENTS

ABBREVIATIONS

DC : Down Conversion

Er : Erbium

FIR :Fluorescence Intensity Ratio

FWHM :Full width half maximum

Ln : Lanthanide

Li : Lithium

NIR : Near-infrared

Nb : Niobium

O : Oxygen

RE : Rare Earth

Te : Tellurium

TeO_2 : Tellurite

TWL : Er^{3+}/Yb^{3+} Doped TeO2-WO_3-LiNbO3

UC : Up Conversion

UV : Ultraviolet

VIS : Visible

Yb :Ytterbium

W : Wolfram (Tungsten)

SYMBOLS

$\boldsymbol{\lambda}$	: Lambda
$\boldsymbol{T}$	: Temperature
$\mathbf{^oC}$	: Centigrade degree
$\boldsymbol{k_B}$	: Boltzman constant
$\boldsymbol{\alpha}$	: Alpha
$\boldsymbol{\beta}$	: Beta
$\boldsymbol{\gamma}$	: Gamma
$\boldsymbol{\nu}$	: Frequency
$\boldsymbol{h}$	: Planck constant
$\boldsymbol{I}$	: Intensity
$\boldsymbol{g}$	: Degeneracy
Tg	: Glass transition temperature
Tc	: Crystallization temperature
Tm	: Melting temperature
$\boldsymbol{\Delta T}$	: Thermal stability
$\boldsymbol{\Delta E}$	: Energy gap
N	: Number of electron
$\boldsymbol{\sigma}$	: Refractive index
$\boldsymbol{S}$	: Thermal sensitivity
Z	: Atomic number

LIST OF TABLES

Page

LIST OF FIGURES

Page

SYNTHESIS, TEMPERATURE SENSING AND WHITE LIGHT PRODUCTION PROPERTIES OF THE LITHIUMNIOBATE AND TUNGSTENOXIDE MODIFIED TeO_2+Yb_2O_3+Er_2O_3 OPTICAL GLASSES

SUMMARY

Tellurium-based glasses doped with rare earths (RE) have been studied in recent years from various aspects due to their many important optical and physical advantages.

In this study, glass materials were obtained by synthesizing Yb^{3+}/Er^{3+} doped TeO_2-WO_3-$LiNbO_3$ lattices with different ratios by melting method. The lattices of our glass materials were modified by increasing the Er^{3+} ion concentration. The up-conversion mechanism under 980 nm laser excitation, absorption properties, optical band gaps and Urbach energies in the range of 200-1100 nm, luminescence properties, thermal properties and white light parameters in the wavelength range of 400-850 nm, and the variation of rare earth ions as a function of concentration were investigated.

The transitions of Er^{3+} ions from their ground state, which is $^4I_{15/2}$, to different excited states, such as $^4F_{3/2,5/2}$, $^2H_{11/2}$, $^4S_{3/2}$, $^4F_{9/2}$, $^4I_{11/2}$, were observed. At laser excitation of 400-850 nm, the emission bands $^2H_{11/2}\rightarrow{}^4I_{15/2}$, $^4S_{3/2}\rightarrow{}^4I_{15/2}$, $^4F_{9/2}\rightarrow{}^4I_{15/2}$ and $^4I_{9/2}\rightarrow{}^4I_{15/2}$ UC of Er^{3+} ion transitions were observed.

It was found that there were small differences in the measured color parameters of the TWL glasses with increasing power. When comparing the TWL glasses as a function of concentration changes, it was found that the Er^{3+} concentration shifted slightly from the red to the green range with increasing power.

In the optical thermometry study, measurements could be made on the TWL1, TWL2 and TWL3 glass samples. In these measurements, two green emission bands, ~527 nm and ~551 nm, were observed. It was found that the intensity at the $^2H_{11/2}\rightarrow{}^4I_{15/2}$ transition at 300 K was quite low compared to the $^4S\rightarrow{}^4I$ transition at 573 K.

On study aims to contribute to the literature on the fabrication of Er^{3+}/Yb^{3+} doped TeO_2-WO_3 glass materials, the design of photonic devices, and the development of temperature and light sensors.

LİTYUMNİOBAT VE TUNGSTENOKSİT KATKILI TeO_2+Yb_2O_3+Er_2O_3 OPTİK CAMLARIN SENTEZ, SICAKLIK ALGILAMA VE BEYAZ IŞIK ÜRETİMİ ÖZELLİKLERİ

ÖZET

Nadir toprak (RE) iyonları ile katkılanmış tellür esaslı camlar birçok önemli optik ve fiziksel avantajları sebebiyle son yıllarda farklı yönleriyle araştırılmıştır.

TeO_2 esaslı cam malzemeler dayanıklı olmaları, mekanik olarak kolay hazırlanmaları, düşük erime sıcaklığına sahip olmaları gibi birçok fiziksel avantajları sayesinde fotonik alanında ve lazer uygulamalarında kullanılmaya elverişlidir. Bunun yanı sıra farklı latislerin oluşmasına imkan sağlayan çok iyi bir konak malzemedir [1][2][3].

TeO_2 en önemli seçim kriterlerinden biri olan düşük fonon enerjisini sağlamasına rağmen[4][5][6], tellürit camların 290^oC olan cam geçiş sıcaklıklarını onların termal olarak dayanıklılığını azaltır. Bu durumda latise WO_3 katkılanarak cam geçiş sıcaklığı 370^oC'ye çıkarılabilir ve bu sayede tellürit camın termal olarak dayanıklılığı arttırılmış olur [7].

RE^{3+} iyonları katkılı optik malzemeler, çeşitli lazer uyarımları altında yukarı ve aşağı dönüşüm süreçleri ile elektromanyetik spektrumda ışıma yapma özellikleri sayesinde lazer uygulamalarında, optik yükselticiler, güneş pillerinde, görüntüleme cihazlarında ve termal sensörlerde kullanımı oldukça yaygındır [8].

Lantanit iyonlarından Er^{3+} iyonunun arttırılmış üst enerji dönüşüm ışıldaması, Yb^{3+}'dan Er^{3+}'a yüksek verimli rezonans yoluyla üretilir. $^2H_{11/2}$ ve $^4S_{3/2}$'nin termal olarak çiftlenmiş enerji seviyelerinin floresans yoğunluk oranına (FIR) dayalı sıcaklık algılama gibi uygulamalarda kullanılması için oldukça avantaj sağlar [9]. Temassız FIR tekniği, hem termal olarak ulaşması zor hem de elektromanyetik olarak zorlu ortamlarda kusursuz sıcaklık ölçümü sağlar [10]. Bunun yanı sıra Er^{3+} iyonlarının termalleşmiş çift olan $^2H_{11/2}$ ve $^4S_{3/2}$ enerji seviyelerinden yayılan üst enerji dönüşüm yeşil ışığının yoğunluk oranı sıcaklığa bağlı olarak değişir. Yoğunluklardaki bu değişiklik, FIR tekniği ile karakterize edilir[8].

Literatürde yapılan çalışmalarda Er^{3+}/Yb^{3+} ortak katkılı tellürit camlar yeşil ve kırmızı emisyonlar için oldukça elverişli olmalarının yanı sıra, yapılan çalışmalar bu camların iyi termal kararlılık gösterdiği ve emisyon spektrumlarının çoğunlukla yakın kızılötesi bantta olduğu tespit edilmiştir [10]–[16]. Yb^{3+} 'nın 980 nm'deki Er^{3+} geçişi $^4I_{13/2}$ 'ye yol açar [10].

TeO_2 esaslı camlar; yüksek kırılma indisleri, düşük fonon enerjileri, geniş iletim bölgesine sahip olmaları ve yüksek şeffaflığa sahip olmaları gibi silikat, fosfat, almanat gibi camlarla kıyaslandığında birçok avantaja sahiptir [17]–[21].

Farklı ışıldayan renklere sahip olmaları ve elektromanyetik spekturumun görünür bölgesinde eşsiz spektral özelliklere sahip olmaları ve UV ile NIR bölgelerinde lüminesans göstermeleri sayesinde lantanit iyonları, renk üretimi,aydınlatma, LED'ler gibi birçok alanda kullanıma uygundur [22].

Lantanit iyonlarından Er^{3+} katkılı tellürit esaslı camlar, verimli üst enerji dönüşümü emisyonları ve yakın kızılötesi bantları gibi avantajları sayesinde araştırma konusudur [23], [24]. Latislerde duyarlılaştırıcı olarak kullanılan en popüler lantanit iyonu Yb^{3+}'dır. Yb^{3+} iyonu, $^2F_{7/2} \rightarrow ^2F_{5/2}$ geçişi sayesinde çok miktarda enerji emer ve lazer için 850-1000 nm arasında yüksek enerji emme verimliliği sağlar. Bunun yanı sıra Er^{3+}, Tm^{3+}, Ho^{3+} gibi aktif RE^{3+} iyonlarına da enerji aktarma avantajına sahiptir. Yüksek uyarılmış yarı kararlı duruma sahip olmaları sayesinde yakın kızılötesi bölgesinden görünür bölgeye üst enerji dönüşüm lüminesansı elde edilmesini sağlar [25].

Yb^{3+} iyonları, RE^{3+} iyonlarının verimliliğini arttırmak için alıcı veya aktivatör olarak da kullanılabilir. Yb^{3+} iyonlarının enerji transferi yoluyla alıcı veya aktivatör olarak olarak RE^{3+} iyonlarının uyarma verimliliğini arttırır ve absorpsiyon kesiti geniştir [26]. RE^{3+} iyonları ile katkılı cam malzemeler, $^4I_{15/2} \rightarrow ^2H_{11/2}$ (522 nm) uyarıldığında $^4S_{3/2}$ durumundan yeşil emisyon bandı olan $^4I_{15/2}$ temel durumuna yavaş bir lüminesans bozunma eğrisi gösterir [26]. Yb^{3+} iyonu 980 nm dalga boyu uyarımı altında komşuya hızlı ve kolay enerji transferi, büyük absorpsiyon kesitine sahiptir [27].

Er^{3+} katkılı camlara duyarlılaştırıcı olarak Yb^{3+} iyonu katkılandığında, Yb^{3+} ile Er^{3+} iyonları arasında verimli enerji aktarım mekanizmasının arttığı gözlenmiştir [27]–[29].

Daha önce yapılan çalışmalarda Er^{3+} iyonlarının uyarılmış durumundan temel duruma geçişleri 550 nm ve 670 nm olmak üzere iki emisyon bandı gözlenir. 550 nm dalgaboyunda $^4S_{3/2} \rightarrow ^4I_{15/2}$ geçişleri ve 670 nm'de $^4F_{9/2} \rightarrow ^4I_{15/2}$ geçişlerine denk gelen yeşil ve kırmızı emisyon bandı görülür [30].

Çalışma kapsamında, değişik oranlarda Yb^{3+}/Er^{3+} ikili katkılı TeO_2-WO_3-$LiNbO_3$ latislerini eritme yöntemi ile sentezlenerek cam malzemeler elde edilmiştir. Eritme yöntemiyle sentezlenmiş 5 adet camın hazırlanmasında kullanılan tüm kimyasallar, Libror AEG 120- Shimadzu hassas elektronik tartı ile tartıldı. Beşer gram olarak hazırlanan kimyasal tozlar, karışım miktarları ayarlanarak mermer havanda karışırıldı. Kimyasal toz karışımlarıyla dolu plattin kap, her bir numune için Carbolite type ELF 11/6 marka elektrikli fırında eritildi.

Numuneler, 950^{o}C ye ulaştıktan sonra 1 saat bekletildi. Önceden 150^{o}C ısıtılan EHRET TK/L4061 marka etüve alındı ve burada da 1 saat bekletildi. Cam malzemelerin latisleri, Er^{3+} iyon konsantrasyonu arttırılarak değiştirilmiştir. 1 mol malzeme için molar oran olarak (84-x mol%)TeO_2+(10 mol%)WO_3 +(3 mol%)Yb_2O_3 +(3 mol%)$LiNbO_3$ +(x mol%)Er_2O_3 formülasyonu kullanıldı.

Elde edilen tüm optik cam malzemelerin 980 nm lazer uyarımı altında üst-enerji dönüşüm mekanizması, 200-1100 nm aralığında soğurma özellikleri, optik band aralıkları ve Urbach enerjileri, 400-850 nm dalga boyu aralığında lüminesans özellikleri, termal özellikleri ve beyaz ışık parametreleri nadir toprak iyon konsantrayonuna bağlı değişimi incelenmiştir. Üst enerji dönüşüm ışıldamasına dayalı beyaz ışık üretimi için kullanılabilirliği ve beyaz ışık üretimini etkileyen optik parametreler araştırılmış ve üst enerji dönüşüm mekanizması sayesinde ölçülmüş olan CCT, CRI, CIE x-y değerleri de tablolar halinde sunulmuştur.

Absorpsiyon spektrumda 487,524,546,654,800 ve 980 nm dalga boylarında $^4F_{3/2,5/2}$, $^2H_{11/2}$, $^4S_{3/2}$, $^4F_{9/2}$, $^4I_{9/2}$, $^4I_{11/2}$ olmak üzere altı absorpsiyon bandı gözlenmiştir. 980 nm'de gözlemlenen absorpsiyon bandı, Yb^{3+} iyonunun bir $^2F_{7/2}\rightarrow{}^2F_{5/2}$ geçişi sergilediği görüldü.

Er^{3+} iyonlarının $^4I_{15/2}$ olan temel durumundan $^4F_{3/2,5/2}$, $^2H_{11/2}$, $^4S_{3/2}$, $^4F_{9/2}$, $^4I_{11/2}$ olmak üzere farklı uyarılmış durumlara geçişleri gözlemlendi. 400-850 nm lazer uyarımında Er^{3+} iyon geçişlerinden (527,551,663 ve 800 nm) $^2H_{11/2}\rightarrow{}^4I_{15/2}$, $^4S_{3/2}\rightarrow{}^4I_{15/2}$, $^4F_{9/2}\rightarrow{}^4I_{15/2}$ ve $^4I_{9/2}\rightarrow{}^4I_{15/2}$ üst enerji dönüşüm emisyon bandları gözlemlendi. TWL camlarının ölçülen renk parametrelerinde gücün artmasıyla küçük farklar olduğu gözlendi. TWL camları konsantrasyon değişikliklerine göre karşılaştırıldıklarında Er^{3+} konsantrasyonu arttıkça kırmızı bölgeden yeşil bölgeye hafifçe kaydığı gözlendi.

Optik termometri incelemesinde, TWL1, TWL2 ve TWL3 cam numunelerinden ölçüm alınabildi. Bu ölçümlerde, ~527 nm ve ~551 nm olmak üzere iki yeşil emisyon bandı gözlemlendi. 300K'de $^2H_{11/2}\rightarrow{}^4I_{15/2}$ geçişindeki yoğunluk, 573 K'deki $^4S\rightarrow{}^4I$ geçişine göre oldukça düşük olduğu gözlendi.

Çalışma kapsamında Er^{3+}/Yb^{3+} katkılı TeO_2-WO_3 cam malzemelerin fotonik cihazların yapımında, sıcaklık ve ışık sensörlerinin geliştirilmesinde literatüre katkı sağlamak amaçlanmıştır.

CHAPTER I

INTRODUCTION

Numerous studies have been conducted on glasses obtained by doping various rare earth ions with host glass materials to develop glasses with pronounced luminosity [9]. These glasses are widely used in many industrial fields, such as sensors, solar cells, etc. [12], [31]. These sensors are based on the measurement of the fluorescence intensity ratio (FIR) of materials doped with RE ions or transition ions. The non-contact FIR technique allows precise temperature measurement in both thermally difficult to access and electromagnetically challenging environments [10]. In this technique, rare earths (RE) are preferred due to their energy levels [12]. It has been observed that materials with UC luminescence, a nonlinear optical process that emits high-energy photons, enable noncontact temperature sensing [10], [14], [15]. It was found that these materials are very suitable for the development of host materials with low phonon energy [14].

Tellurite-based glasses are quite favourable host materials for rare earth luminescence due to their low melting temperature [31], higher linear and nonlinear refractive index compared to silicate glasses [7], [16], chemical resistance and thermal stability [11], and wide transmission range [15]. In addition to these properties, one of the most important reasons for their preference is that they increase the efficiency of UC thanks to their low phonon energy[31]. With these properties, they precede the widely preferred oxide glasses such as silicates and borates[16]. When all these properties are evaluated, tellurite-based glasses become very suitable host materials for rare-earth ions. TeO_2-based host glass materials UC have been prepared by doping many different principal components such as WO_3, ZnO, PbO [11]. However, in addition to these advantages, tellurite glasses also have the disadvantage of not being durable at high optical densities due to their low glass transition temperatures[7]. Tellurite glasses doped with WO_3 have been investigated as a solution to reduce this drawback [7], [16], [32], [33]. Positive changes in the physicochemical properties of WO_3 doped glasses were observed [16]. While the transition temperature of TeO_2 glass is 290^oC, it was

observed that the transition temperature of WO_3-doped TeO_2 glass material is 370^0C [7] . Another important advantage of WO_3-TeO_2 glass materials is that they have high phonon energy compared to others [33].

3-valent rare-earth ions such as Er^{3+}, Yb^{3+}, Tm^{3+}, Ho^{3+} increase UC luminescence thanks to their ability to transfer their energy to the neighbour ion [34], [35]. The first study in this field showed that the ratio of fluorescence intensity depends on the ratio of green light emitting quantum levels to the concentration of Er^{3+} ion [31], [36], [37]. However, although the Er^{3+} ions produce an emission band of about 1.5 μm, doping alone has no advantage other than low luminescence efficiency[7][10]. For this reason, the optical properties were investigated by doping Yb^{3+} ions, which exhibit strong absorption, into the matrix[31], [38]. Thanks to the Yb^{3+} contribution, the large absorption cross section, the $^4I_{15/2}\rightarrow{}^4I_{11/2}$ transition of the Er^{3+} ion at 980 nm, was increased, making the weak ground state absorption efficient [10], [38], [39]. This enhancement is due to efficient resonance energy transfer from the Yb^{3+} ion to the Er^{3+} ion [11]. In addition to the fact that Er^{3+} /Yb^{3+} codoped tellurite glasses are very good for green and red emission, studies have shown that these glasses have good thermal stability and their emission spectra are mainly in the near-infrared region [11], [39]. The Er^{3+} transition of Yb^{3+} at 980 nm leads to $^4I_{13/2}$ [14].

Er^{3+}/Yb^{3+} doped tellurite-based glasses are UC glasses that exhibit temperature sensitive behavior using the FIR technique. This technique (FIR) analyzes the integrated intensity ratio of two different emission bands of fluorescent materials to determine the temperature [12].

The Er^{3+} UC radiation increases due to the energy transfer from Yb^{3+} to Er^{3+}. The use of the thermally coupled energy levels of $^2H_{11/2}$ and $^4S_{3/2}$ to determine the intensity ratio of fluorescence is one of the most important examples of the application of Er^{3+} to temperature measurement [9], [10].

In this study, TeO_2-WO_3-$LiNbO_3$ glasses doped with Er^{3+} and Yb^{3+} ions were fabricated and their thermal and optical properties were investigated. Upon excitation

at about 980 nm, UC luminescence in the green and red regions was observed, and the mechanism of energy transfer were analyzed. The optical parameters affecting the usability and generation of white light based on UC luminescence were studied.

By exciting of our glass samples doped with lanthanide ions (Ln^{3+}) in the UV and NIR-IR ranges, using the spectral data obtained thanks to the UC mechanism: the light emitted by our glasses at all frequencies of the colors red, green, blue (red, grain, blue/ RGB) , and the luminance efficiency were measured. CCT, CRI, CIE x-y values measured with the UC mechanism are also presented in tables.

CHAPTER II

GENERAL INFORMATION

II.1. Tellurite Glasses

TeO_2-based glasses are well suited glasses for optical devices, thanks to their many advantages, such as their many electromechanical properties, high nonlinear behaviour, and low phonon energy. TeO_2 is a conditional glass former because it allows glass formation by combining heavy metal oxides or earth metals [40].

The fact that TeO_2 glasses are suitable for use in photonics, laser applications, even telecommunications, and electric storage vehicles; Physical properties such as high linear and nonlinear refractive indices, easy mechanical preparation, durability, low melting temperature, high thermal stability and similar physical properties have great impact. In addition, they are host materials that can be transformed into different glass materials, as they allow the preparation of different compositions. In previous studies, it has been observed that some rare earth ions improve luminescence properties [1]–[3].

There are many reasons why TeO_2-based glasses are preferred over silicate, phosphate, and laminate glasses. First, they have higher refractive index and nonlinear refractive index thansilicate and fluoride glasses. Second, their phonon energies are lower (~750

cm-1) compared to oxide glasses. The third important feature is that the transmission zone of silicate glasses is 0.2-3 mm, while that of tellurite glasses is between 0.35-5 mm. One of the most important reasons why they are preferred over fluoride glasses is their glass stability. Moreover, they have high transparency at wavelengths up to 5.5 μm [17]–[21] .

Considering the nonlinear optical properties of TeO_2 glasses, as well as their high chemical stability, many properties have become a research topic attracting the attention of researchers [41]. In addition, tellurite glasses transmit broad wavelengths ranging from 0.5 μm to 6 μm and have a high concentration of rare-earth ions and a high refractive index compared to other glasses. It offers the possibility to create glasses with different properties using different modifiers, which allow us to change the optical properties at will. [42], [43].

Doping with $LiNbO_3$, one of the most important ferroelectric materials, gives tellurite-based glasses highly efficient electrooptical, piezoelectric and pyroelectric properties. This has resulted in materials suitable for use in areas such as wave devices and waveguides. These devices are mostly fabricated from $LiNbO_3$ single crystals, and by modelling these crystalline lines, suitable applications for photonic devices have been developed [44]. The structural features of the TeO_2-$LiNbO_3$ pair are also of interest. While $LiNbO_3$ is a ferroelectric material with a high Curie temperature, TeO_2-based glasses are an asymmetric trigonal bipyramid of TeO_4 and have a lone pair of electrons in the equatorial position [45]. Alkali or alkaline earth metals are incorporated into tellurite glasses as converters, and tellurite becomes a potential material for optical sensing and biochemical applications thanks to the change of host material. This is because tellurite as a host matrix offers very efficient luminescence and low phonon energy compared to other hosts such as phosphate, borate, and silicate. The reason it is doped with other oxides is that TeO_2 alone cannot form glass. The ability of this guest material to accommodate strong metal oxides and rare earth ions is due to its weaker Te-O bonds [4]–[6].

Up-conversion fluorescence in TeO_2 glasses; It is pumped at 980 nm, which will allow the development of amplifiers with high output power and broadband gain. This means that the phonon energy must be increased. However, the glass transition temperature of tellurite glasses of 290^oC makes them thermally weak. At this point, in addition of WO_3 to tellurite glasses increases the phonon energies compared to other tellurite glasses and raises the glass transition temperature to 370^oC [7].

In addition, TeO_2 can be doped with metal oxides such as WO_3 to make it a more efficient glass former, and this doping gives the glasses linear refractive index property [16], [19]–[21], [46].

WO_3 is preferred because of its electrochemical properties and low cost. TeO_2-WO_3 compounds provide linear and highly nonlinear optical properties while offering high mechanical and thermal resistance [46][16].

The addition of transition metals with empty d-orbital cations such as WO_3 or TiO_2 can increase the efficiency. This is because TeO_2-based glasses have Te^{4+} single electron pair [32], [47]–[50] and a Te-O-Te [51], [52] bonding structure. This improves the optical properties [32].

II.2. Rare Earth (REE) Elements

It is a metal group consisting of 17 heavy elements including rare earths, Sc, Y, and the lanthanide group. Nowadays, rare earths are very important for the construction of many technological tools and high-tech applications that we often use in our Daily life.

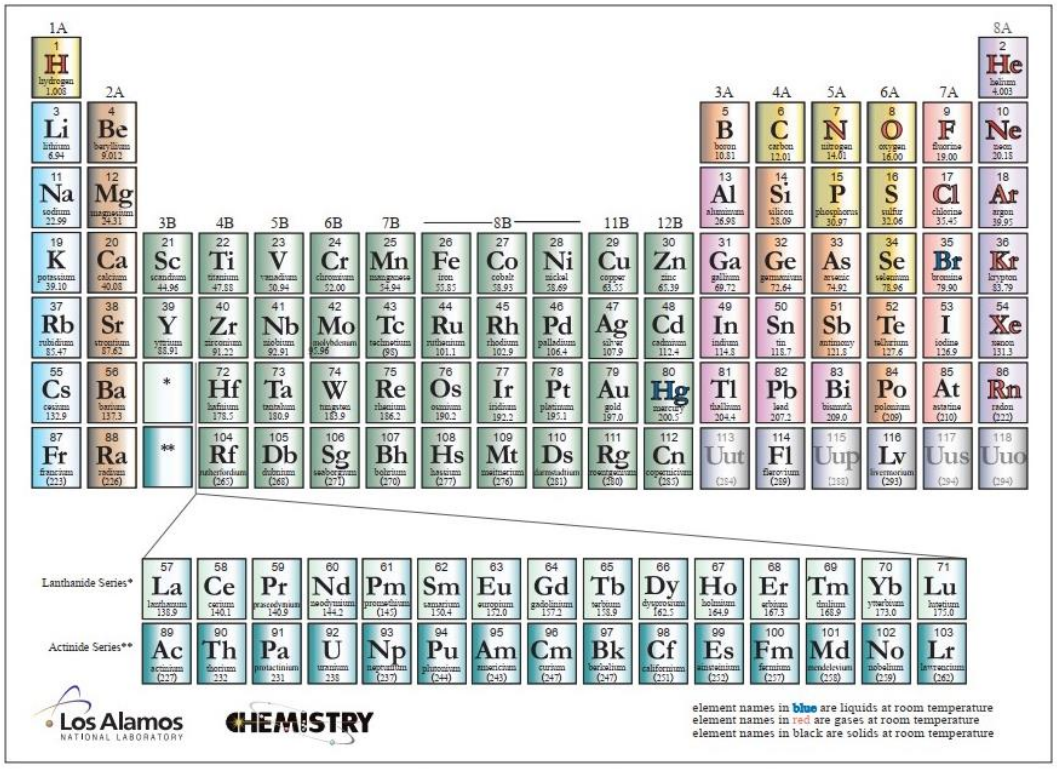

Figure 2.1: The Periodic System of the Element [53].

Electron shells of an atom; They are called K,L,M,N,O,P and Q or 1,2,3,4,5,6,7. It is the electrons in the outer shell that determine the conductive and chemical properties. At the same time, each shell contains a subshell with atomic orbitals. These subshells are also referred to as s,p,d,f (Jensen 2007).

Atomic structures of lanthanides; f orbitals are filled and consist of seven suborbitals. Lanthanides are characteristic 3+ cations. This is because they have a $4f^{n+1}$,$5s^2$,$5p^6$,$6s^2$ configuration and lose 4f electrons and $6s^2$ electrons.

Erbium has 6 isotopes and its atomic number is 68. Whereas ytterbium has 7 stable isotopes and its atomic number is 70 [22].Lanthanides glow when heated in the spectral range between ultraviolet (UV) and near-infrared (NIR), that is, they exhibit luminescence.

Lanthanide ions are preferred in many fields such as lighting, color manufacturing and LEDs thanks to their various luminescent colors. They are also widely used in energy conversion applications (UV or IR) thanks to their unique spectral properties in the visible region of the electromagnetic spectrum (Andres and Chauvin 2012).

Ion	$4f^n$	4f electrons							S	L	J	$^{2S+1}L_J$
Ce^{3+}	$4f^1$	↑							1/2	3	5/2	$^2F_{5/2}$
Pr^{3+}	$4f^2$	↑	↑						1	5	4	$^3H_4$
Nd^{3+}	$4f^3$	↑	↑	↑					3/2	6	9/2	$^4I_{9/2}$
Pm^{3+}	$4f^4$	↑	↑	↑	↑				2	6	4	$^5I_4$
Sm^{3+}	$4f^5$	↑	↑	↑	↑	↑			5/2	5	5/2	$^6H_{5/2}$
Eu^{3+}	$4f^6$	↑	↑	↑	↑	↑	↑		3	3	0	$^7F_0$
Gd^{3+}	$4f^7$	↑	↑	↑	↑	↑	↑	↑	7/2	0	7/2	$^8S_{7/2}$
Tb^{3+}	$4f^8$	↑↓	↑	↑	↑	↑	↑	↑	3	3	6	$^7F_6$
Dy^{3+}	$4f^9$	↑↓	↑↓	↑	↑	↑	↑	↑	5/2	5	15/2	$^6H_{15/2}$
Ho^{3+}	$4f^{10}$	↑↓	↑↓	↑↓	↑	↑	↑	↑	2	6	8	$^5I_8$
Er^{3+}	$4f^{11}$	↑↓	↑↓	↑↓	↑↓	↑	↑	↑	3/2	6	15/2	$^4I_{15/2}$
Tm^{3+}	$4f^{12}$	↑↓	↑↓	↑↓	↑↓	↑↓	↑	↑	1	5	6	$^3H_6$
Yb^{3+}	$4f^{13}$	↑↓	↑↓	↑↓	↑↓	↑↓	↑↓	↑	1/2	3	7/2	$^2F_{7/2}$

Table 2.1: Electronic Configurations of Trivalent Lanthanide ions in the ground state [54] .

II.3. Er^{3+}/Yb^{3+} Doped Glass Materials

Glass materials spiked with RE^{+3} are versatile. The luminescence properties of these ions vary depending on the host material with which they are doped. Glass materials are not naturally uniformly ordered, which means that the energy levels of the lanthanide ions with which they are doped exhibit regional differences. For example, glass hosts silicate, phosphate, tellurite, chalcogenide, etc. They differ from each other in terms of phonon energies, physicochemical and conductive properties. The most important selection criterion among these characteristics is low phonon energy.

Tellurite glasses are generally preferred because they have low phonon energy and many advantages such as high chemical and mechanical resistance and corrosion

resistance [55]. Tellurite glasses are effective glass materials that can be transformed in different ways by various external stimuli.

Many studies have been conducted on the near-infrared bands and UC emissions, and it has been shown that glasses based on Er^{3+} telluride are very efficient compared to oxide glasses. The Er^{3+} emission spectrum obtained by UC pumping at wavelengths of 800-980 nm has two thermal levels ($_2H^{11/2}$ and $^4S_{3/2}$). The main energy transfer between 500-570 nm wavelength is produced by radiative decays in the ground state of $^4I_{15/2}$ (green emission band) and occurs by filling up the excited intermediate level.

In glass materials doped with rare-earth ions, a slower luminescence decay curve from the $^4S_{3/2}$ state to the ground state, i.e., the $^4I_{15/2}$ - $^2H_{11/2}$ green emission band, is observed when excited at 522 nm.

In their study, Li et al [56] investigated the temperature dependent UC emission in Er^{3+} doped transparent ceramic material, and found that the density changes with increasing temperature. Three emission bands, 540, 564, and 682 nm, were observed under 980 nm laser excitation. The study found that the peak intensity at 564 nm wavelength was higher at low temperatures when two different temperatures were considered.

Another important point of the study is that the lifetime of green emission ($^4S_{3/2}$ level) is more affected by red emission ($^4F_{9/2}$ level) than temperature, and the intensity the UC conversion emission band is highest at 540 nm at room temperature.

Among the RE^{3+} ions, the Yb^{3+} ion is used to increase the efficiency of the activator RE^{3+} ions because it matches the emission wavelengths of relatively inexpensive lasers and also has a large absorption cross section. Manzani et al. [57] observed that the sensitivity of both tellurite glasses to other glasses and host material to host material varies greatly.

It was observed that erbium ions can be produce strong emission in compositions where the Yb^{3+} ion concentration is kept relatively high compared to the Er^{3+} ion concentration. One of the advantages of the Yb^{3+} ion is that it offers both easy and fast

energy transfer to its neighbor and a large absorption cross-section at 980 nm excitation.

Research has noted the decreasing Er^{3+} luminescence spectrum in glass materials, and the strong ion-phonon interaction has been suggested as the reason. This interaction is caused by small energy gaps between adjacent excitation levels [58]. By adding sensitizers such as Yb^{3+} to the compositions of glasses doped with Er^{3+} ions, the absorption bandwidth of Er^{3+} ions can be brought to about 100 nm.

In addition to using Yb^{3+} ions as sensitizers in this way, they are also used as activating additives in glass materials. Thanks to its broad luminescence band, it is used in femtosecond lasers. Its broad absorption and luminescence lifetime make it very suitable for use in Ti: sapphire, Nd: YAG or InGaAs lasers.

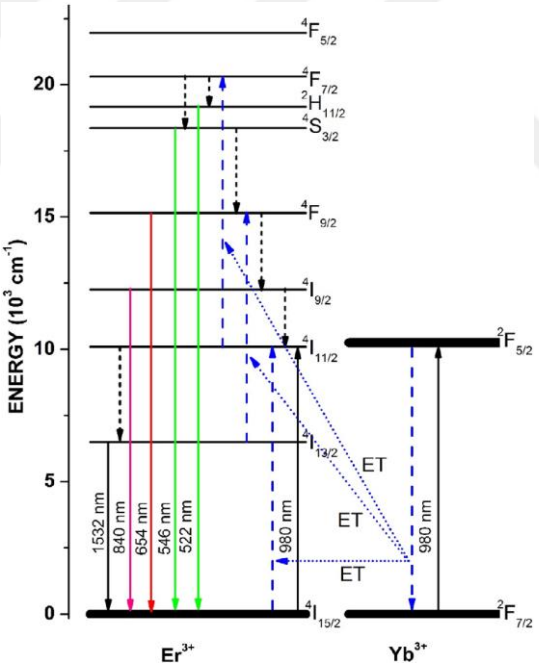

Figure 2.2: Energy level diagram of the energy transfer processes between Er3+ and Yb3+ ions [59].

Ytterbium ions provide radiation absorption and emission due to the presence of two split energy states, the $^2F_{7/2}$ ground level and the $^2F_{5/2}$ excitation level.

II.4. Color Parameters

Electromagnetic waves have a wide spectrum of propagation. Different wave intervals in the narrow spectrum that the human eye can perceive are perceived as different colors, from the longest to the shortest, between red and purple [60].

Colors perceived at different wavelengths are divided into three primary colors according to the trichromatic color vision of the human eye [61]. Although the trichromatic theory was proposed by Thomas Young in the 1800s, it was proven by Maxwell's experiment in 1860 that the three primary colors correspond to red, green, and blue. The trichromatic theory is based on the assumption that the three primary colors are the same [60].

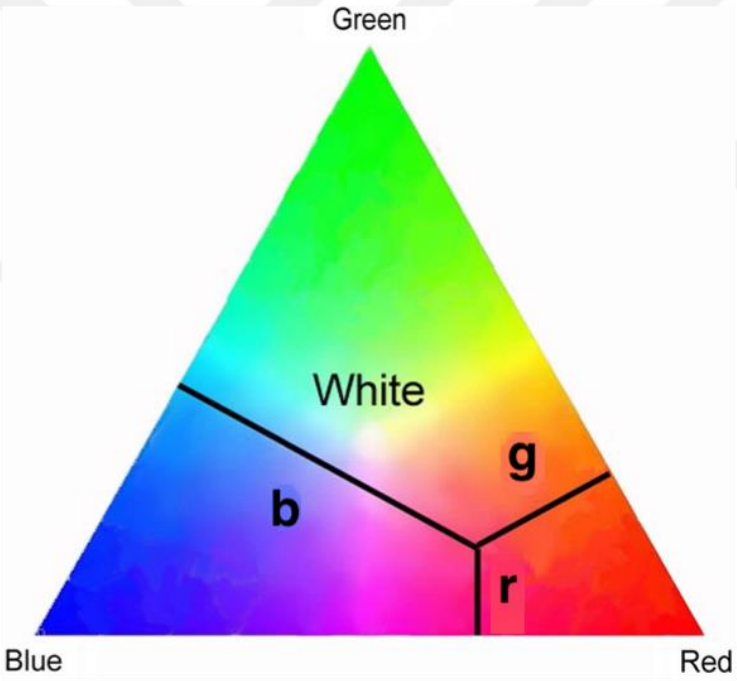

Figure 2.3: Maxwell's triangle [60]

II.4.1. Trichromatic theory

The trichromatic theory assumes that there are three types of cones or receptors on the retina that detect the three primary colors, and that all colors are the reaction degree of

the receptors. The standard observer functions were defined by the CIE (International Commission on Illumination) (1931). These functions have three main sensitivities in each of the spectra of visible wavelengths[61].

II.4.2. Colorimetry

Colorimetry is the technique of determining the three primary colors perceived by the human eye (red, green, and blue) by placing them in three-dimensional color space and reducing the color perception to CIE tristimulus values.

A CIE chart is a two-dimensional chart because only two variables are used to express chromaticity. If you plot a CIE color diagram, you will get a horseshoe-shaped curve [60], [61].

Gassmann (1853) established a set of rules for color addition and matching experiments. These rules later formed the basic principles of colorimetry.

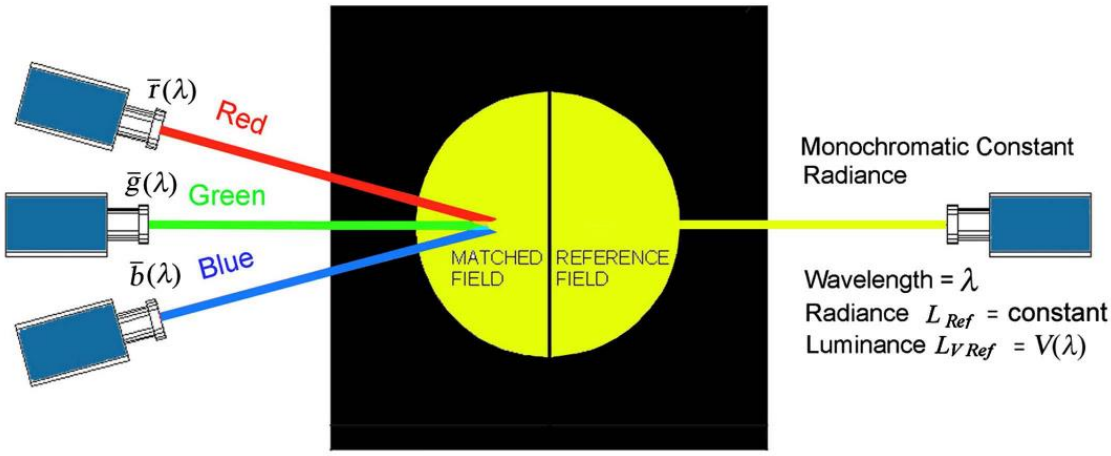

Figure 2.4: Color-matching fields with a monochromatic reference field [60] .

Figure 2.4 shows the setup of a color matching experiment. In the experimental setup, one half of the screen, which is divided into two parts, is the illuminated area and the whole has a viewing angle of 2 degrees, the other half is illuminated with a monochromatic light beam. One half of the area is the area that should correspond to

the reference area. 3 beams of pure monochromatic light, red, green and blue, illuminate the matching area [60].

II.4.3 Chromaticity coordinates r,g,b

A coordinate system is divided into three orthogonal axes and these axes are called r, g, and b. The distance of any point in the coordinate system from the origin is determined by the brightness of the point on that line. The Schroedinger spectrum bag (1920) is the representation of the spectroscopic image pair of points with coordinates as a curve in space [60].

As shown in the figure 2.5 , these points are located at coordinates (1,0,0), (0,1,0) and (0,0,1).

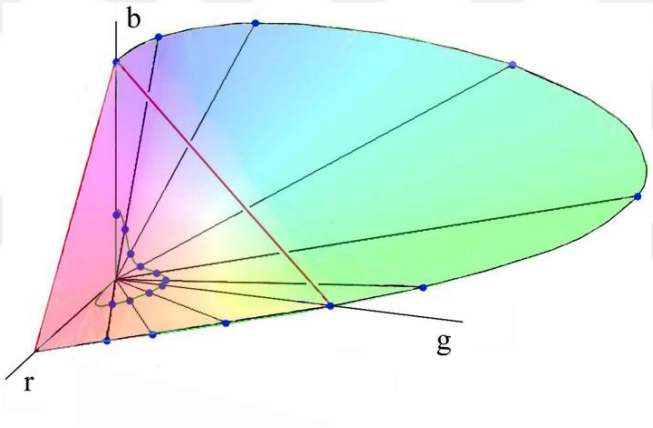

Figure 2.5: Projection of points with coordinates $\bar{r}(\lambda)$, $\bar{g}(\lambda)$, and $\bar{b}(\lambda)$ to a plane passing through points (1,0,0), (0,1,0), and (0,0,1) [60].

In Figure 2.6, the plane in which r(λ) is plotted against g(λ) represents the coordinate plane showing the location of all spectrally pure colors.

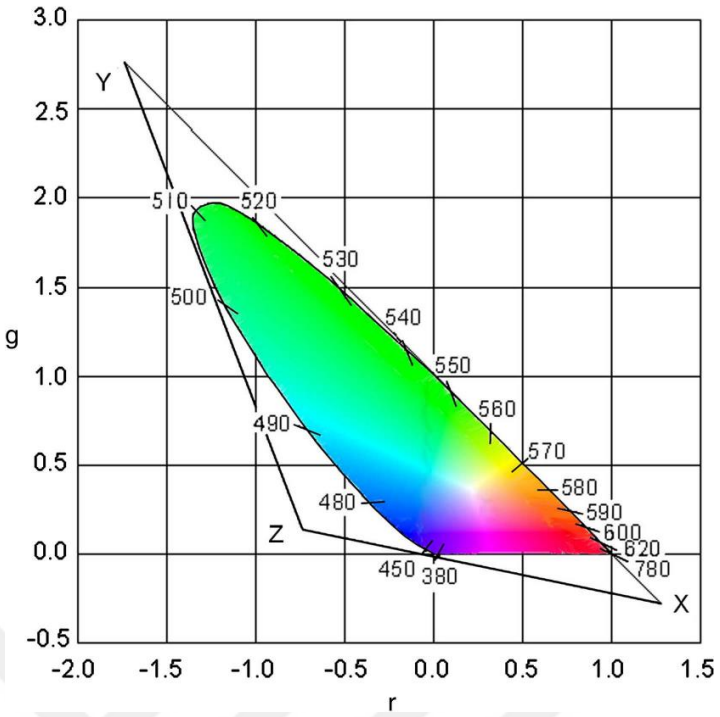

Figure 2.6: Chromaticity diagram for r versus g [60].

By normalizing tristimulus values;

$$r = \frac{R}{R+G+b} \tag{2.1}$$

$$g = \frac{G}{R+G+B} \tag{2.2}$$

$$b = \frac{B}{R+G+B} \tag{2.3}$$

$$r + g + b = 1 \tag{2.4}$$

The r, g, and b values were obtained to determine the hue and saturation of any color [60].

The values of chromaticity coordinates for an area of 2 degrees determined in the convention CIE for spectrally pure colors are given in the table:

Wavelength (nm)	$r(\lambda)$	$g(\lambda)$	$b(\lambda)$	Wavelength (nm)	$r(\lambda)$	$g(\lambda)$	$b(\lambda)$
380	0.0272	−0.0115	0.9843	585	0.7071	0.2952	−0.0023
385	0.0268	−0.0114	0.9846	590	0.7617	0.2402	−0.0019
390	0.0263	−0.0114	0.9851	595	0.8087	0.1928	−0.0015
395	0.0256	−0.0113	0.9857	600	0.8475	0.1537	−0.0012
400	0.0247	−0.0112	0.9865	605	0.8800	0.1209	−0.0009
405	0.0237	−0.0111	0.9874	610	0.9059	0.0949	−0.0008
410	0.0225	−0.0109	0.9884	615	0.9265	0.0741	−0.0006
415	0.0207	−0.0104	0.9897	620	0.9425	0.0580	−0.0005
420	0.0181	−0.0094	0.9913	625	0.9550	0.0454	−0.0004
425	0.0142	−0.0076	0.9934	630	0.9649	0.0354	−0.0003
430	0.0088	−0.0048	0.9960	635	0.9730	0.0272	−0.0002
435	0.0012	−0.0007	0.9995	640	0.9797	0.0205	0.0002
440	−0.0084	0.0048	1.0036	645	0.9850	0.0152	0.0002
445	−0.0213	0.0120	1.0093	650	0.9888	0.0113	0.0001
450	−0.0390	0.0218	1.0172	655	0.9918	0.0083	0.0001
455	−0.0618	0.0345	1.0273	660	0.9940	0.0061	0.0001
460	−0.0909	0.0517	1.0392	665	0.9954	0.0047	0.0001
465	−0.1281	0.0762	1.0519	670	0.9966	0.0035	0.0001
470	−0.1821	0.1175	1.0646	675	0.9975	0.0025	0.0000
475	−0.2584	0.1840	1.0744	680	0.9984	0.0016	0.0000
480	−0.3667	0.2906	1.0761	685	0.9991	0.0009	0.0000
485	−0.5200	0.4568	1.0632	690	0.9996	0.0004	0.0000
490	−0.7150	0.6996	1.0154	695	0.9999	0.0001	0.0000
495	−0.9459	1.0247	0.9212	700	1.0000	0.0000	0.0000
500	−1.1685	1.3905	0.7780	705	1.0000	0.0000	0.0000
505	−1.3182	1.7195	0.5987	710	1.0000	0.0000	0.0000
510	−1.3371	1.9318	0.4053	715	1.0000	0.0000	0.0000
515	−1.2076	1.9699	0.2377	720	1.0000	0.0000	0.0000
520	−0.9830	1.8534	0.1296	725	1.0000	0.0000	0.0000
525	−0.7386	1.6662	0.0724	730	1.0000	0.0000	0.0000
530	−0.5159	1.4761	0.0398	735	1.0000	0.0000	0.0000
535	−0.3304	1.3105	0.0199	740	1.0000	0.0000	0.0000
540	−0.1707	1.1628	0.0079	745	1.0000	0.0000	0.0000
545	−0.0293	1.0282	0.0011	750	1.0000	0.0000	0.0000
550	0.0974	0.9051	−0.0025	755	1.0000	0.0000	0.0000
555	0.2121	0.7919	−0.0040	760	1.0000	0.0000	0.0000
560	0.3164	0.6881	−0.0045	765	1.0000	0.0000	0.0000
565	0.4112	0.5932	−0.0044	770	1.0000	0.0000	0.0000
570	0.4973	0.5067	−0.0040	775	1.0000	0.0000	0.0000
575	0.5751	0.4283	−0.0034	780	1.0000	0.0000	0.0000
580	0.6449	0.3579	−0.0028				

Table 2.2: Chromaticity coordinates r(λ), g(λ), and b(λ) for spectrally pure colors and for a 2-deg field (from CIE 1931) [60] .

II.4.4. Chromocity coordinates (x,y,z)

Chromaticity Coordinates; (similar to r,g,b- space) As can be seen in Figure 2.7, it is found by determining the points corresponding to the color matching functions in the coordinate system in terms of x(λ), y(λ) and z(λ) for spectrally pure colors.

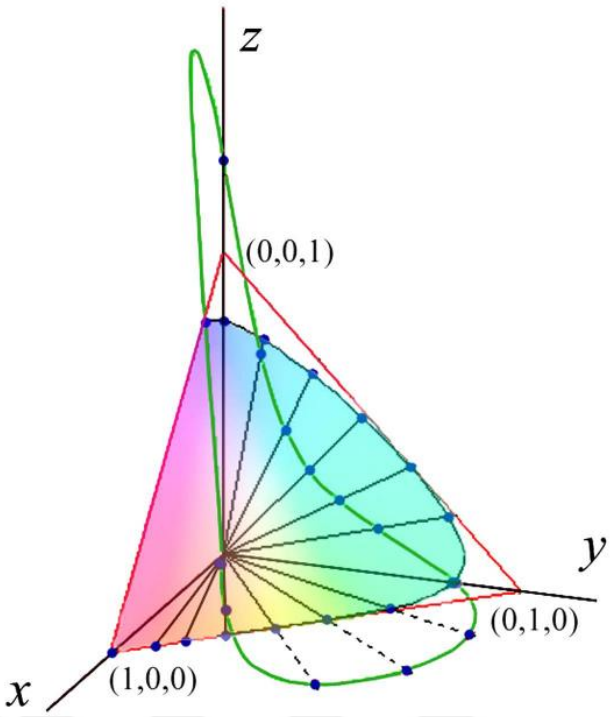

Figure 2.7: Projectionof points with coordinates x(λ), y(λ), z(λ) to a plane passing through points (1,0,0), (0,1,0), (0,0,1) [60].

Just as in r , g , and b-space, the functions are normalized to wavelength:

$$x(\lambda) = \frac{\bar{x}(\lambda)}{\bar{x}(\lambda)+\bar{y}(\lambda)+\bar{z}(\lambda)} \tag{2.5}$$

$$y(\lambda) = \frac{\bar{y}(\lambda)}{\bar{x}(\lambda)+\bar{y}(\lambda)+\bar{z}(\lambda)} \tag{2.6}$$

$$z(\lambda) = \frac{\bar{z}(\lambda)}{\bar{x}(\lambda)+\bar{y}(\lambda)+\bar{z}(\lambda)} \tag{2.7}$$

For a color that is not monochromatic, i.e., that has more than one wavelength, the chromaticity coordinates are determined as follows;

$$x = \frac{X}{X+Y+Z} \tag{2.8}$$

$$y = \frac{Y}{X+Y+Z} \tag{2.9}$$

$$z = \frac{Z}{X+Y+Z} \tag{2.10}$$

The chromaticity coordinates are linearly dependent on each other.

$$x + y + z = 1 \tag{2.11}$$

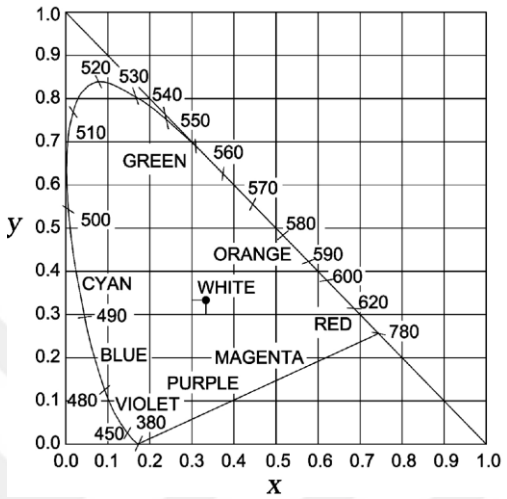

Figure 2.8: Cromaticity x-y diagram for a 10-deg field (from CIE, 1964) [60]

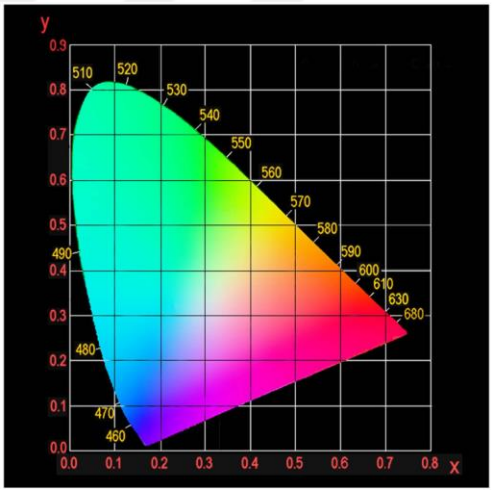

Figure 2.9: Color chromaticity x-y diagram for a 2-deg field (from CIE, 1932) [60]

CIE chromaticity diagram, in which all pure spectral colors are represented as a horseshoe-shaped curve [60]. This diagram is used to represent hue and saturation, not brightness level (Figure 2.12).

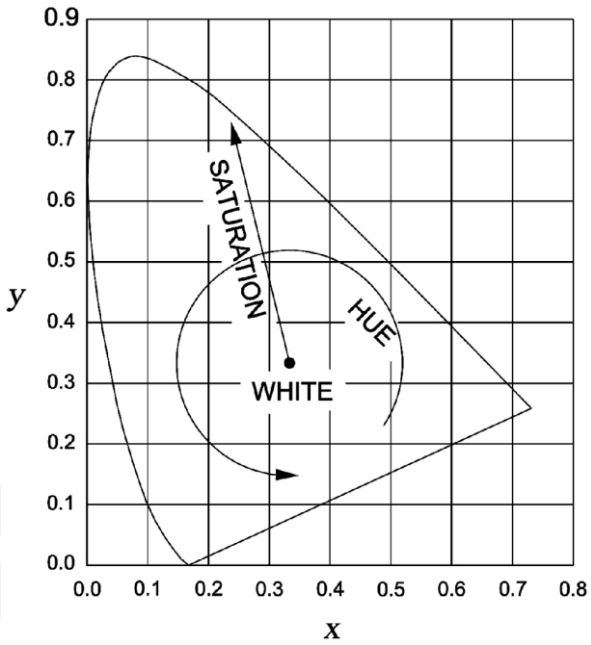

Figure 2.10: Hue and saturation variation in the chromaticity diagram [60]

II.5. Optical Thermometry

II.5.1. Luminescence thermometry

The measurement of luminescence properties with respect to temperature is called luminescence thermometry. To express the performance of luminescence thermometry, the values S (sensitivity) and S_R (relative sensitivity) are used. They are calculated as in Formula 2.12;

$$S = \left|\frac{dQ}{dT}\right|$$

$$S_R = \frac{S}{Q} = \frac{1}{Q}\left|\frac{dQ}{dT}\right| \qquad (2.12)$$

The most popular materials used for luminescence are broad band gap inorganic lanthanides and transition metal ion doped materials. Their use in illumination, plasmas, solid-state lasers, nanotechnology, bioimaging and many other fields has increased. The emissions of rare earth ions and transition metal ions span the ranges UV-NIR-VIS. Moreover, their properties, such as their suitability for synthesis, temperature stability, and widest temperature measurement range among all materials, make them the first choice for luminescence temperature measurement experiments.

The excitation bands and emissions in the luminescence spectrum are defined by the bandwidth and band position. These parameters are temperature dependent. The factors causing this dependence are changes in the refractive index, changes in the energy levels of the electronic levels etc.

The plot made by calculating the ratio of the intensities of different emission bands in luminescent material, is the most popular method for luminescence thermometry. This method, used for rare-earth additions, uses the ratio of emission intensities (caused by the electron transition terminating at various stark sublevels) to emission intensities resulting from the closely excited state of the lanthanide ions. This method can also be used for UC emissions.

When the energy difference between the two thermally dependent excited energy states of the lanthanide ions is ≤2000 cm^{-1}, the electrons change from lower energy to higher energy [62].

In this case, the electronic population of both levels is distributed according to the Boltzman principle;

$$N_H = N_L \cdot \exp(-\Delta E/k_B T) \tag{2.13}$$

In the equation in Equation 2.13, N_H is high, N_L is the number of electrons in the low excited state, ΔE is the energy difference, k_B is the Boltzmann constant, and T is the absolute temperature.

Equation 2.14, defines the luminescence intensity ratio (L-IR) of high (I_H) and low (I_L) excited state emission. g is the excited state degeneracy, h is the Planck constant, ν is the emission frequency, and A is the spontaneous emission rate.

$$\mathrm{LIR(T)} = \frac{\mathrm{I_H(T)}}{\mathrm{I_L}}$$

$$= \mathrm{c}.\frac{\mathrm{g_H A_H h\nu_H}}{\mathrm{g_L A_L h\nu_L}}.\exp\left(-\frac{\Delta \mathrm{E}}{\mathrm{k_B T}}\right) = \mathrm{B}.\exp(-\Delta \mathrm{E}/\mathrm{k_B T}) \qquad (2.14)$$

Taking the logarithm of equation 2.14, we show that it has a linear dependence on the inverse temperature (equation 2.15).

$$\log(LIR) = Log(B) - \frac{\Delta E}{k_B} \cdot \frac{1}{T} \qquad (2.15)$$

High energy states cannot be filled at low temperatures. This is because the electrons do not have enough energy to fill the energy gap between them, so the rate of non-radiative relaxation from the higher energy level to the lower is large. The result is that the lower ΔE is, the lower the temperature at which the LIR scheme can be used [54].

II.5.2. Fluorescence intensity ratio

The IR transmission of glasses down to 4.5 μm in the near - infrared and visible range, high rare-earth resolution, optical quality, slow corrosion rates, and high refractive indices make them very attractive for spectroscopic studies [55], [63], [64] .

Tellurium-based glasses are coming to the fore because their phonon energies are lower than those of common oxide glasses such as silicate, borate, and phosphate [65]. Absorption and emission spectra in the UV (ultraviolet) – VIS (visible) – NIR (vear-infrared) range have been studied.

IR infrared radiation has a wavelength of 0.75-1000 μm, NIR (near - infrared) 0.750-3 μm, M-IR (mid- infrared) 3-30 μm and F-IR (far infrared) with 30-1000 μm wavelengths. Infrared) is divided into 3 regions. IR spectroscopy; used to determine

the properties of a material such as transmittance, gradient index, and refractive index [55].

To get an idea of the temperature at which the system is in thermal equilibrium, we can look at the populations of the energy levels of the thermal pairs. These populations gives us an indication the Boltzman population distribution. Thanks to a technique called FIR (fluorescence density ratio), information about the temperature of the thermal equilibrium of the system can be obtained by studying the emission of the thermally coupled level of a trivalent rare- earth ion. This technique was introduced in 1990 by Berthou e Jorgensen [66]. Berthou e Jorgensen [66] experimented with fluorinated optical fiber glass doped with Yb^{3+}/Er^{3+} [55].

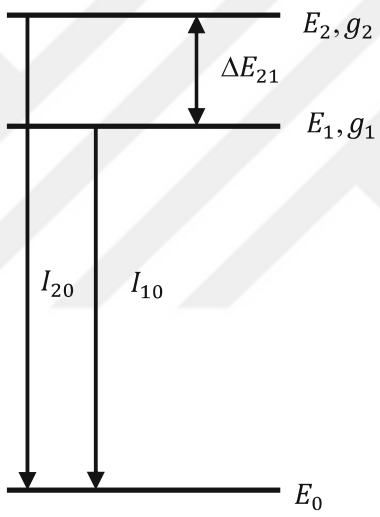

Figure 2.11: Simplified diagram for three energy level thermometry system [55].

As shown in Figure 2.13, the fluorescence intensity of two closely spaced energy levels was recorded as a function of temperature analyzed in the three-level system. By thermal excitation: due to the small energy gap between the two excited states, the population of the upper- level can be brought to a lower- level. The population of ions rising to this upper level is explained by the Boltzman distribution law.

The redistribution of the population of emitting levels with the increase of temperature causes the emission intensities of these levels to change.

In Figure 2.13, N_1 and N_2 are the populations. ΔE_{21} is the energy gap between two thermalized levels in the absorption spectrum. It can be determined experimentally. T is the absolute temperature and K_B is the Boltzman constant [66], [67].

As the population ratio;

$$\frac{N_2}{N_1} = e^{\left(\frac{\Delta E_{21}}{K_B T}\right)} \tag{2.16}$$

definable.

The thermalized emission density can be described as in equation 2.17.

$$I_{20} = N_2 h\upsilon_{20}\beta_{20}A_{20}g_2 \tag{2.17}$$

In the equation, I_{20}/I_{10} is the thermalized emission intensity caused by the radiative decay that occurs during the transition from any state to the lower state. The ion population is proportional to N_2/N_1. The branching rate is related to the β_{20}/β_{10} transition, the spontaneous radiative emission rate A_{20}/A_{10}, the degeneracy of the g_2/g_1 level, and the average photon energy $h\nu_{20}/h\nu_{10}$.

Equation 2.18 calculates the FIR of two transitions (the ratio of their integrated areas) corresponding to thermalized energy levels;

$$FIR = R = \frac{A_{E_{20}}}{A_{E_{10}}} = \frac{N_2 h\upsilon_{20}\beta_{20}A_{20}g_2}{N_1 h\upsilon_{10}\beta_{10}A_{10}g_1} \tag{2.18}$$

In Equation 2.19, it is related to the temperature of the optical sensor using the ratio of the fluorescence intensity between the two thermalized emissions [68], [69]:

$$R = \frac{\upsilon_{20}\beta_{20}A_{20}g_2}{\upsilon_{10}\beta_{10}A_{10}g_1} e^{\left(\frac{\Delta E_{21}}{K_B T}\right)} \tag{2.19}$$

If we make it a little simpler, $C = \frac{v_{20}\beta_{20}A_{20}g_2}{v_{10}\beta_{10}A_{10}g_1}$ for;

$$R = Ce^{\left(\frac{\Delta E_{21}}{K_B T}\right)} \tag{2.20}$$

In this way, the absolute temperature is determined.

The system is in thermal equilibrium. The equation as a function of linear T^{-1} can be written as

$$\ln(R) = a + b\frac{1}{T} (a = \ln(C)\ and\ b = \frac{-\Delta E_{21}}{K_B} \tag{2.21}$$

The parameter C depends on the electronic transitions. This intensity ratio is independent of the power density of the source, since the intensity of each emission band is proportional to the population of levels.

Thermal sensitivity (S) is a measure of how sensitive a temperature sensor is to a given temperature change. This parameter, which determines the quality of the optical sensor, $(s = \frac{dR}{dT})$ is given by the rate of change of the density ratio (R) with temperature.

The thermally bond system is calculated as in Equation 2.22;

$$S = R\left(\frac{\Delta E_{21}}{K_B T^2}\right) \tag{2.22}$$

In Equation 2.23, the equation giving the relative change in temperature per degree, R, shows performance of thermometry;

$$S_R = \frac{1}{R}\left|\frac{dR}{dT}\right| = \frac{S}{R} = \frac{\Delta E_{21}}{K_B T^2} \tag{2.23}$$

This parameter is usually used to compare different thermometers and is expressed in $\%K^{-1}$ [55], [63], [70]–[73].

II.6. Cooperative Energy Transfer

In mechanisms of energy transfer, an excited ion (called a sensitizer or donor) transfers excitation energy to an activator (or acceptor ion). In rare cases, there is a second-class process in which two ions combine to absorb (or emit) a photon [74] .

Optical thermometry has become a focus of research thanks to the luminescence properties of RE doped materials, that exploit the temperature dependence of wavelength, fluorescence intensity ratio (FIR) and emission intensity. The luminescence properties of RE luminescent materials are temperature dependent and consist of hosts, activators/sensitizers.

II.6.1. Down -conversion

The development of rare earth luminescent materials has accelerated, with luminescent materials in up-conversion, down-conversion, and both modes.

RE photoluminescence is called DC luminescence or Stokes luminescence. This is due to the principle of Stokes' theorem that low energy long wavelength radiation is emitted and luminescent materials absorb high energy short wavelength radiation. DC Luminescence is a very effective mechanism to obtain visible fluorescence emissions. To achieve intense visible fluorescence emission, DC luminescence is widely preferred, especially in solar energy applications. Research has shown that DC luminescent materials are not suitable for biological applications due to the excitation wavelength of UV or visible light. It is very popular for use in solar cells because it can convert light that the UV part cannot react to into visible and IR light and make it absorbable.

II.6.2. Up -conversion

In addition, many temperature measurement and biomedical temperature measurement studies are based on UC luminescence, which is preferred. Unlike DC, UC luminescence is an anti-Stokes mechanism. The UC mechanism emits high energy

short wavelength photons and absorbs multiple low energy long wavelength photons after multiple photon addition, which is due to the energy level properties of the RE ions. These materials have very high performance in optical thermometry. In UC luminescent materials, the energy of the absorbed photons is lower than that of the emitted ones. The most common Ln^{3+} ion used as a sensitizer is Yb^{3+} . The Yb^{3+} ion absorbs a large amount of energy thanks to the $^2F_{7/2} \rightarrow {}^2F_{5/2}$ transition and provides high energy absorption efficiency for the laser between 850-1000 nm. Moreover, it can transfer energy to the active ions Er^{3+}, Tm^{3+} and Ho^{3+} and has a highly excited metastable state. Therefore, it provides UC luminescence from the NIR region to the visible region [75].

CHAPTER III

MATERIAL AND METHOD

Within the scope of the topic of my master's thesis, 5 glasses were produced by the melting process. Tungsten oxide telluride glasses were prepared with the various compositions listed in Table 3.1. The rare earth ions Er^{+3} , Yb^{+3} were used as additives along with tungsten oxide tellurite which we used as host material in our basic formulation. The formulation used in our synthesis corresponds to the molar ratio for 1 mol of our material: (84-x mol%)TeO_2 +(10 mol%) WO_3 +(3mol%)Yb_2O_3 +(3mol%)$LiNbO_3$+(x mol%)Er_2O_3.

Table 3.1: The formulations of the samples

	TeO_2	WO_3	$LiNbO_3$	Yb_2O_3	Er_2O_3
TWL1	76.925	10	10	3	0.075
TWL2	76.85	10	10	3	0.15
TWL3	76.7	10	10	3	0.3

TWL4	76.5	10	10	3	0.5
TWL5	72.5	15	10	2	0.5

All chemicals used in the preparation of our 5 glasses, synthesized by melting, were weighed using a Libror AEG 120- Shimadzu precision electronic balance. Each sample was synthesized in an amount of 5 gr, and the amount of doping is detailed below.

The chemical powders prepared in five grams were emptied into the marble mortar by adjusting the mixture amounts and mixing carefully to make them homogeneous. The platinum container filled with the chemical powder mixtures was placed in the Carbolite brand electric furnance, type ELF 11/6, for each sample for each sample and the lid of the platinum container was closed to minimize material loss due to evaporation that may occur during melting.

After the samples reached 950^{o} C, 1 hour was sufficient for the melting process. The mixture in the platinum crucible, which was removed from the furnace using long tongs, was carefully poured into stainless steel molds and placed in the EHRET TK/L4061 frunace, which was preheated to 150^{o} C considering the transition temperature of the steel molds, and left for 1 hour for glazing.

All the synthesized samples were obtained as transparent. The two major surfaces of the samples were ground and polished to make the surfaces smooth and parallel to best transmit light and minimize scattering (absorption and luminescence spectra). Distilled water and different abrasive thicknesses were used in grinding to obtain parallel and smooth surfaces. Then felt, aluminum oxide, and distilled water were used for polishing.

In this preparation to obtain the absorption and luminescence spectra of parallel and smooth polished surfaces, the last step was to pass all samples through pure water and store them in storage containers to remove any oil, dirt, and dust that might have

accumulated on them from handling and touching. After all these processes, the absorbance and luminescence data were provided.

III.1 Investigation of Optical Properties

To investigate their spectroscopic properties, the surfaces of all samples were ground and polished to make them parallel. The physical properties were determined. Absorption spectra and UC luminescence spectra were obtained. All measurements were performed at room temperature.

III.1.1 Absorption spectroscopy

Absorption spectra were recorded with the Cary 100 UV-VIS Spectrometer in the range 400-850 nm and, with the Cary 5000 UV-VIS-NIR, version 1.12 in the range 300-1100 nm.

III.1.2 Luminescence spectroscopy

No Princeton Instruments SP 2500i monochromator was used for the luminescence emission and UC spectra of the sample at 980 nm. As detector: luminescence measurements in the IP-NIR (800-1700 nm) range, Acton series ID-441-C InGaAs and UV-VIS (440-110 nm) luminescence measurements were performed using the SI-440 Silicon Photodiode Detector 980 m CW laser diodes (Apollo Instruments diode lasers – Model No: S30-808-6) were used as pump sources. Pump powers of the lasers: 3 mW for 980 nm CW LD. Acton Spectra Hub and Spectra Sense program were used as detector interface (spectrometer).

III.2 Measurement of White Light Parameters

CIE 1931 x-y standards were used to determine and compare the white light parameters (CIE 1931 x-y Chromaticity Diagram- color chart). For CIE x-y, CCT and CRI measurements, the light emitted on our samples at 980 nm UC was determined using the Asense Tek Lighting Passport illumination meter.

Table 3.2: White light parameters and photographs of TWL1 glass sample recorded according to varying power with varying current under excitation with a 980 nm laser.

Current Value	Up Conversion Spectrum	CIE-1931 Diagram	Emission Picture	CCT and CRI	CIE x-y
0.59 A	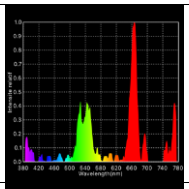	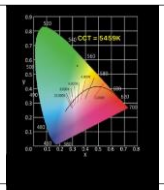	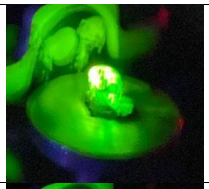	5459 K 55	0.3365-0.5585
0.72 A	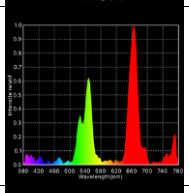	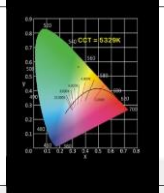	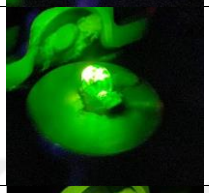	5329 K 50	0.3442-0.5641
0.92 A	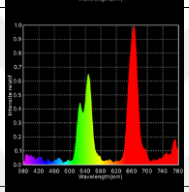	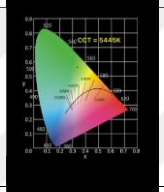		5445 K 50	0.3374-0.5619
1.03 A	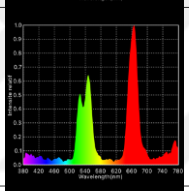	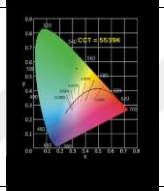		5539 K 52	0.3320-0.5532
1.26 A	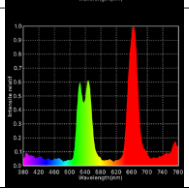	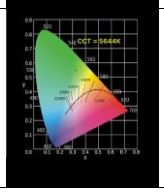		5644 K 54	0.3262-0.5484

Table 3.2 (continued): White light parameters and photographs of TWL1 glass sample recorded according to varying power with varying current under excitation with a 980 nm laser.

1.38 A	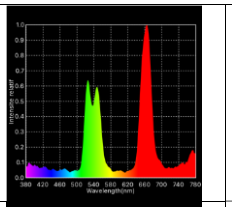	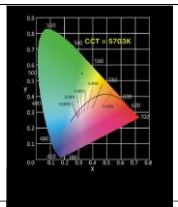		5703 K 54	0.3232-0.5447
1.50 A	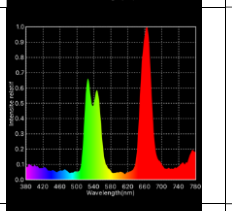	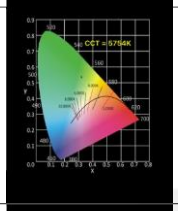	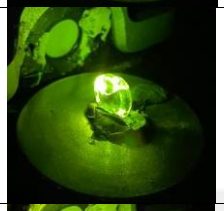	5754 K 55	0.3207-05363
1.70 A	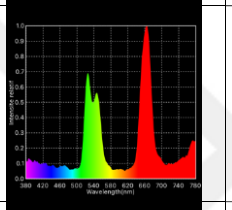	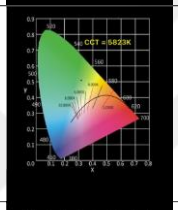	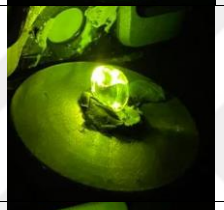	5823 K 58	0.3183-0.5097
1.85 A	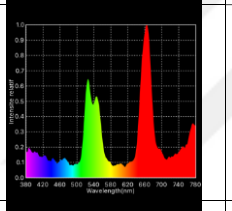	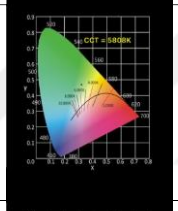		5808 K 63	0.3206-0.4689
1.99 A	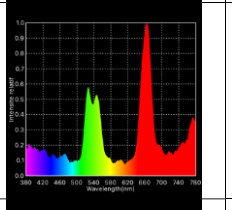	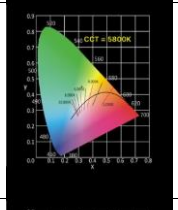		5800 K 64	0.3217-0.4489
2.13 A	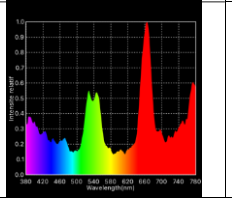	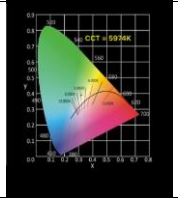		5974 K 73	0.3189-0.3897
2.26 A	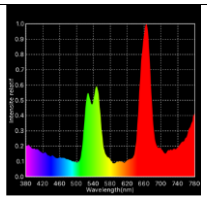	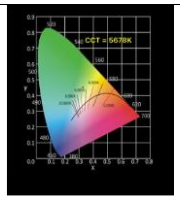		5678 K 63	0.3263-0.4520

Table 3.3: White light parameters and photographs of TWL2 glass sample recorded according to varying power with varying current under excitation with a 980 nm laser.

Current Value	Up Conversion Spectrum	CIE-1931 Diagram	Emission Picture	CCT and CRI	CIE x-y
2.51 A	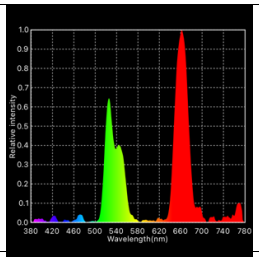	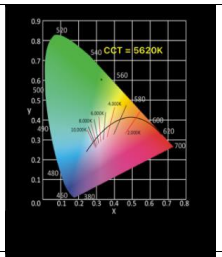	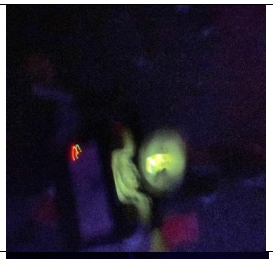	5620 K 45	0.3270 - 0.6039
2.38 A	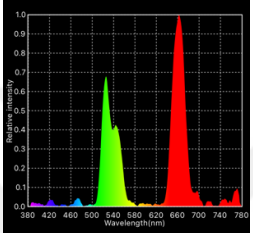	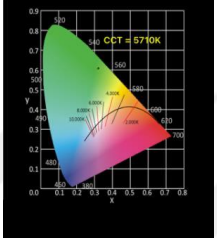		5710 K 45	0.3212 - 0.6087
2.26 A	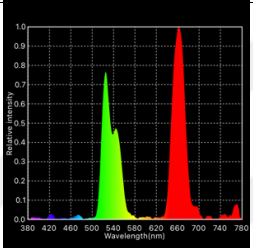	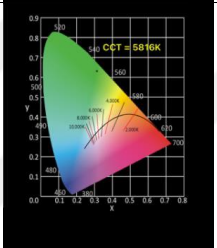		5816 K 37	0.3136 - 0.6311
2.16 A	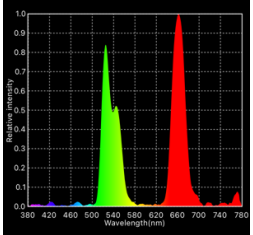	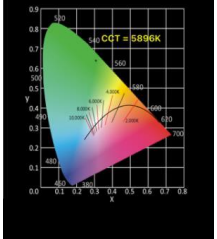	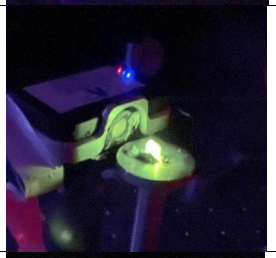	5896 K 34	0.3081 - 0.6388
1.99 A	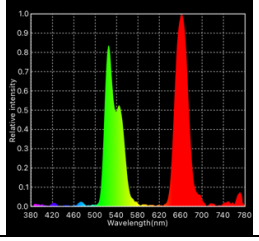	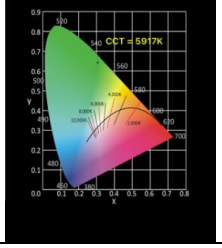	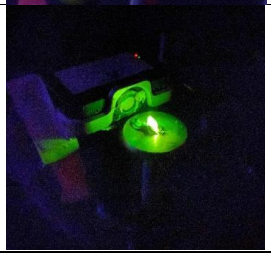	5917 K 30	0.3064 - 0.6432

Table 3.3 (continued): White light parameters and photographs of TWL2 glass sample recorded according to varying power with varying current under excitation with a 980 nm laser.

1.90 A	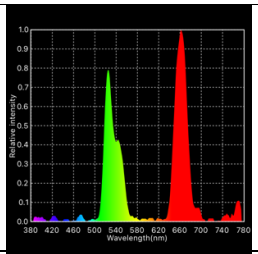	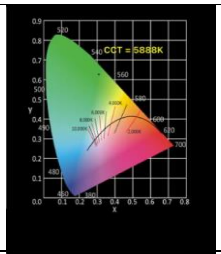	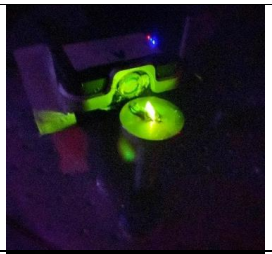	5888 K 40	0.3092 - 0.6270
1.76 A	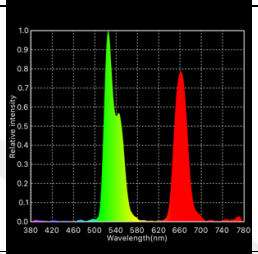	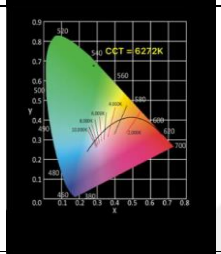	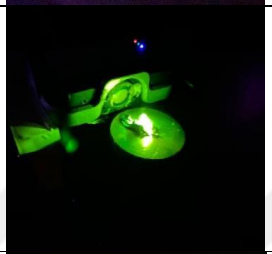	6272 K 11	0.2799 - 0.6762
1.60 A	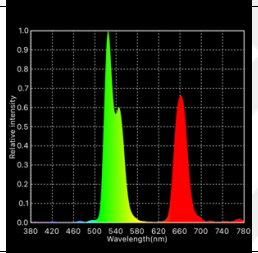	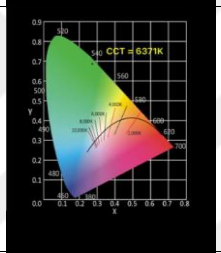		6371 K 2	0.2720 - 0.6864
1.51 A	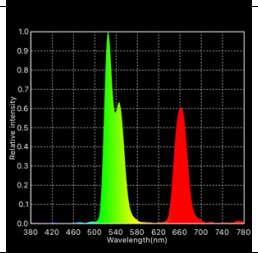	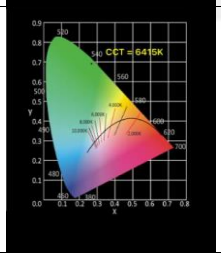		6415 K -2	0.2683 - 0.6917
1.35 A	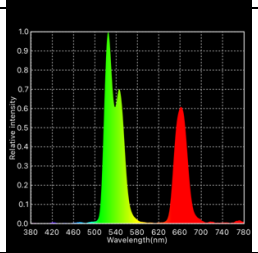	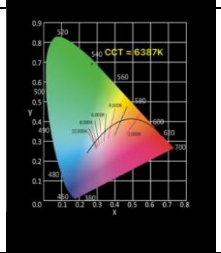		6387 K -2	0.2704 - 0.6906
1.23 A	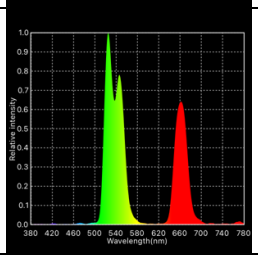	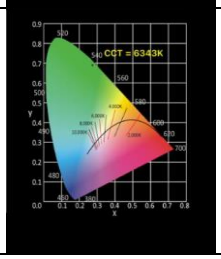		6343 K -3	0.2735 - 0.6900

Table 3.3 (continued): White light parameters and photographs of TWL2 glass sample recorded according to varying power with varying current under excitation with a 980 nm laser.

1.14 A	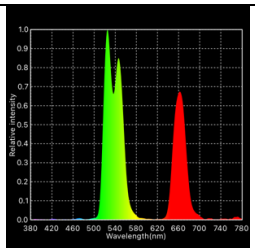	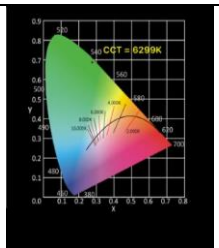		6299 K -2	0.2768 - 0.6880
1.00 A	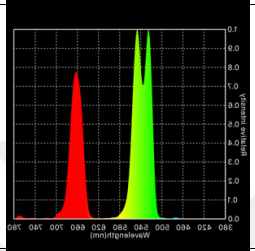	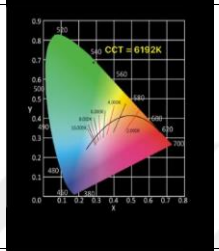		6192 K -6	0.2845 - 0.6851
0.91 A	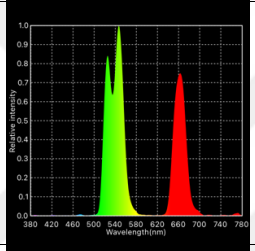	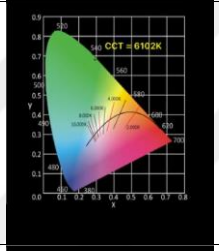		6102 K -6	0.2912 - 0.6809
0.75 A	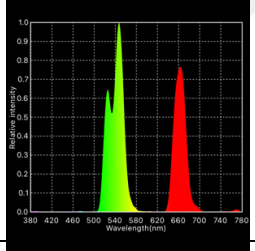	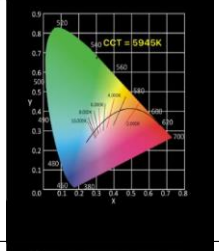	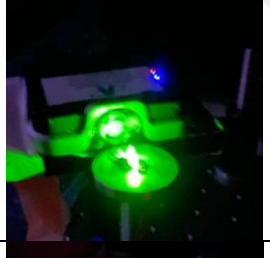	5945 K -5	0.3027 - 0.6735
0.60 A	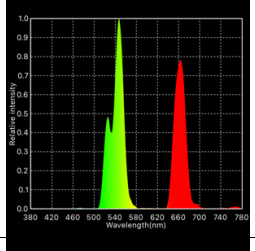	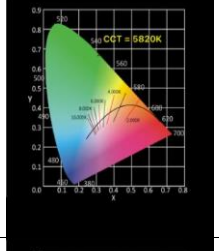	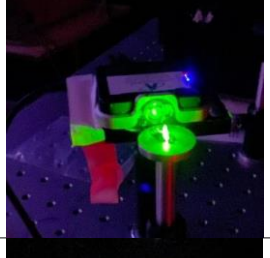	5820 K -4	0.3119 - 0.6671
0.50 A	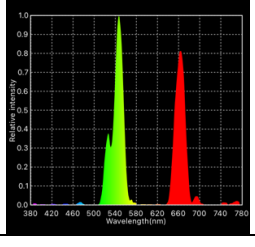	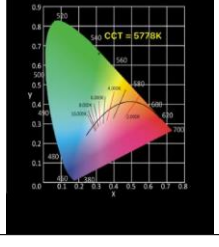		5778 K 15	0.3152 - 0.6591

Table 3.4: White light parameters and photographs of TWL3 glass sample recorded according to varying power with varying current under excitation with a 980 nm laser.

Current Value	Up Conversion Spectrum	CIE-1931 Diagram	Emission Picture	CCT and CRI	CIE x-y
0.50 A	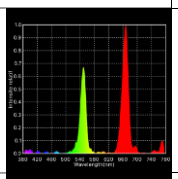	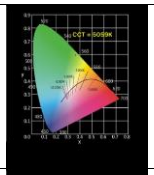		5059 K 38	0.3630 - 0.5964
0.75 A	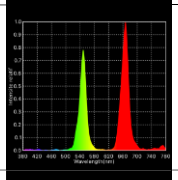	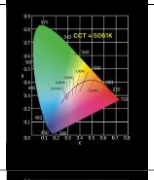	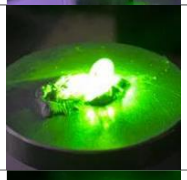	5061 K 37	0.3639 - 0.6087
1.00 A	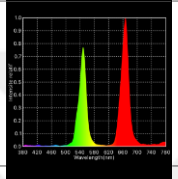	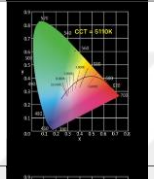		5110 K 39	0.3604 - 0.6065
1.25 A	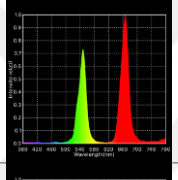	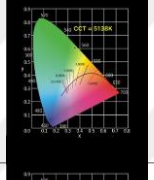	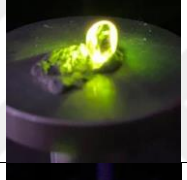	5138 K 41	0.3583 - 0.6044
1.50 A	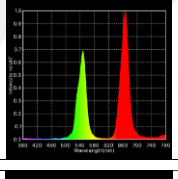	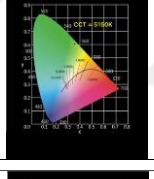	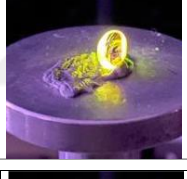	5150 K 41	0.3576 - 0.6050
1.75 A	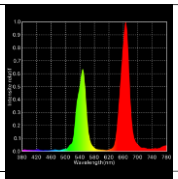	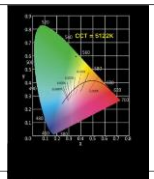	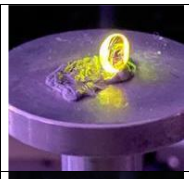	5122 K 44	0.3588 - 0.5951
2.00 A	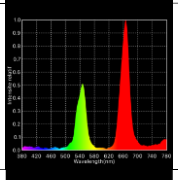	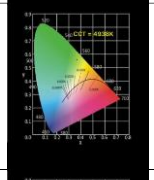	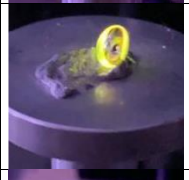	4938 K 47	0.3674 - 0.5583
2.26 A	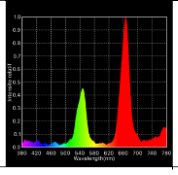	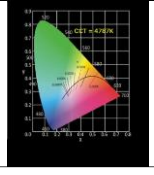	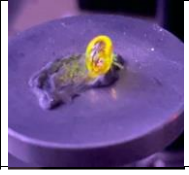	4787 K 51	0.3719 - 0.5194

Table 3.5: White light parameters and photographs of TWL4 glass sample recorded according to varying power with varying current under excitation with a 980 nm laser.

Current Value	Up Conversion Spectrum	CIE-1931 Diagram	Emission Picture	CCT and CRI	CIE x-y
0.50 A	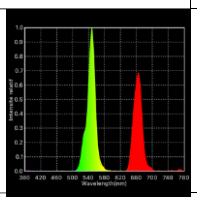	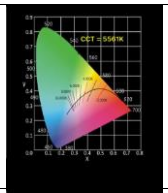	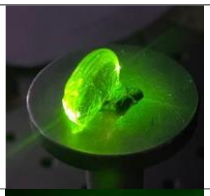	5561 K 8	0.3306-0.6518
0.75 A	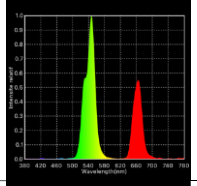	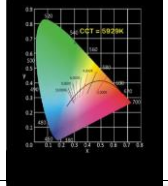		5929 K 7	0.3041-0.6688
1.00 A	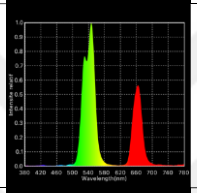	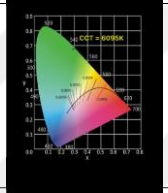		6095 K 7	0.2921-0.6756
1.26 A	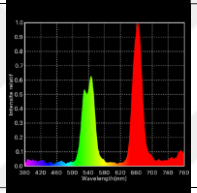	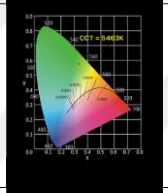	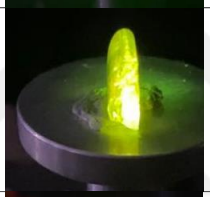	5463 K 49	0.3366-0.5762
1.50 A	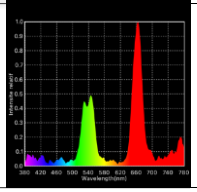	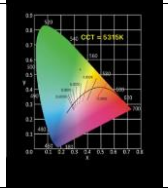	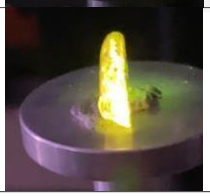	5315 K 54	0.3439-0.5330
1.75 A	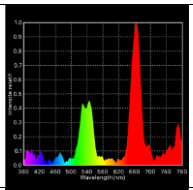	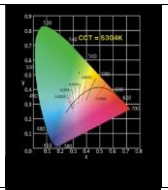	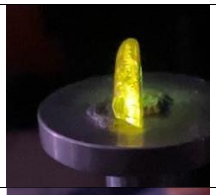	5304 K 56	0.3437-0.5130
2.00 A	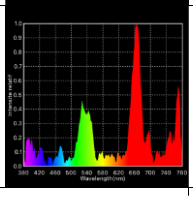	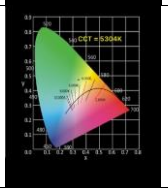	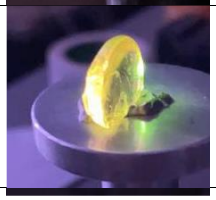	5304 K 65	0.3421-0.4722

Table 3.6: White light parameters and photographs of TWL5 glass sample recorded according to varying power with varying current under excitation with a 980 nm laser.

Current Value	Up Conversion Spectrum	CIE-1931 Diagram	Emission Picture	CCT and CRI	CIE x-y
2.27 A	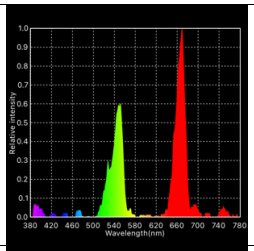	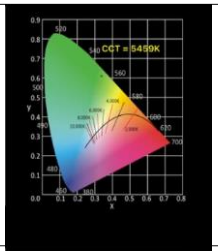		5459 K 41	0.3373-0.6101
2.13 A	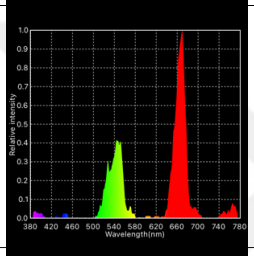	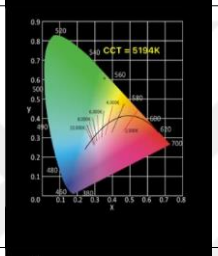	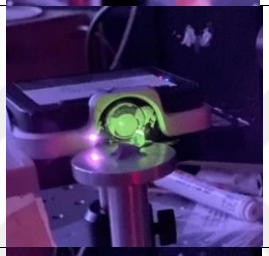	5194 K 43	0.3547-0.6068
1.93 A	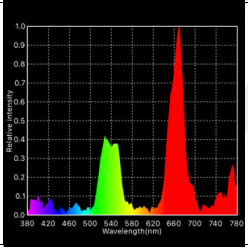	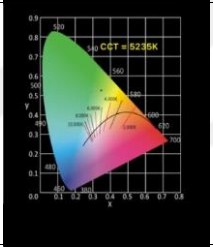		5235 K 57	0.3479-0.5254
1.79 A	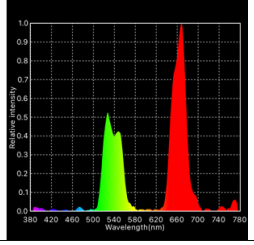	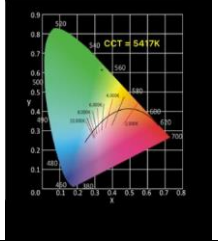		5417 K 39	0.3401-0.6137

Table 3.6 (continued): White light parameters and photographs of TWL5 glass sample recorded according to varying power with varying current under excitation with a 980 nm laser.

1.65 A	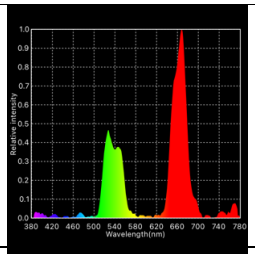	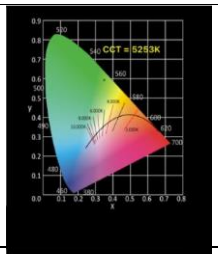	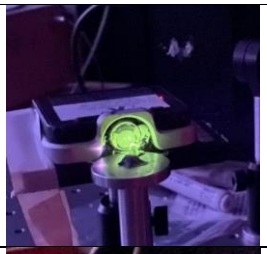	5253 K 46	0.3501-0.5927
1.57 A	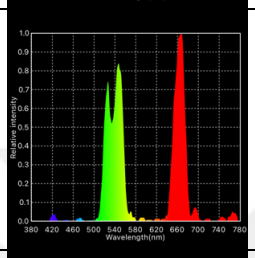	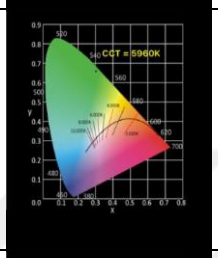	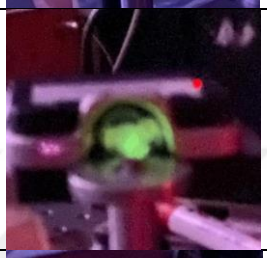	5960 K 22	0.3026-0.6590
1.46 A	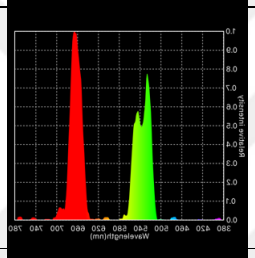	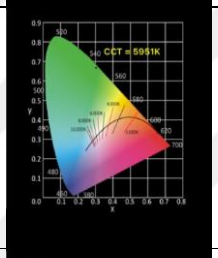		5951 K -6	0.3027-0.6674
1.26 A	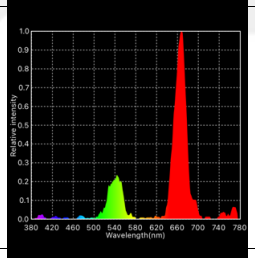	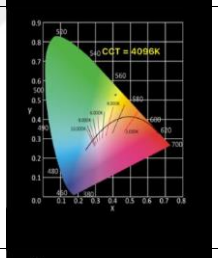		4096 K 39	0.4148-0.5265
1.15 A	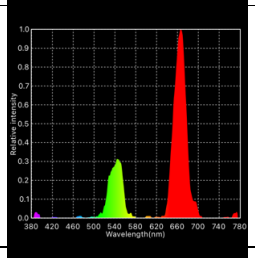	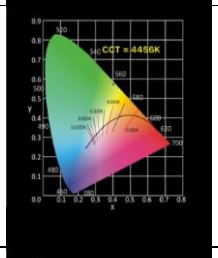		4456 K 35	0.4006-0.5715
1.02 A	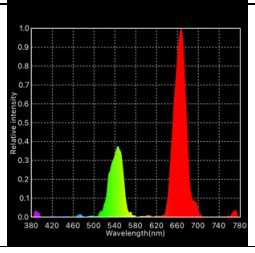	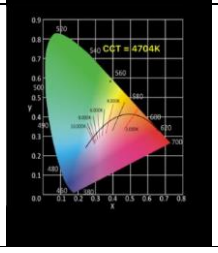		4704 K 38	0.3855-0.5827

Table 3.6 (continued): White light parameters and photographs of TWL5 glass sample recorded according to varying power with varying current under excitation with a 980 nm laser.

0.90 A	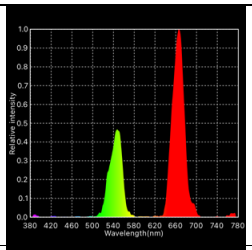	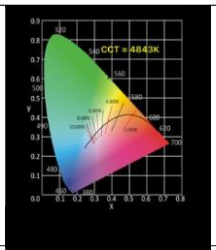	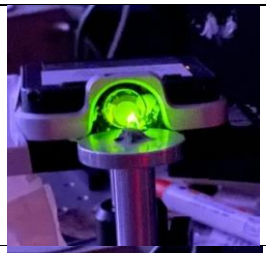	4843 K 28	0.3783-0.6016
0.75 A	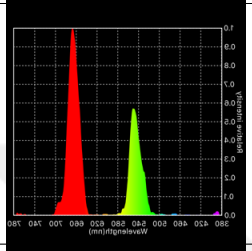	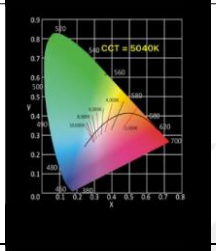		5040 K 28	0.3658-0.6139
0.6 A	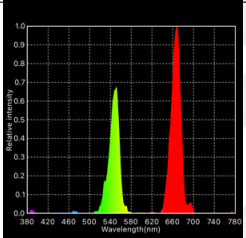	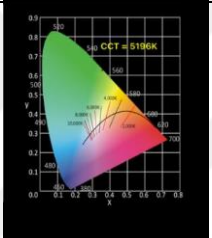	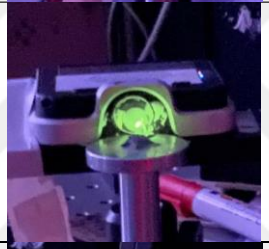	5196 K 24	0.3557-0.6264
0.5 A	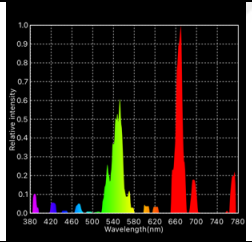	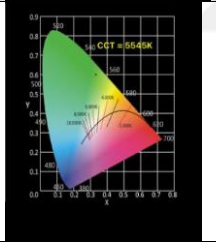	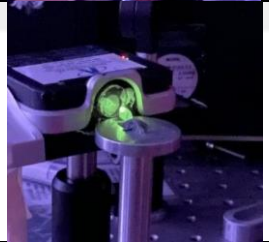	5545 K 35	0.3317-0.6007

CHAPTER IV

RESULT AND DISCUSSIONS

IV.1. Absorption spectrum

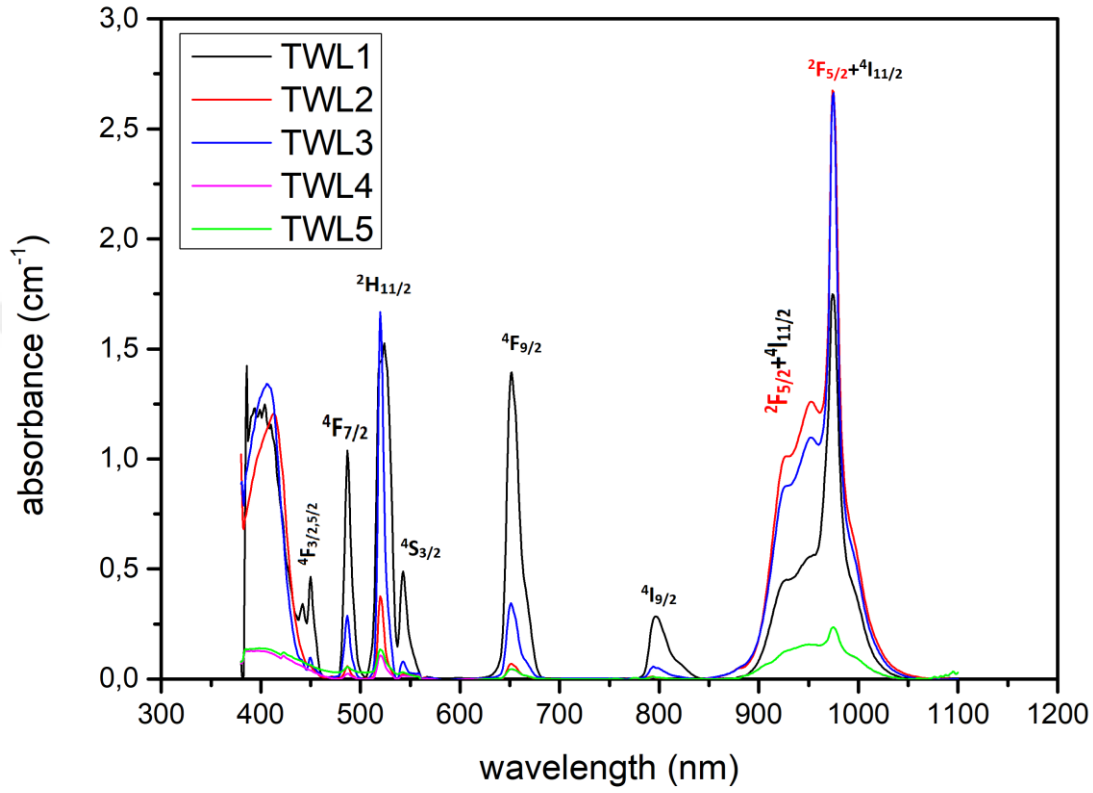

Figure 4.1: TWL glasses absorbance

The absorption spectra of doped glasses measured between 400-1200 nm are shown in Figure 4.1. In the measured regions, various transitions of Er^{3+} ions from the ground state to the excited states $^4F_{3/2,5/2}$, $^2H_{11/2}$, $^4S_{3/2}$, $^4F_{9/2}$, $^4I_{9/2}$, $^4I_{11/2}$ were observed, these transitions at 487, 524, 546, 654, 800 and 980 nm respectively.

The absorption band observed at 980 nm indicates that the Yb^{3+} ion exhibits a $^2F_{7/2} \rightarrow {}^2F_{5/2}$ transition [38]. The UC emission spectra are shown in Figure 4.29,30,31,32,33 by excitation of Er^{3+}/Yb^{3+} doped TeO_2-WO_3 glasses at different powers at 980 nm in the range 400-850 nm. Four UC emission bands were observed

originating from Er^{3+} ion transitions: $^2H_{11/2}\rightarrow{}^4I_{15/2}$, $^4S_{3/2}\rightarrow{}^4I_{15/2}$, $^4F_{9/2}\rightarrow{}^4I_{15/2}$ and $^4I_{9/2}\rightarrow{}^4I_{15/2}$ at wavelengths of 527, 551, 663 and 800 nm, respectively [38], [76], [77].

To determine which mechanism is involved in the UC process, the number of photons responsible for the various UC emissions from glass materials must be determined.

$$I\alpha P^n \tag{4.1}$$

In this expression, I is the emission intensity of UC and P is the pump power. n is the number of photons we want to know [78]. The log linear feet of the power graph of UC emission intensity give the slope corresponding to the number of photons.

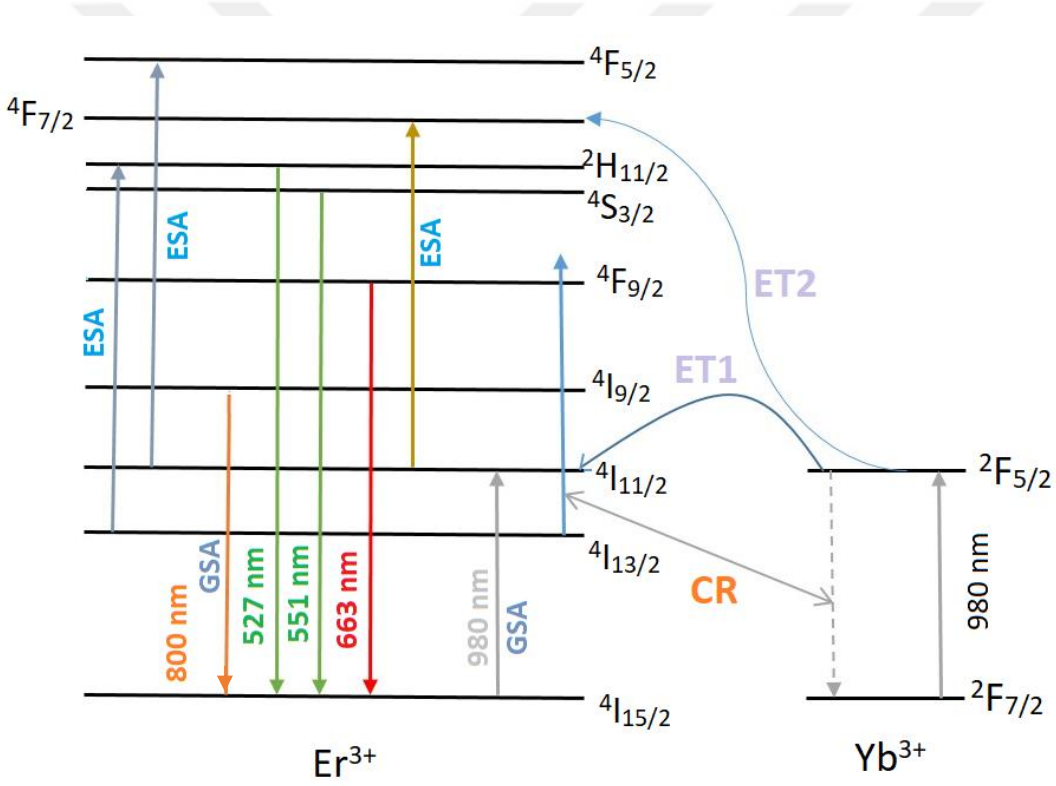

Figure 4.2: Simplified energy level diagram of Er^{3+} and Yb^{3+} ions, possible infrared and upconversion excitation mechanisms under 980 nm excitation are indicated.

At 980 nm excitation, the $^4I_{11/2}$, $^4F_{9/2}$, $^4F_{7/2}$, and $^2H_{9/2}$ levels absorb photons and replenish them through the excited state absorption (ESA) and ground state absorption

(GSA)processes [79]. These filled levels radiatively relax to the ground state $^4I_{15/2}$, resulting in the transitions $^4F_{5/2}\rightarrow{}^4I_{15/2}$ (493 nm) , $^2H_{11/2}\rightarrow{}^4I_{15/2}$ (527 nm), $^4S_{3/2}\rightarrow{}^4I_{15/2}$ (551 nm), $^4F_{9/2}\rightarrow{}^4I_{15/2}$ (663 nm) and $^4I_{9/2}\rightarrow{}^4I_{15/2}$ (800 nm). These emission transitions are enhanced by the energy transfer from Yb^{3+} ions to different excited states of Er^{3+} ions. This is because the absorption cross section of Yb^{3+} ions is stronger than that of Er^{3+} ions at 980 nm excitation [80].

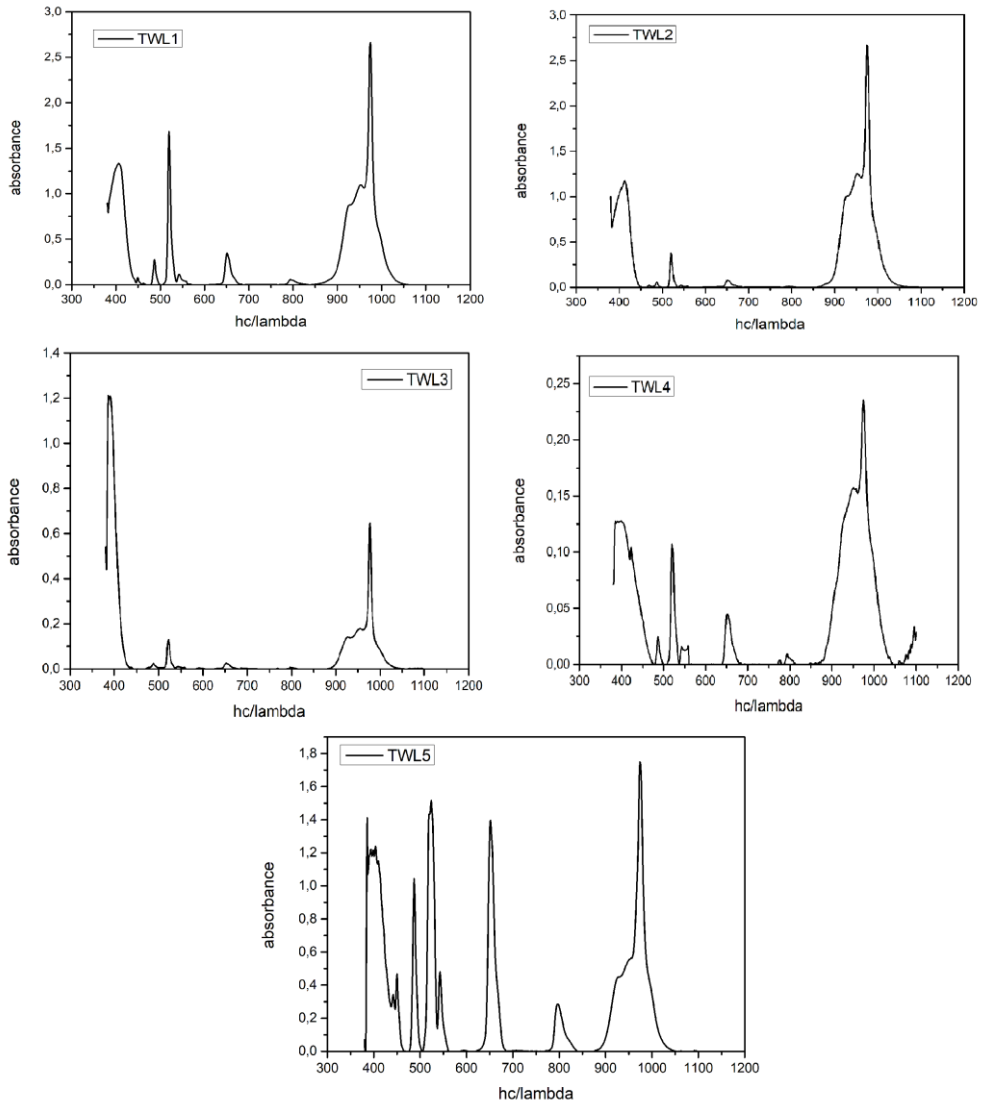

Figure 4.3: TWL1,2,3,4,5 glasses absorbance

IV.2 Optical Band Gap Analysis

To determine the fundamental absorption limits, it is possible to obtain information on the optical transitions and electronic band structure of crystalline and non-crystalline materials in the UV region. Using the optical absorption spectra, the optical bandwidth, E_{opt}, and the Urbach energy, ΔE, can be calculated. There are two types of optical transitions, direct and indirect, with respect to the absorption band in such materials. In both cases, the electromagnetic wave interacts with the valence electrons and pushes the ions from the ground state to the excited state. The absorption coefficient α(ν) with respect to the photon energy of the direct and indirect transitions is expressed by Davis and Mott in the following equation 4.2.

$$\alpha(\omega) = \frac{B(\hbar\omega - E_{opt})^n}{\hbar\omega} \quad (4.2)$$

Here B is a constant and $\hbar\omega$ is the photon energy. For direct and indirect transitions, the value of n is given as ½ and 2. The equivalent is found by extrapolating 4.2 as $(\alpha\,\hbar\,\omega)^{1/2}=0$ and $(\alpha\,\hbar\,\omega)^{2}=0$ [81]–[87].

Figures Indirect band gap for TWL1,2,3,4,5:

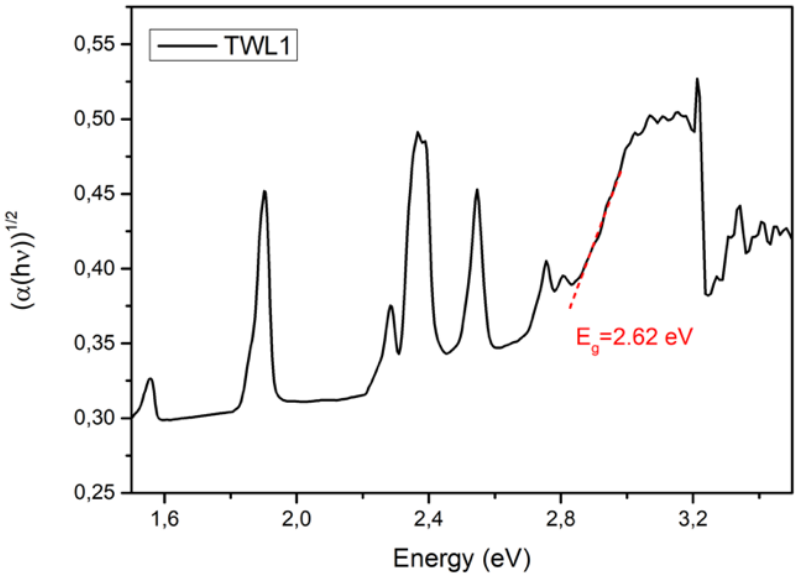

Figure 4.4: Indirect band gap for TWL1

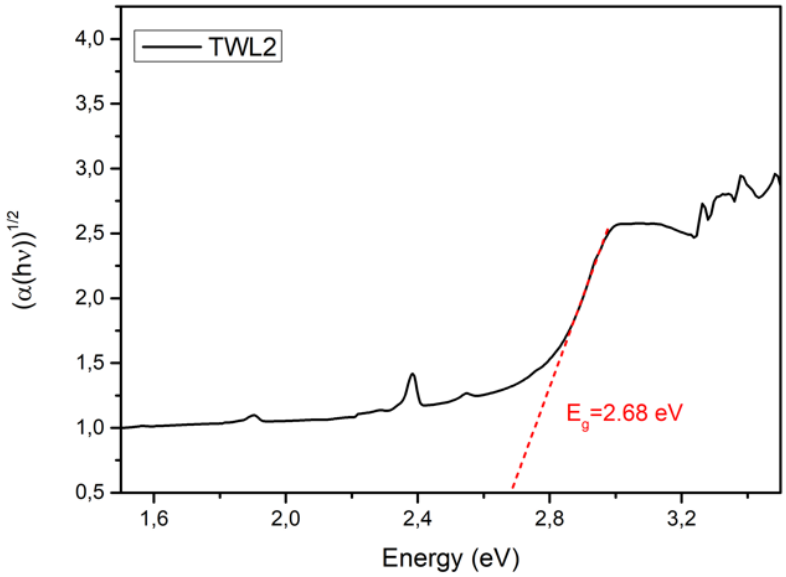

Figure 4.5: Indirect band gap for TWL2

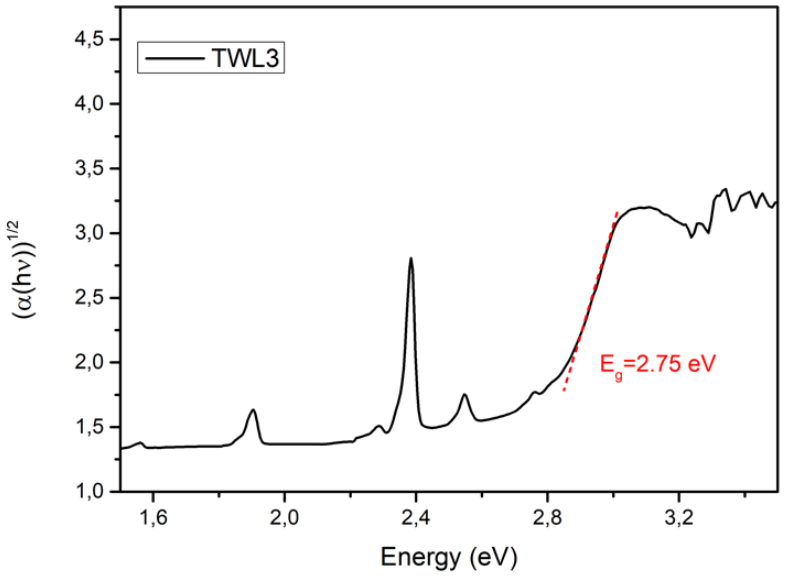

Figure 4.6: Indirect band gap for TWL3

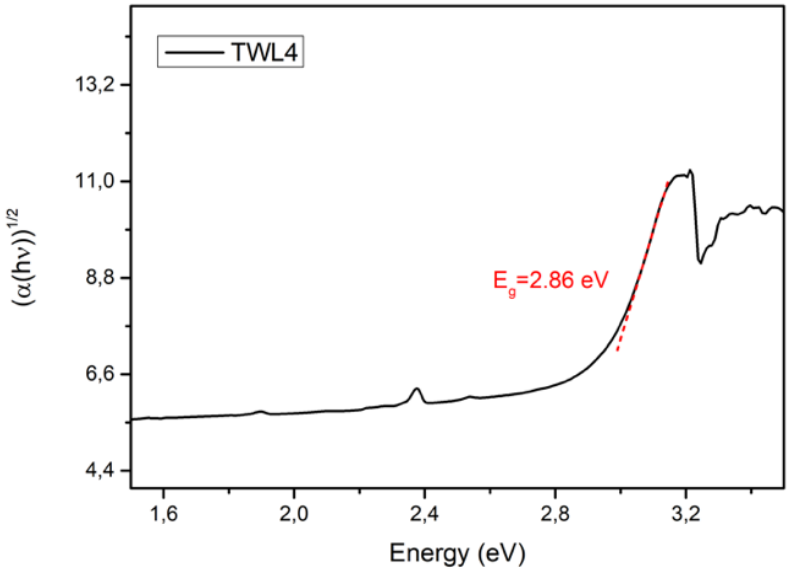

Figure 4.7: Indirect band gap for TWL4

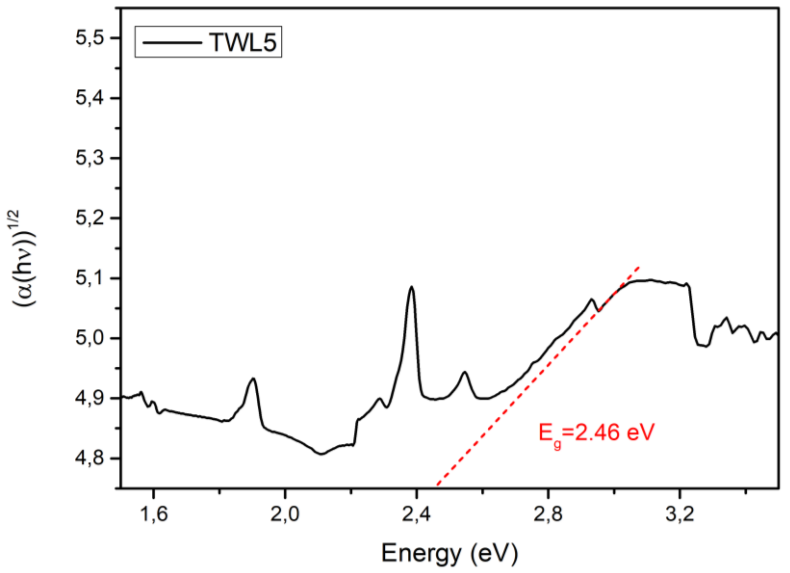

Figure 4.8: Indirect band gap for TWL5

The absorption coefficient α(ω) is given by the equivalent 4.3. If the Urbach energy is ΔE, it results from the slope of the graph of ln(α(ω)) in equation 4.3 with respect to $\hbar$ ω [81]–[90].

$$ln\alpha(\omega) = \left(\frac{\hbar\omega}{\Delta E}\right) - C \quad (4.3)$$

The absorption spectrum is used to calculate the optical band gap in glass materials. The absorption coefficient (α) is determined using the Beer-Lambert law [91]. In our study, the direct-indirect optical band gap and Urbach energy in Er^{3+}/Yb^{3+} doped TeO_2-WO_3 glasses were investigated.

As determined by Tauc and Mott [92], [93]. The absorption coefficient (α), optical band gap (E_g), and incident photon energy (hν) are given by the following equation 4.4.

$$\alpha h\upsilon = A(h\upsilon - E_g)^r \quad (4.4)$$

In the equation, A represents the proportionality constant, and r takes the values ½ and 3/2 for directly allowed and directly forbidden transitions, respectively [94]. In our study, the r value was included in the equation as ½ to calculate the direct optical band gap of RE ion-doped glasses. The curves (direct band gap) between $(\alpha\nu h)^2$ and incident radiation "h (eV)" for all doped glasses are shown in Figures 4.9,10,11,12,13.

The values of the optical band gap (E) for the glass materials were given as equation 4.4.

Figures are Direct band gap for TWL1,2,3,4,5;

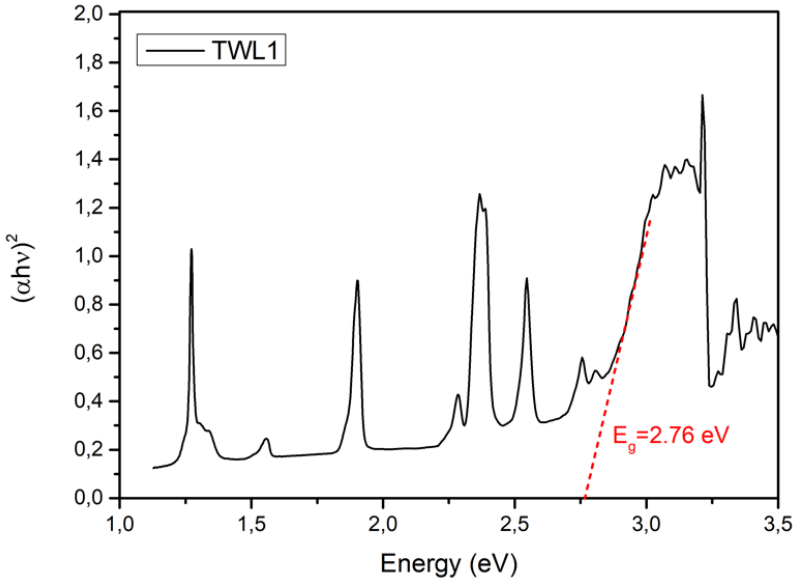

Figure 4.9: Direct band gap for TWL1

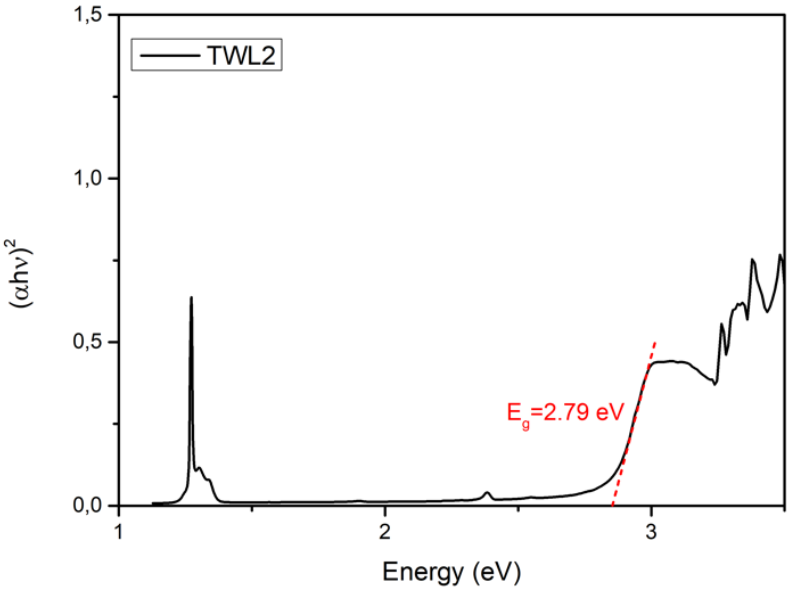

Figure 4.10: Direct band gap for TWL2

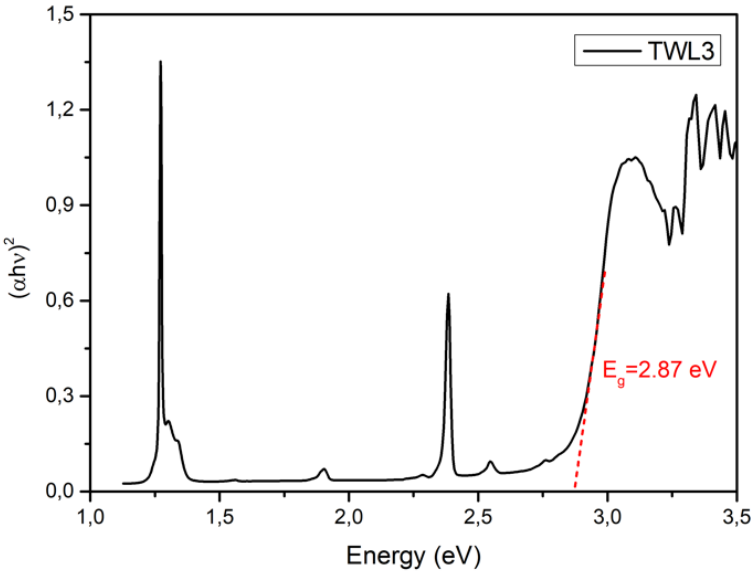

Figure 4.11: Direct band gap for TWL3

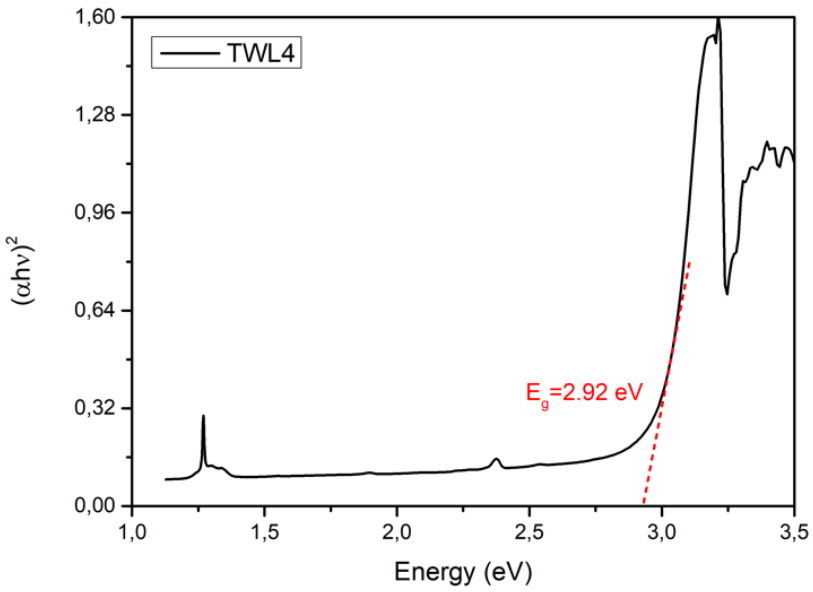

Figure 4.12: Direct band gap for TWL4

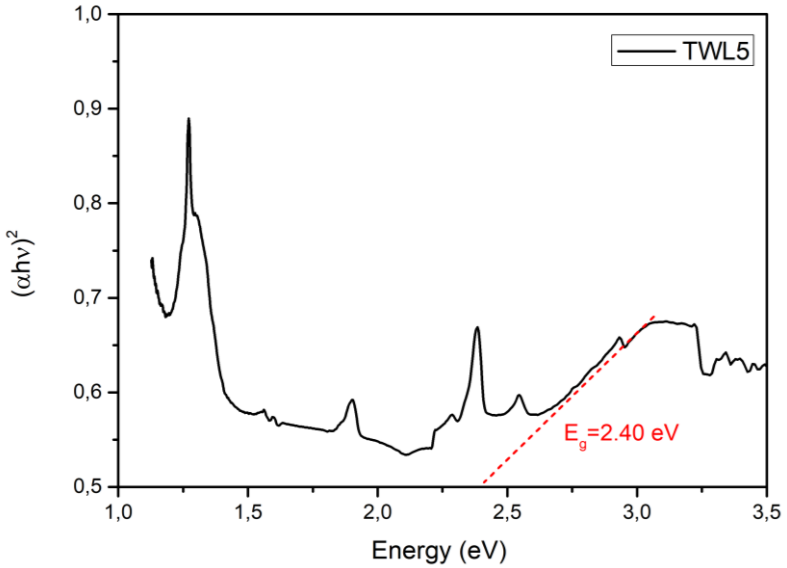

Figure 4.13: Direct band gap for TWL5

The Urbach energy is the name for the forbidden energy gap indicating disorder in the structure of amorphous solid materials. In the Urbach energy, the absorption coefficient and the incoming photon energy are expressed by the following equation;

$$\alpha = Bexp(\frac{h\nu}{E_U}) \quad (4.5)$$

Figures 4.14,15,16,17,18 shows the plot of photon energy versus log absorption coefficient values for TWL glasses. In the diagram, the Urbach energy is obtained from the reciprocal of the slope of the linear part between ln(α) and h. The value of the Urbach energy was found to be 0.75, 0.39, 0.34, 0.42, 9.55 eV. The values are in agreement with previous studies [38].

Figures are Urbach Energy for TWL1,2,3,4,5;

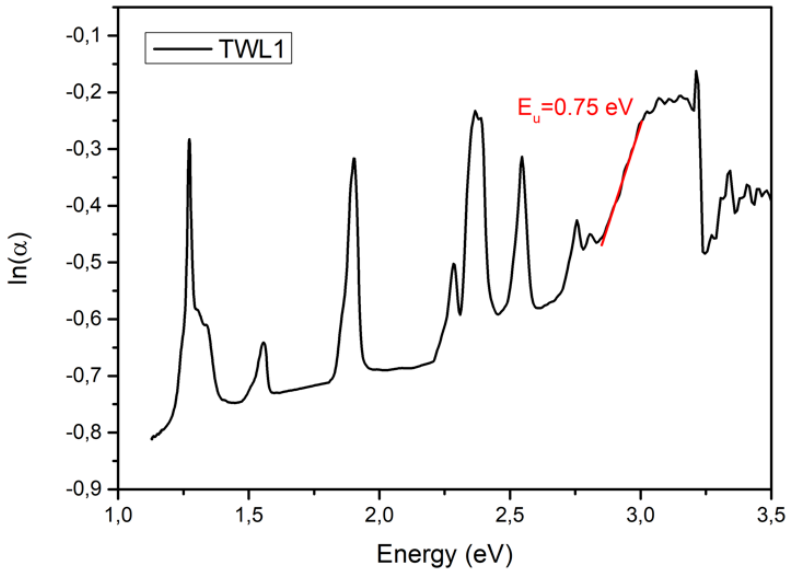

Figure 4.14: Urbach energy for TWL1

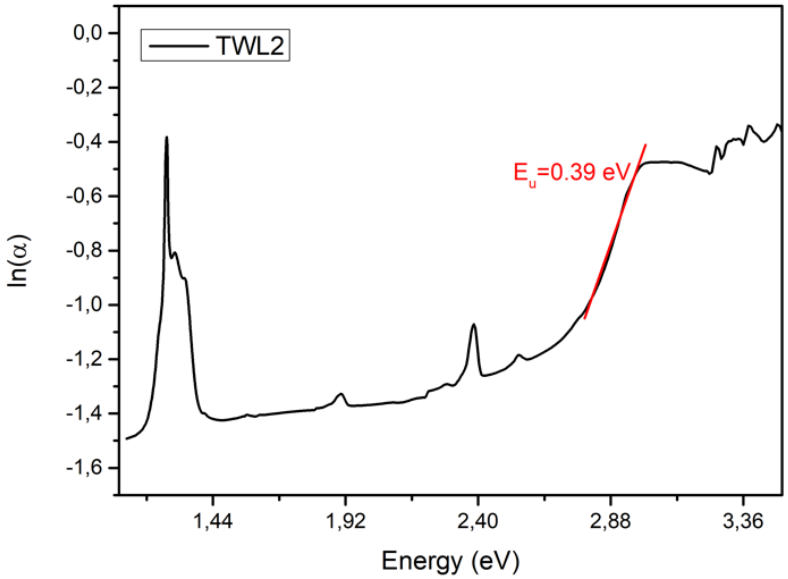

Figure 4.15: Urbach energy for TWL2

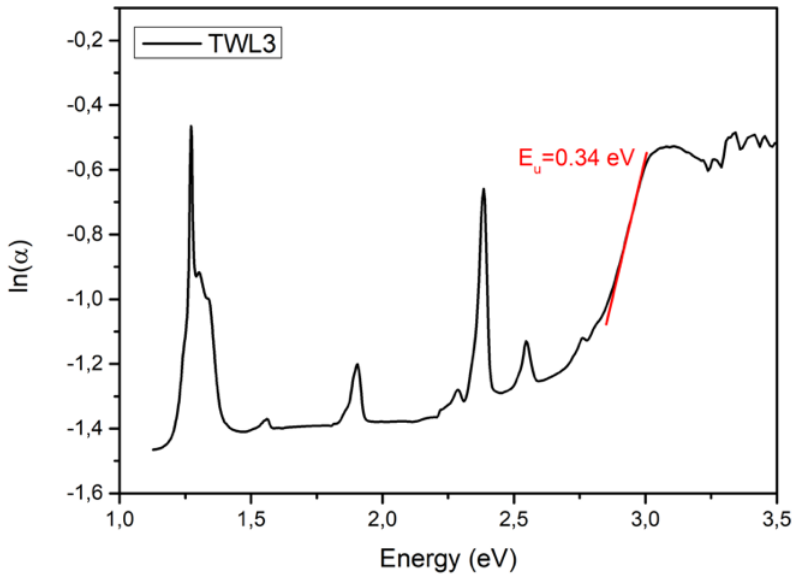

Figure 4.16: Urbach energy for TWL3

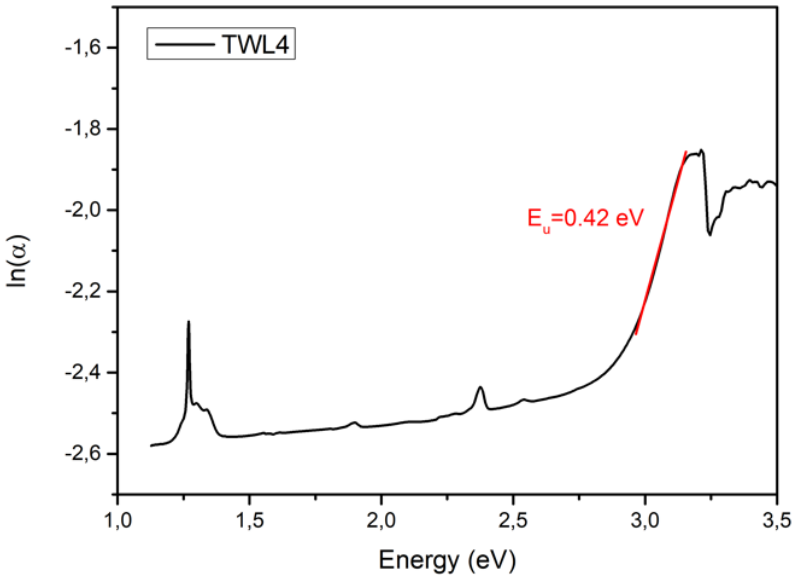

Figure 4.17: Urbach energy for TWL4

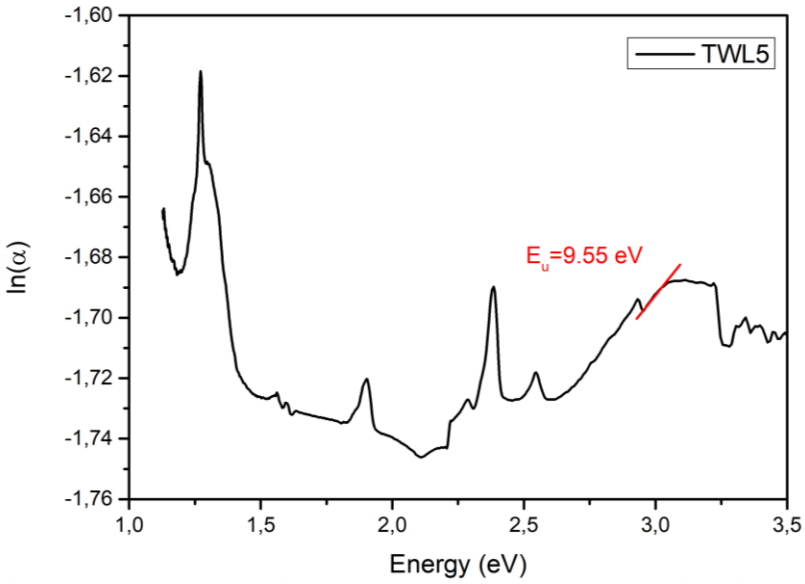

Figure 4.18: Urbach energy for TWL5

IV.3. Photoluminescence Characteristics

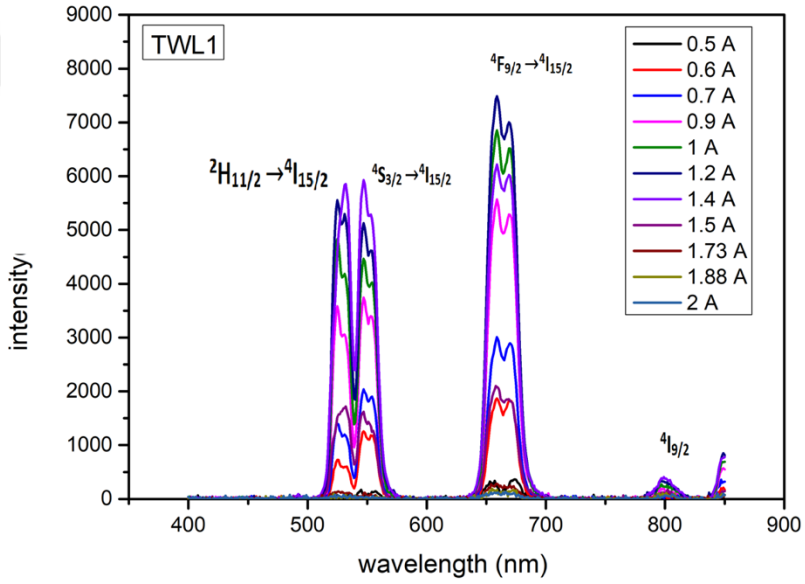

Figure 4.19: Up-conversion emission intensities of TWL1 glass as function of excitation power.

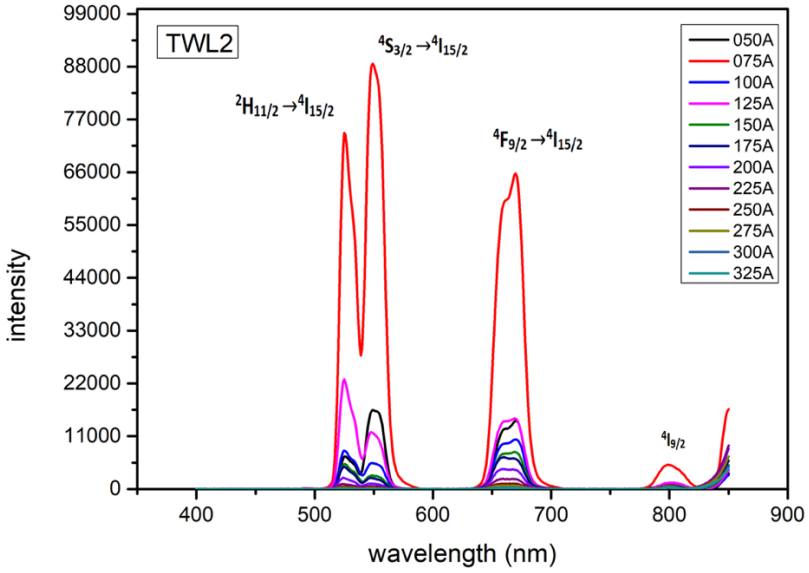

Figure 4.20: Up-conversion emission intensities of TWL2 glass as function of excitation power.

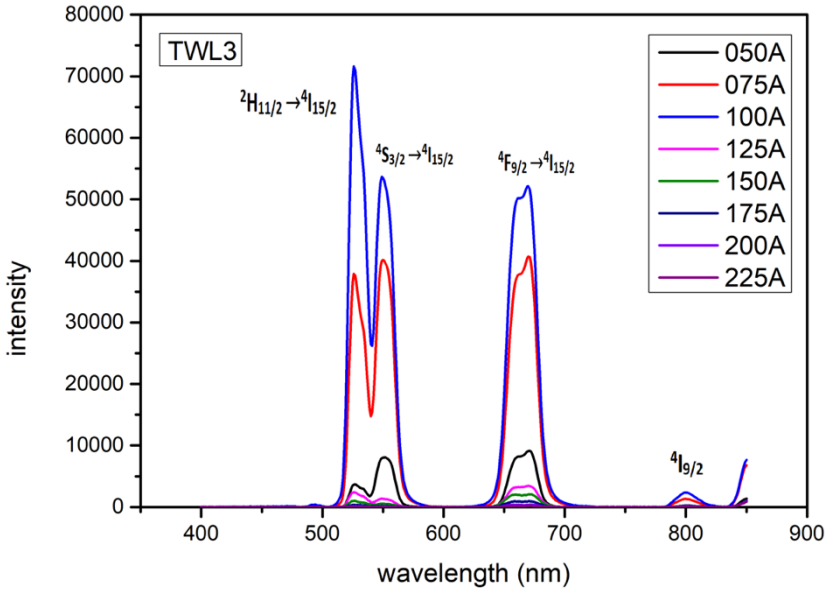

Figure 4.21: Up-conversion emission intensities of TWL3 glass as function of excitation power.

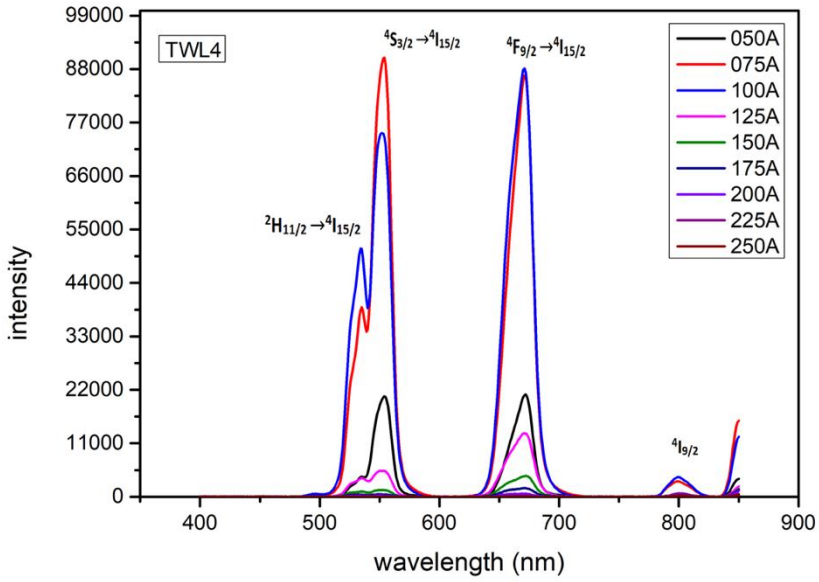

Figure 4.22: Up-conversion emission intensities of TWL4 glass as function of excitation power.

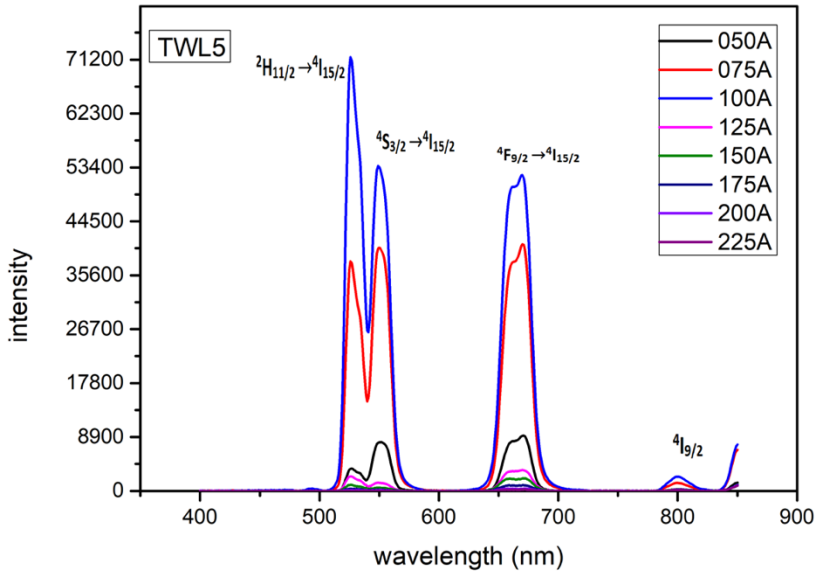

Figure 4.23: Up-conversion emission intensities of TWL5 glass as function of excitation power.

Graphs of change in transitions, bandwidths and peaks for Er^{3+} and Yb^{3+} doped glass materials presented in the findings section were obtained from 980 UC luminescence

spectra, their luminescence intensities measured as a function of excitation power and read from the 980 nm UC luminescence change data as a function of changing power with the change in output current logI/logP and using the number of photons entering the UC processes, is determined. The resulting graph and corresponding peaks are given below.

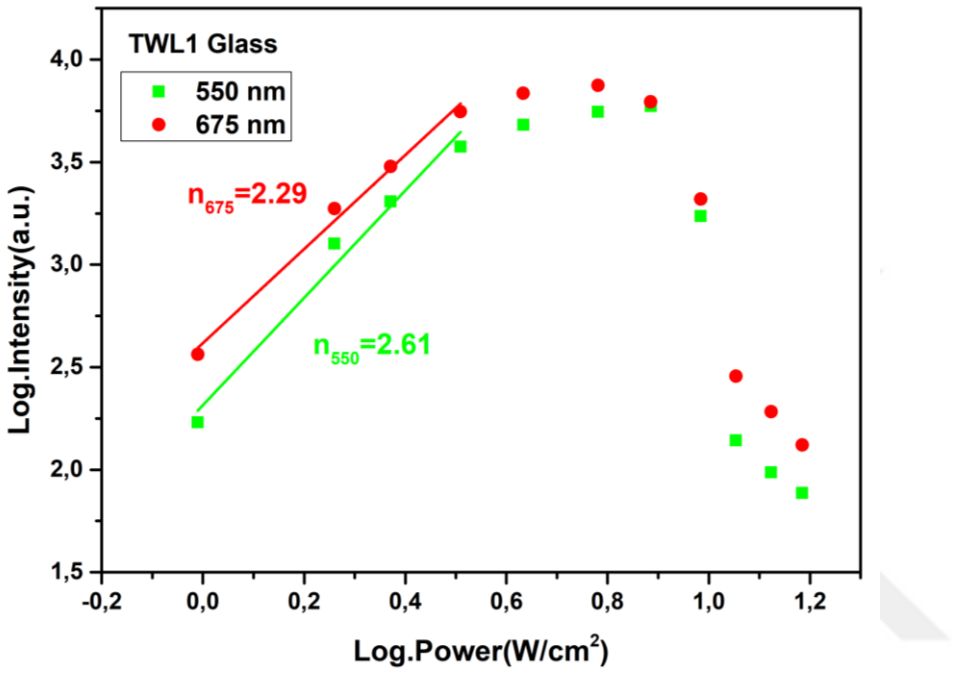

Figure 4.24: Slopes of the change in luminescence intensity due to the change in power at prominent peaks of the TWL1 glass matrix

The mechanism causing the UC-luminescence observed in the green region in the graphs of TWL1 as a function of logI excitation strength are energy transfer and thermal radiation mechanisms. (Figure 4.24)

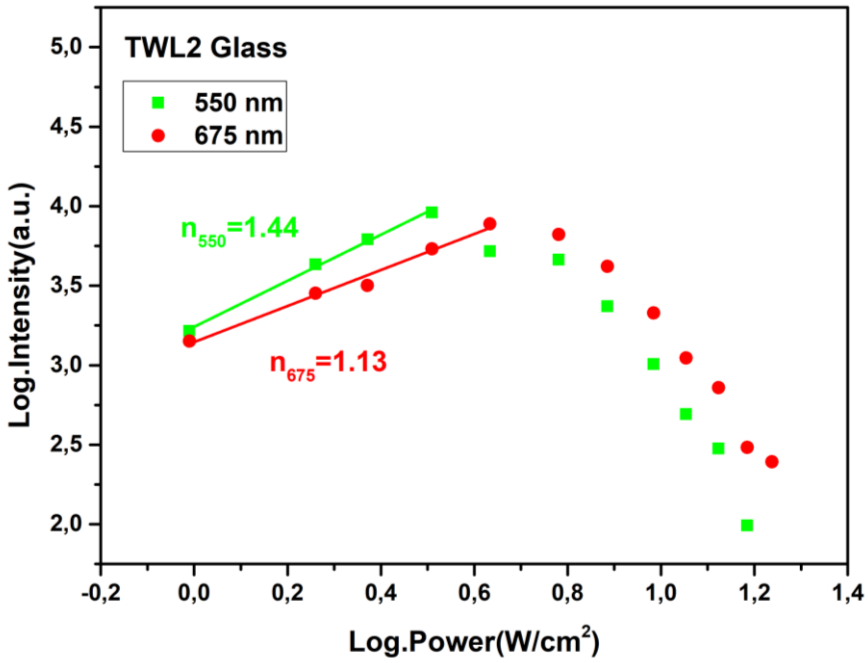

Figure 4.25: Slopes of the change in luminescence intensity due to the change in power at prominent peaks of the TWL2 glass matrix.

The mechanisms responsible for the UC-luminescence observed in the excitation power-dependent graphs of logI of TWL2 glass are energy transfer and thermal radiation mechanisms. (Fig 4.25).

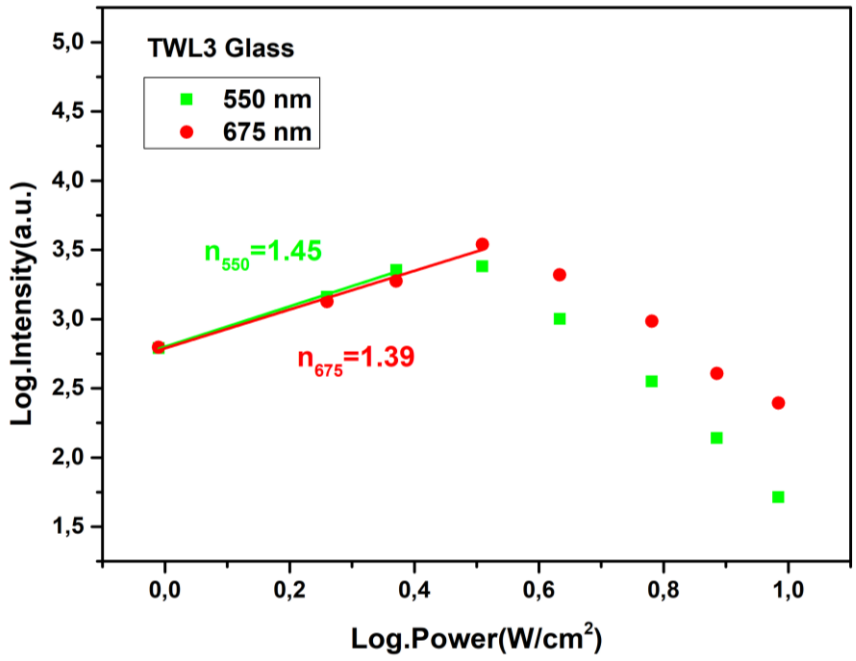

Figure 4.26: Slopes of the change in luminescence intensity due to the change in power at prominent peaks of the TWL3 glass matrix.

The mechanisms responsible fort he UC- luminescence observed in the excitation power dependent graphs of logI of TWL3 glass are the mechanisms of energy transfer and thermal radiation. (Fig 4.26)

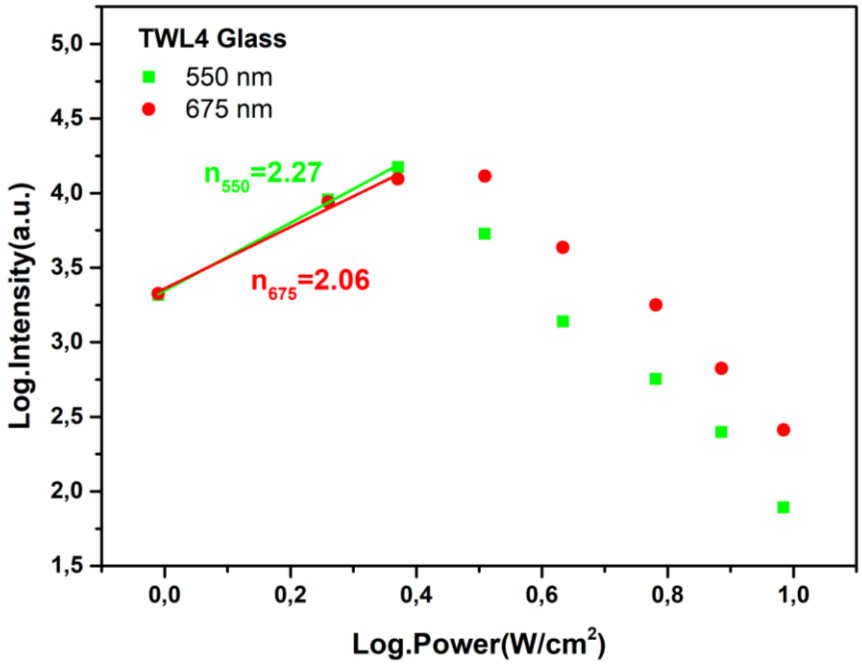

Figure 4.27: Slopes of the change in luminescence intensity due to the change in power at prominent peaks of the TWL4 glass matrix.

The mechanisms responsible for the UC -luminescence observed in the excitation power-dependent graphs of logI of TWL4 glass are energy transfer and thermal radiation mechanisms. (Figure 4.27).

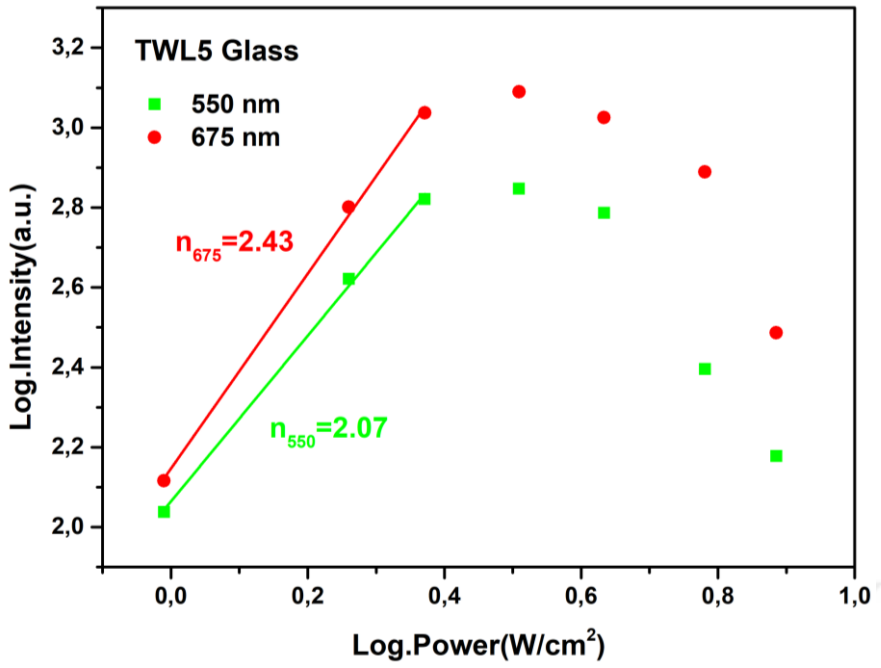

Figure 4.28: Slopes of the change in luminescence intensity due to the change in power at prominent peaks of the TWL5 glass matrix.

The mechanisms responsible for the UC -luminescence observed in the excitation power-dependent graphs of logI of TWL5 glass are energy transfer and thermal radiation mechanisms. (Fig 4.28).

In TWL glasses, the intensity of Er^{3+} UC -emission increases with excitation power. A slope of about two was found for the variation of UC -emissions at wavelengths of 600 nm and above with the variation of power. This result suggests that the observed emissions are associated with the absorption of at least two photons. UC -The emission intensities at wavelengths longer than 600 nm deviate from linearity. This effect indicates that thermal luminescence mechanisms are more effective for high-energy UC emissions.

IV.4. White Light Parameters- CIE x-y, CCT, CRI

The color coordinates of the emission spectra as a function of power were determined.Slight differences were observed with increasing concentritaion of Er^{3+} ion, shifting slightly from pure green to red.

To characterize the color of the emitted light, the purity of the emitted color must be calculated [79]. The formula in which we can see the effect of power change on color purity;

$$Colour\ purity = \frac{\sqrt{(x_s-x_i)^2+(y_s-y_i)^2}}{\sqrt{(x_d-x_i)^2+(y_d-y_i)^2}} x100\% \quad (4.6)$$

In the formula (x_s,y_s) stands for a sample coordinate, (x_d,y_d) for the coordinates of the dominant wavelength, (x_i,y_i) for the coordinates of the illumination point[38].

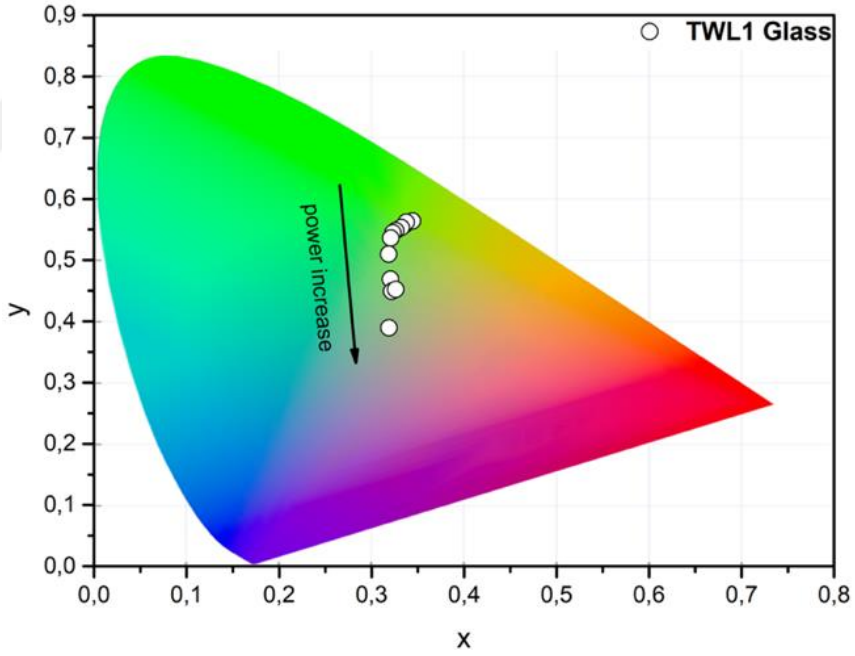

Figure 4.29: Color coordinates for TWL1 glass

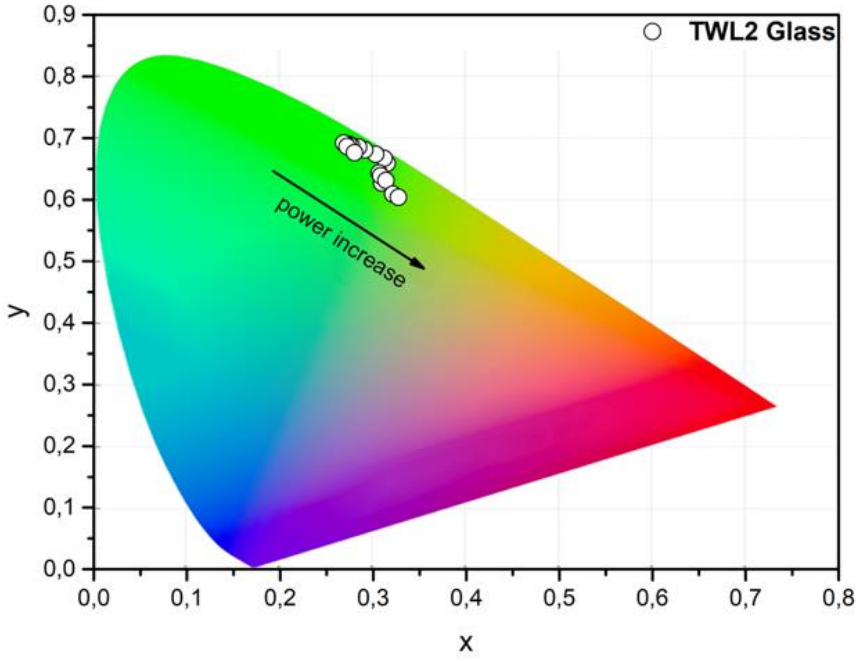

Figure 4.30: Color coordinates for TWL2 glass

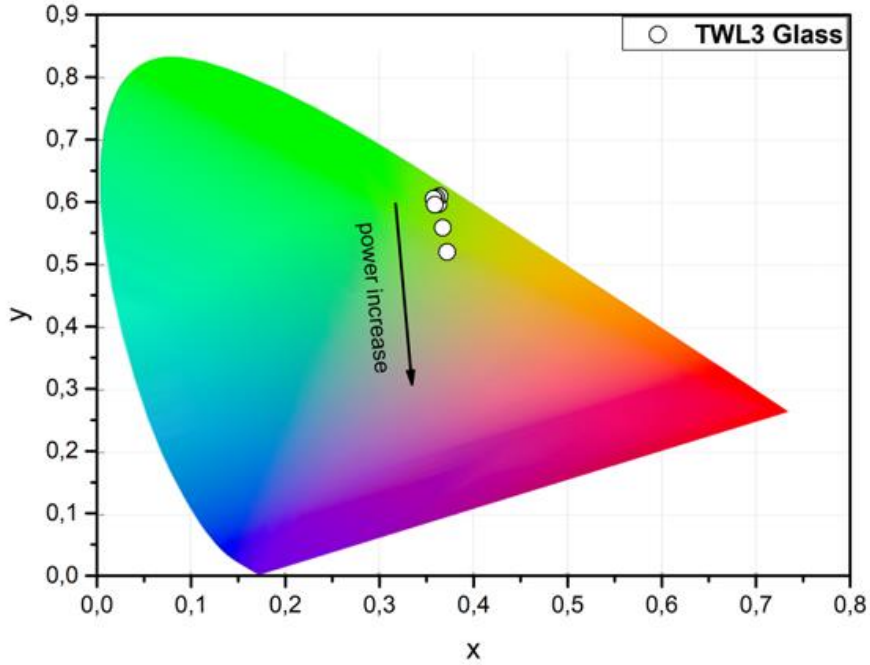

Figure 4.31: Color coordinates for TWL3 glass

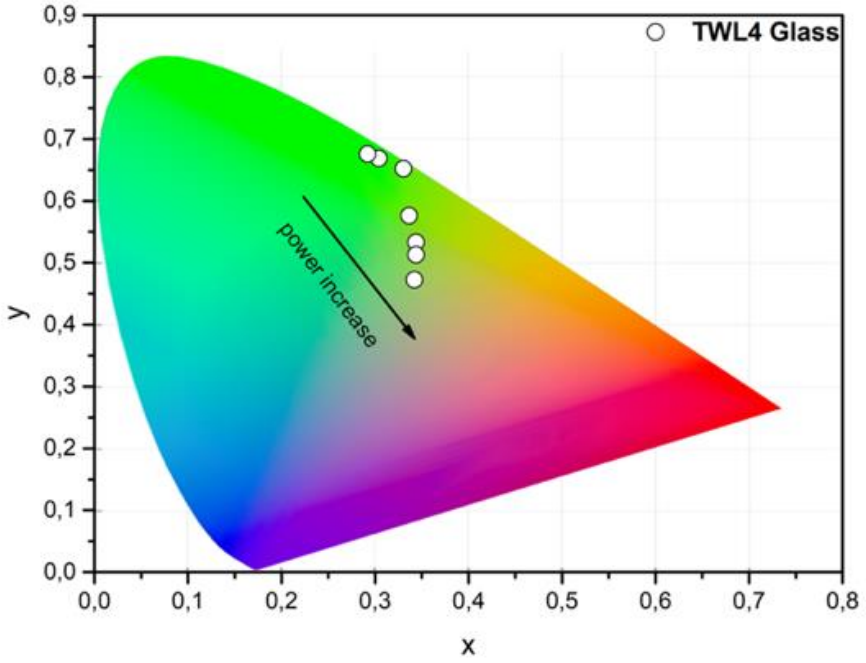

Figure 4.32: Color coordinates for TWL4 glass

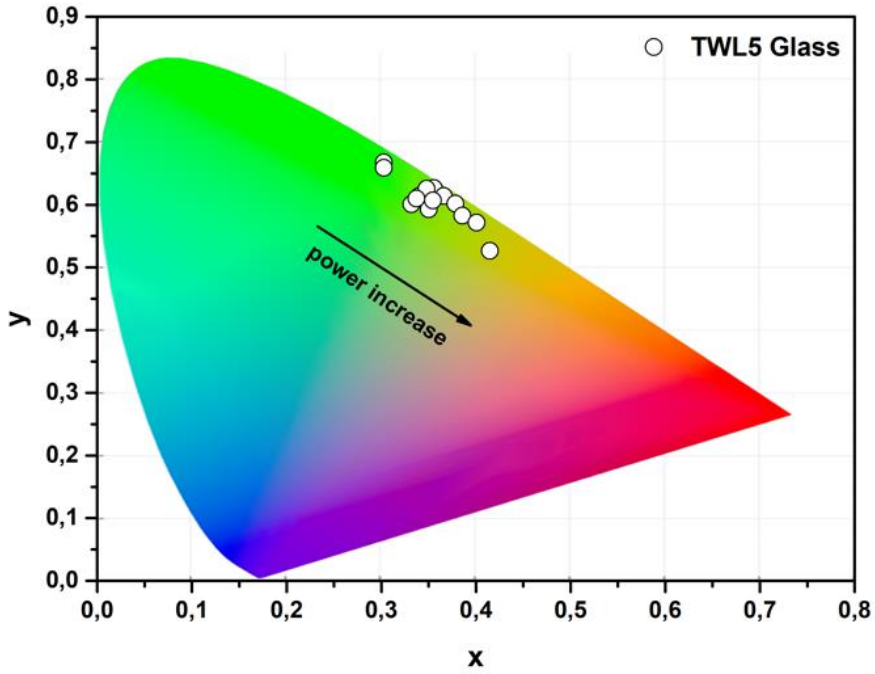

Figure 4.33: Color coordinates for TWL5 glass

The CIE x-y coordinates for pure white light are (0.333, 0.333), while the CT values are between 3000 and 7500 K, as they correspond to the values provided by the blackbody source. Daylight also has CT values that range from 2000 K to 10,000 K. In addition, CRI values range from 0-100. The relationship between CCT and CIE 1931 x-y chroma coordinates is shown in Figure 2.7.

In this study, the white light parameters of UC luminescence obtained as a function of variation of power at varying output current were measured under 980 nm laser excitation on glass matrices with different proportions of lanthanide doping using an illuminescence meter. The values obtained are listed in the following table.

When comparing the values from the literature with the measured values, white light based on UC and thermal processes was observed in all doped materials to varying degrees. The parameters of white light, the tables for the studied glass matrices are given below.

Table 4.1: White light parameters for TWL1 recorded by illuminansmetra, with different luminescence intensity and output current.

Current Value	**CIE (x-y)**	**CCT(K)**	**CRI**
0.59 A	0.3365-0.5585	5459K	55
0.72 A	0.3442-0.5641	5329 K	50
0.92 A	0.3374-0.5619	5445 K	50
1.03 A	0.3320-0.5532	5539 K	52
1.26 A	0.3262-0.5484	5644 K	54

1.38 A	0.3232-0.5447	5703 K	54
1.50 A	0.3207-0.5363	5754 K	55
1.70 A	0.3183-0.5097	5823 K	58
1.85 A	0.3206-0.4689	5808 K	63
1.99 A	0.3217-0.4489	5800 K	64
2.13 A	0.3189-0.3897	5974 K	73
2.26 A	0.3263-0.4520	5678 K	63

Table 4.2: White light parameters for TWL2 recorded by illuminansmetra, with different luminescence intensity and output current.

Current Value	**CIE (x-y)**	**CCT(K)**	**CRI**
0.50 A	0.3152-0.6591	5778 K	15
0.60 A	0.3119-0.6671	5820 K	-
0.75 A	0.3027-0.6735	5945 K	-
0.91 A	0.2912-0.6809	6102 K	-
1.00 A	0.2845-0.6851	6192 K	-
1.14 A	0.2768-0.6880	6299 K	-

1.23 A	0.2735-0.6900	6343 K	-
1.35 A	0.2704-0.6906	6387 K	-
1.51 A	0.2683-0.6917	6415 K	-
1.60 A	0.2720-0.6864	6371 K	2
1.76 A	0.2799-0.6762	6272 K	11
1.90 A	0.3092-0.6270	5888 K	40
1.99 A	0.3064-0.6432	5917 K	30
2.16 A	0.3081-0.6388	5896 K	34
2.26 A	0.3136-0.6311	5816 K	37
2.38 A	0.3212-0.6087	5710 K	45
2.51 A	0.3270-0.6039	5620 K	45

Table 4.3: White light parameters for TWL3 recorded by illuminansmetra, with different luminescence intensity and output current.

Current Value	**CIE (x-y)**	**CCT(K)**	**CRI**
0.50 A	0.3630-0.5964	5059 K	38
0.75 A	0.3639-0.6087	5061 K	37
1.00 A	0.3604-0.6065	5110 K	39

1.25 A	0.3583-0.6044	5138 K	41
1.50 A	0.3576-0.6050	5150 K	41
1.75 A	0.3588-0.5951	5122 K	44
2.00 A	0.3674-0.5583	4938 K	51
2.26 A	0.3719-0.5194	4787 K	51

Table 4.4: White light parameters for TWL4 recorded by illuminansmetra, with different luminescence intensity and output current.

Current Value	**CIE (x-y)**	**CCT(K)**	**CRI**
0.50 A	0.3306-0.6518	5561 K	8
0.75 A	0.3041-0.6688	5929 K	7
1.00 A	0.2921-0.6756	6095 K	7
1.26 A	0.3366-0.5762	5463 K	49
1.50 A	0.3439-0.5330	5315 K	54
1.75 A	0.3437-0.5130	5304 K	56
2.00 A	0.3421-0.4722	5304 K	65

Table 4.5: White light parameters for TWL5 recorded by illuminansmetra, with different luminescence intensity and output current.

Current Value	CIE (x-y)	CCT(K)	CRI
0.50 A	0.3317-0.6007	5545 K	35
0.60 A	0.3557-0.6264	5196 K	24
0.75 A	0.3658-0.6139	5040 K	28
0.90 A	0.3783-0.6016	4843 K	28
1.02 A	0.3855-0.5827	4704 K	38
1.15 A	0.4006-0.5715	4456 K	35
1.26 A	0.4148-0.5265	4096 K	39
1.46 A	0.3027-0.6674	5951 K	-6
1.57 A	0.3026-0.6590	5960 K	22
1.65 A	0.3501-0.5927	5253 K	46
1.79 A	0.3401-0.6137	5417 K	39
1.93 A	0.3479-0.5254	5235 K	57
2.13 A	0.3547-0.6068	5194 K	43

2.27 A	0.3373-0.6101	5459 K	41

IV.5. Temperature Sensing Properties

The investigation of the temperature sensitivity of Er^{3+}/Yb^{3+} doped TeO_2-WO_3 glasses under 980 nm excitation was performed by recording the UC emission spectra of green bands between 300 K and 573 K in the range of 500-600 nm.

Figure 4.43 shows the UC emission spectra at the lowest and highest temperatures, including two green emission bands around 527 nm and 551 nm determined for the $^2H_{11/2} \rightarrow {}^4I_{15/2}$ and $^4S_{3/2} \rightarrow {}^4I_{15/2}$ transitions of the Er^{3+} ion. Figure 4.43 UC Emission spectra for green bands of Er^{3+}-Yb^{3+} codoped TeO_2-WO_3 glass at two extreme temperatures.

From Figure 4.43, it can be seen that the intensity of the two bands changes in opposite directions with increasing temperature. The density corresponding to the $^2H_{11/2} \rightarrow {}^4I_{15/2}$ transition at 300 K is quite low compared to the $^4S \rightarrow {}^4I$ transition. However, the opposite was observed at 573 K. We recorded the UC emission spectra at 573 K in the TWL3 glass, but imbalances in the intensity ratio were observed.

The $^2H_{11/2}$ and $^4S_{3/2}$ levels are thermally coupled and obey the Boltzmann distribution. The ratio of fluorescence intensity of these transitions is used for optical thermometry;

$$FIR = I_{527}/I_{551} = Cexp(-\Delta E/kT) \quad (5.1)$$

Where I_{527} $^2H_{11/2} \rightarrow {}^4I_{15/2}$ are the densities corresponding to I_{551} $^4S_{3/2} \rightarrow {}^4I_{15/2}$. E is the difference in energy levels between $^2H_{11/2}$ and $^4S_{3/2}$. k is the Boltzman constant and T is the absolute temperature [95]. The equation can be written as a linear equation as in eq. 5.2;

$$\ln\left(\frac{I_{527}}{I_{551}}\right) = -\left(\frac{\Delta E}{kT}\right)\left(\frac{1}{T}\right) + \ln(C) \quad (5.2)$$

Plotting ln(I/I) as 1/T gives the slope corresponding to the E/k value and the intersection with ln(C) in Figure 4.36,39,42.

The S-value calculated in Eq. 2.22 S-value calculated is the rate at which the fluorescence intensity changes with a change in temperature. Indicates the sensitivity of the sensor.

$$S = dR/dT = FIR(\Delta E/kT^2) \quad (5.3)$$

Relative sensitivity (S_A) and absolute sensitivity (S_R) as well as sensor sensitivities, i.e., the rate of change of IR with temperature, were calculated using 2.22 and 2.23 equations.

$$S_R = \frac{1}{R}\left|\frac{dR}{dT}\right| = \frac{S}{R} = \frac{\Delta E_{21}}{K_B T^2} \quad (2.23)$$

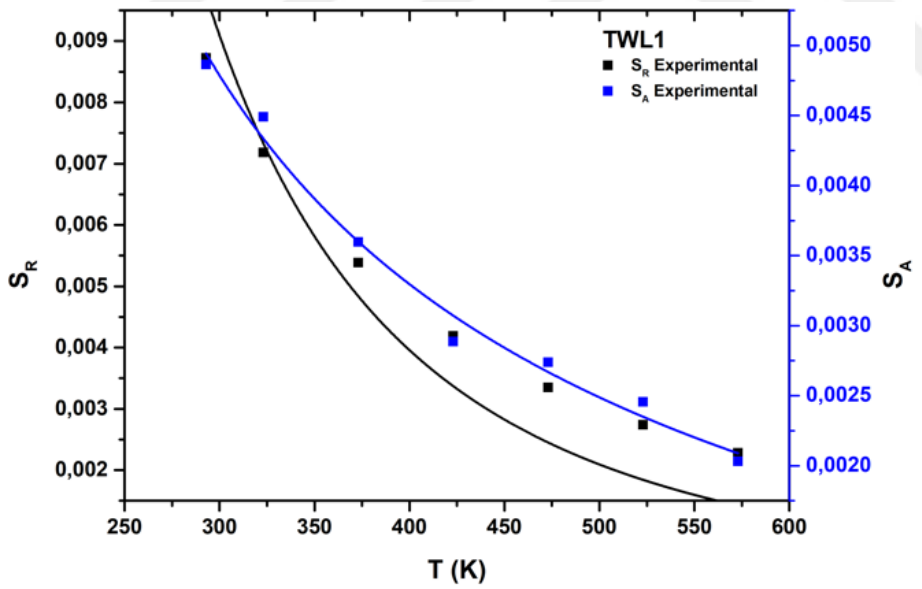

Figure 4.34: Relative and absolute sensitivity vs. temperature for TWL1 glass

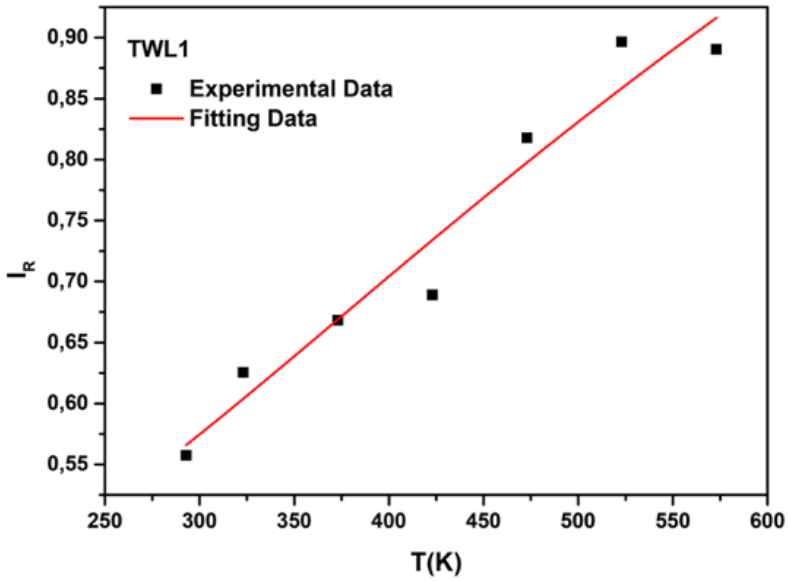

Figure 4.35: The nonlinear relationship between the intensity ratio and temperature of TWL1.

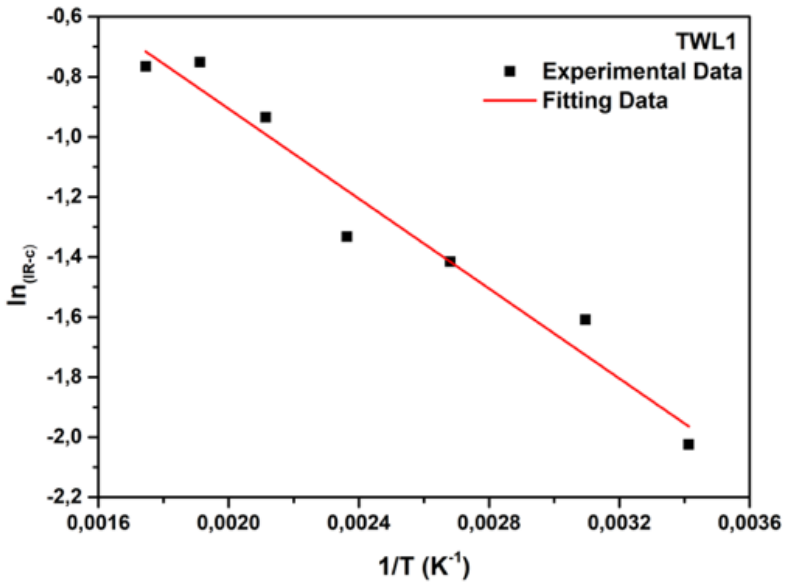

Figure 4.36: Plot of ln(I_{527} nm /I_{551} nm) as a function of inverse absolute temperature for TWL1

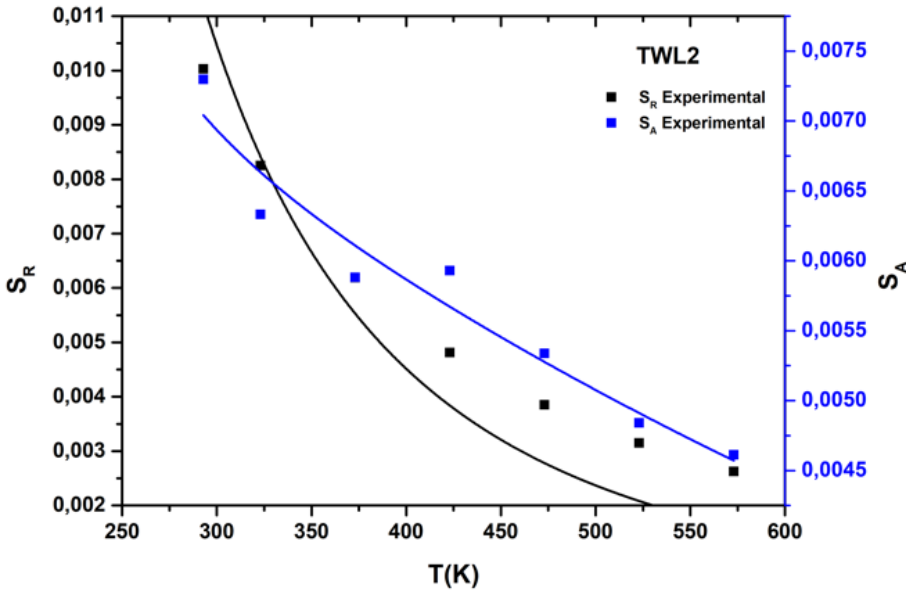

Figure 4.37: Relative and absolute sensitivity vs. temperature for TWL2 glass

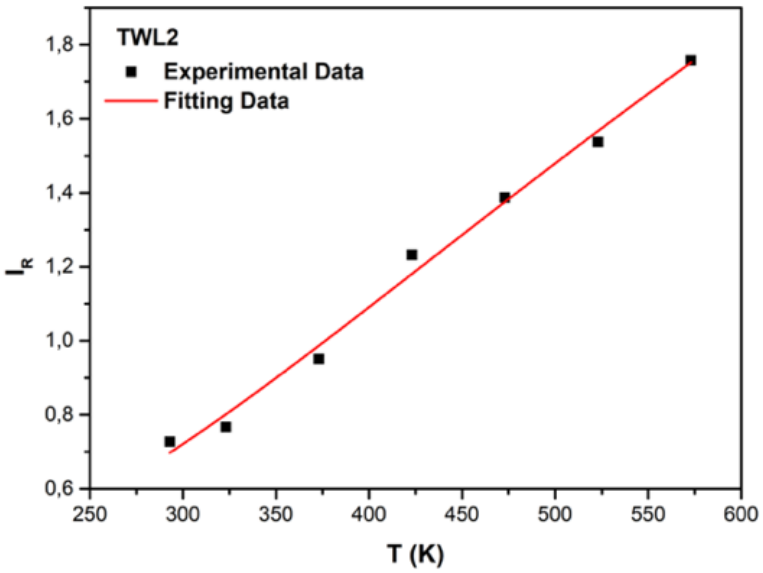

Figure 4.38: The nonlinear relationship between the intensity ratio and temperature of TWL2.

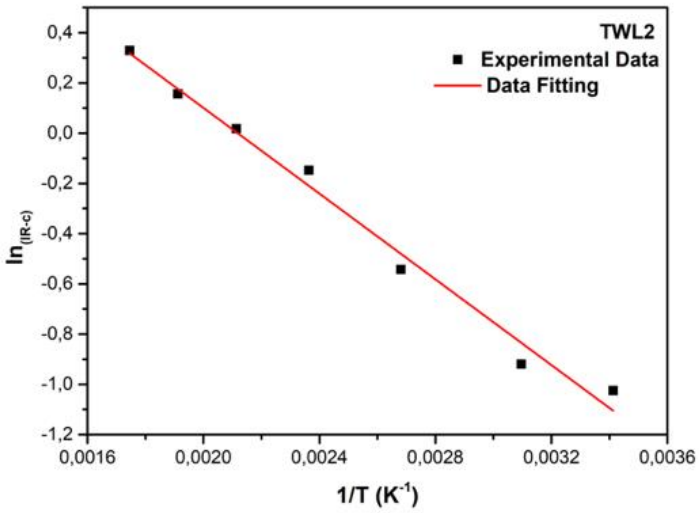

Figure 4.39: Plot of ln(I_{527} nm /I_{551} nm) as a function of inverse absolute temperature for TWL2

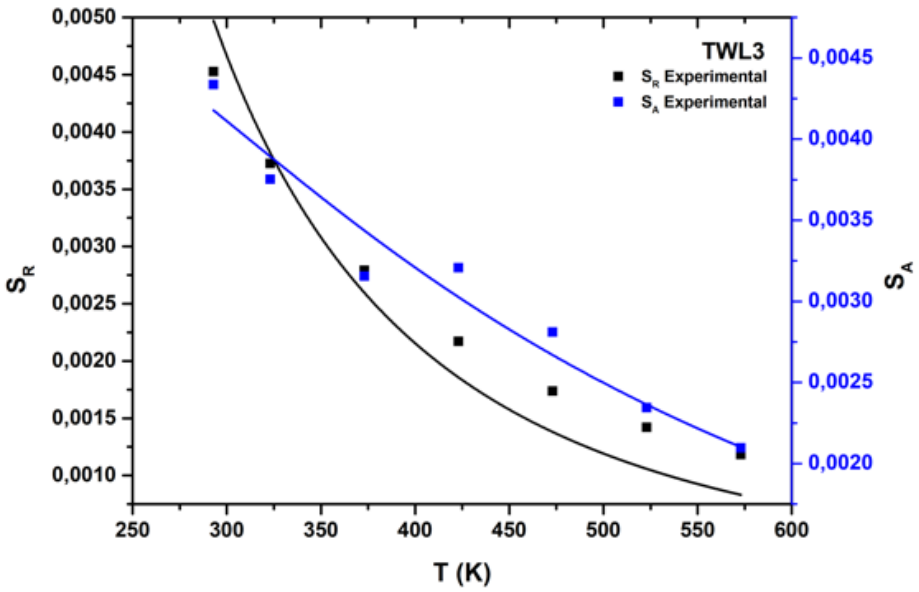

Figure 4.40: Relative and absolute sensitivity vs. temperature for TWL3 glass

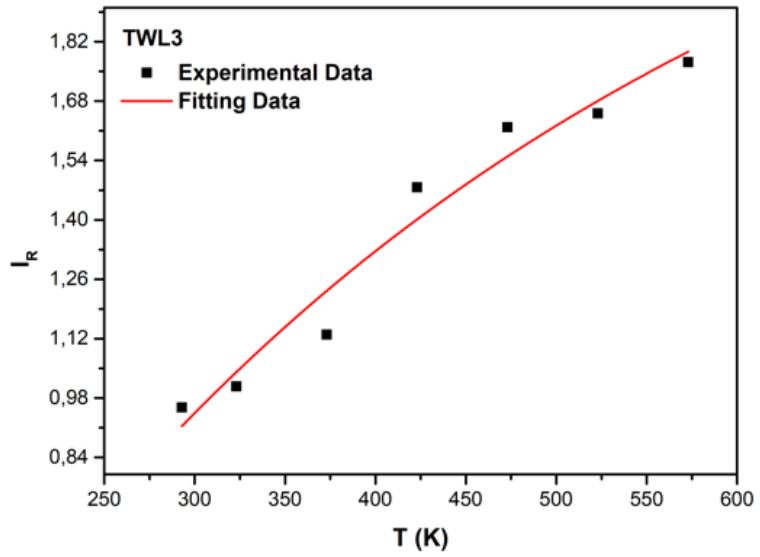

Figure 4.41: The nonlinear relationship between the intensity ratio and temperature of TWL3.

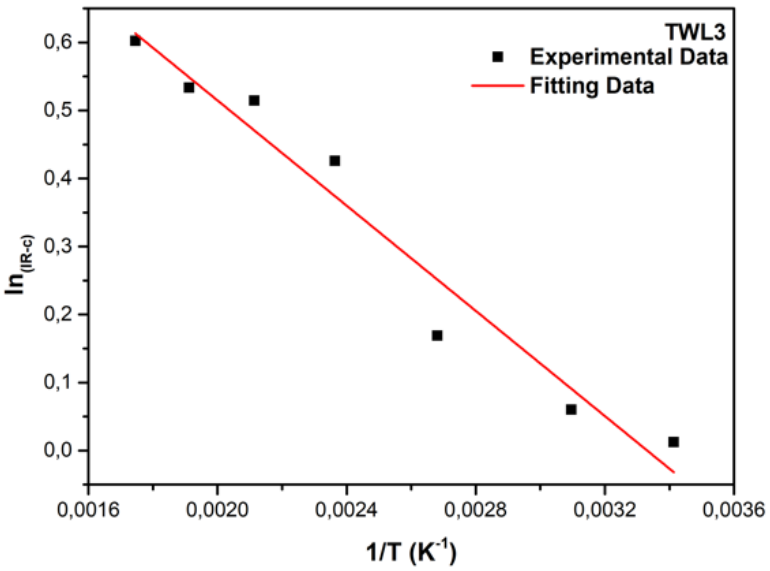

Figure 4.42: Plot of ln(I_{527} nm /I_{551} nm) as a function of inverse absolute temperature for TWL3

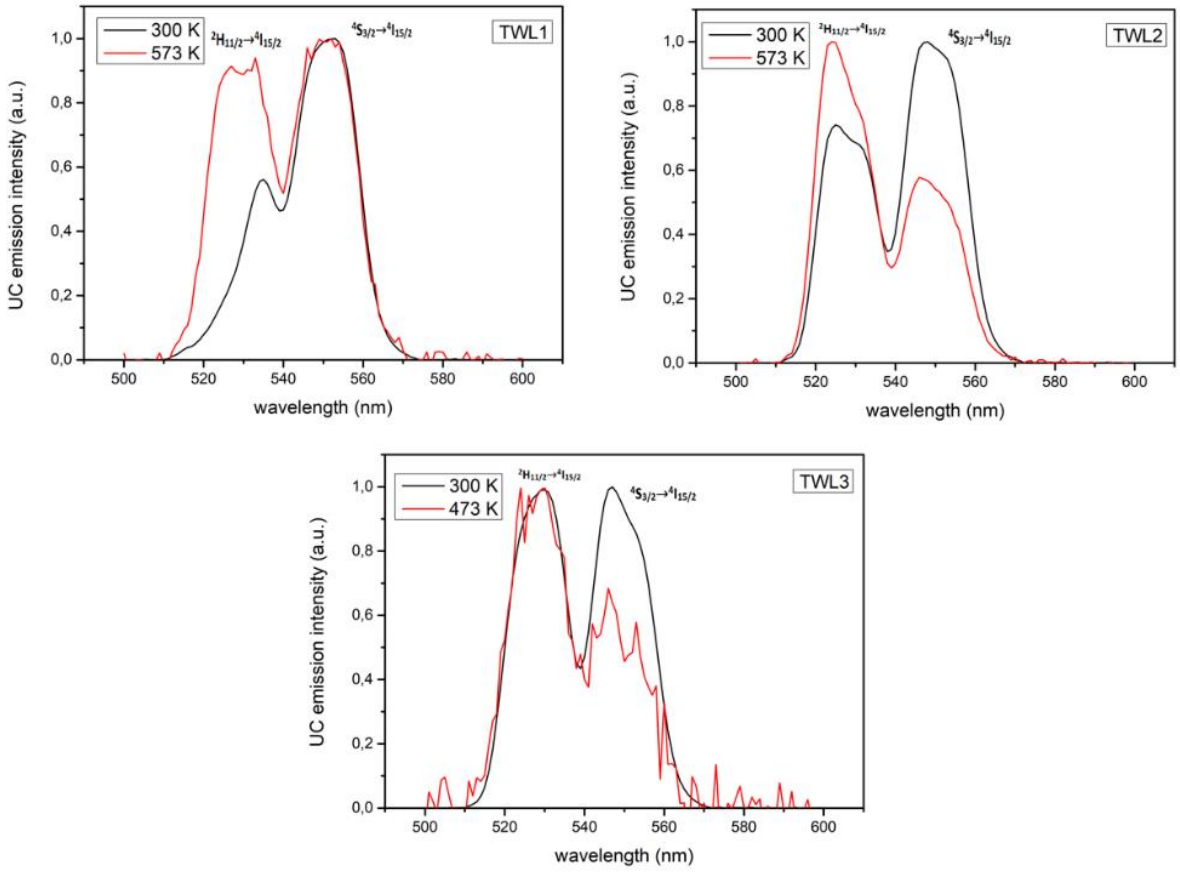

Figure 4.43: The UC emission spectra at the lowest and highest temperatures for TWL1,2,3

REFERENCES

[1] **Pujari N., Birampally K., Edukondalu, A., and Vardhani, C. P**. (2021), "Effect of Li_2O content on structural and optical properties of Li_2O-TeO_2-As_2O_3-B_2O_3 glasses," *J. Phys. Chem. Solids*, vol. **148**, p. 109627, doi: 10.1016/j.jpcs.2020.109627.

[2] **Stambouli, W., Elhouichet, H., Gelloz, B., and Férid, M.** (2013), "Optical and spectroscopic properties of Eu-doped tellurite glasses and glass ceramics," *J. Lumin.*, vol. **138**, pp. 201–208, doi: 10.1016/j.jlumin.2013.01.019.

[3] **Gupta, N. *et al.*** (2017). "Structure-property correlations in TiO_2-Bi_2O_3-B_2O_3-TeO_2 glasses," J. Non. Cryst. Solids, vol. **470**, no. May, pp. 168–177, doi: 10.1016/j.jnoncrysol.2017.05.021.

[4] **Hasim, N., Rohani, M. S., and Sahar**, **M. R.** (2016). "Structural characteristics of Er^{3+} and Nd^{3+} doped lithium niobate tellurite glass," Mater. Sci. Forum, vol. 846, pp. 126–130, doi: 10.4028/www.scientific.net/MSF.846.126.

[5] **Shankar, M.V. and Varma**, **K. B. R.** (1999). "Dielectric and optical properties of surface crystallized TeO_2-$LiNbO_3$ glasses," J. Non. Cryst. Solids, vol. 243, no. 2–3, pp. 192–203, doi: 10.1016/S0022-3093(98)00815-1.

[6] **Shinde, A. B. , Krishna, P. S. R. and Rao, R.**, (2017). "Structure of TeO_2 - $LiNbO_3$ glasses," AIP Conf. Proc., vol. 1832, pp. 10–13, doi: 10.1063/1.4980456.

[7] **Zhao, S., Chen, B., Wen, L. and Hu L.** (2006). "Spectral properties and stability of Er^{3+}-doped TeO_2-WO_3 glass," Mater. Chem. Phys., vol. 99, no. 2–3, pp. 210–213, doi: 10.1016/j.matchemphys.2005.10.011.

[8] **Grishin, I. A., Gur'ev, V.A., Intyushin, E.B., Elliev, Y.E., and Savikin, A.P.** (2004). "Preparation and properties of Er- and Yb-activated TeO_2-WO_3 glasses," Inorg. Mater., vol. **40**, no. 4, pp. 431–433, doi: 10.1023/B:INMA.0000023972.60957.3b.

[9] **Tang, J. *et al.*** (2017). "Study on optical properties and upconversion luminescence of Er^{3+}/Yb^{3+} co-doped tellurite glass for highly sensitive temperature measuring," Opt. Mater. Express, vol. **7**, no. 9, p. 3238, doi: 10.1364/ome.7.003238.

[10] **Li, X. *et al.***, (2016). "Effects of Er^{3+} concentration on down-/up-conversion luminescence and temperature sensing properties in $NaGdTiO_4$: Er^{3+}/Yb^{3+} phosphors," Ceram. Int., vol. **42**, no. 13, pp. 14710–14715, doi: 10.1016/j.ceramint.2016.06.096.

[11] **Tang, J. *et al.***, (2017). "Study on optical properties and upconversion luminescence of Er^{3+}/Yb^{3+} co-doped tellurite glass for highly sensitive temperature measuring," Opt. Mater. Express, vol. **7**, no. 9, p. 3238, doi: 10.1364/ome.7.003238.

[12] **Vetrone, F. *et al.*,**(2007). "Effects of Yb^{3+} concentration on up-conversion luminescence and temperature sensing characteristics of $Tm^{3+}/Yb^{3+}:Y_2O_3$ phosphor" vol. **661**, no. 2004.

[13] **Leal, J. J. *et al.*** (2019). "Effect of TiO_2 on the thermal and optical properties of Er3+/Yb3+ co-doped tellurite glasses for optical sensor," J. Lumin., vol. **208**, no. October 2018, pp. 342–349, doi: 10.1016/j.jlumin.2019.01.004.

[14] **Shen, X., Nie, Q., Xu, T., and Gao, Y.** (2005). "Optical transitions of Er^{3+}/Yb^{3+} codoped TeO_2-WO_3-Bi_2O_3 glass," Spectrochim. Acta - Part A Mol. Biomol. Spectrosc., vol. **61**, no. 13–14, pp. 2827–2831, doi: 10.1016/j.saa.2004.10.030.

[15] **Pandey, A., Kumar, V., Kroon, R. E. and Swart**, **H. C.** (2017). "Photon upconversion in Ho^{3+}-Yb^{3+} embedded tungsten tellurite glass," J. Lumin., vol. **192**, no. July, pp. 757–760, doi: 10.1016/j.jlumin.2017.08.009.

[16] **Fares, H., Jlassi, I., Elhouichet, H., and Férid, M.** (2014). "Investigations of thermal, structural and optical properties of tellurite glass with WO_3 adding," J. Non. Cryst. Solids, vol. 396–397, pp. 1–7, doi: 10.1016/j.jnoncrysol.2014.04.012.

[17] **Balueva, K. V. , Kut'in, D. , Plekhovich, Motorin, S. E. and Dorofeev, V. V.** (2021). "Thermophysical characterization of TeO_2-WO_3-Bi_2O_3 glasses for optical applications," J. Non. Cryst. Solids, vol. **553**, no. October, p. 120465, doi: 10.1016/j.jnoncrysol.2020.120465.

[18] **Hager, I. Z. , El-Mallawany, R., and Bulou, A.** (2011). "Luminescence spectra and optical properties of TeO_2-WO_3-Li_2O glasses doped with Nd, Sm and Er rare earth ions," Phys. B Condens. Matter, vol. **406**, no. 4, pp. 972–980, doi: 10.1016/j.physb.2010.12.041.

[19] **El-Mallawany**, **R. A. H.** (2002). Tellurite glasses handbook : physical properties and data. CRC Press.

[20] **Shaltout, I., Tang, Y., Braunstein, R. and Shaisha, E. E.** (1996). "FTIR spectra and some optical properties of tungstate-tellurite glasses," J. Phys. Chem. Solids, vol. **57**, no. 9, pp. 1223–1230, doi: 10.1016/0022-3697(95)00309-6.

[21] **Kosuge, T., Benino, Y., Dimitrov, V., Sato, R. and Komatsu, T.** (1998). "Thermal stability and heat capacity changes at the glass transition in K_2O-WO_3-TeO_2 glasses," *J. Non. Cryst. Solids*, vol. **242**, no. 2–3, pp. 154–164, doi: 10.1016/S0022-3093(98)00800-X.

[22] **Powell**, **J. E.** (1964). *The Rare-Earth Elements.*, vol. **86**, no. 21.

[23] **Sidkey, M.A., El Mallawany, R.A., Abousehly, A. A. and Saddeek**, **Y. B.** (2002). "Relaxation of longitudinal ultrasonic waves in some tellurite glasses," *Mater. Chem. Phys.*, vol. **74**, no. 2, pp. 222–229, doi:

10.1016/S0254-0584(01)00466-7.

[24] **El-Mallawany, R.** (1995). "Devitrification and vitrification of tellurite glasses," *J. Mater. Sci. Mater. Electron.*, vol. **6**, no. 1, pp. 1–3, 1995, doi: 10.1007/BF00208125.

[25] **Zhao, Y., Wang, X., Zhang, Y., Li,Y., and Yao, X.** (2020). "Optical temperature sensing of up-conversion luminescent materials: Fundamentals and progress," Journal of Alloys and Compounds, vol. **817**. Elsevier Ltd, Mar. 15, 2020, doi: 10.1016/j.jallcom.2019.152691.

[26] **El-Mallawany, R.** (2018). "Tellurite glass smart materials: Applications in optics and beyond," Tellurite Glas. Smart Mater. Appl. Opt. Beyond, no. 1984, pp. 1–297, doi: 10.1007/978-3-319-76568-6.

[27] **Dos Santos, P.V, De Araujo, M.T., Gouveia-Neto, A. S. , Medeiros Neto, J. A. and Sombra, A. S. B.** (1998). "Optical temperature sensing using upconversion fluorescence emission in Er^{3+}/Yb^{3+}-codoped chalcogenide glass," Appl. Phys. Lett., vol. **73**, no. 5, pp. 578–580, 1998, doi: 10.1063/1.121861.

[28] **Gao, Y., Nie, Q. H. , Xu, T. F. and Shen**, **X.** (2004). "Thermal stability and spectroscopic properties of new Er^{3+}/Yb^{3+}-codoped tellurite glasses," Chinese Phys. Lett., vol. **21**, no. 9, pp. 1799–1801, doi: 10.1088/0256-307X/21/9/034.

[29] **Polman**, **A.** (2003). "Absorption and emission spectroscopy in Er," Opt. Mater. (Amst)., vol. 21, pp. 705–712.

[30] **Gapontsev, V. P. , Matitsin, S. M. , Isineev, A. A. and Kravchenko, V. B.** (1982). "Erbium glass lasers and their applications," Opt. Laser Technol., vol. **14**, no. 4, pp. 189–196, doi: 10.1016/0030-3992(82)90095-0.

[31] **Leal, J. J. *et al***. (2019). "Effect of TiO_2 on the thermal and optical properties of Er^{3+} /Yb^{3+} co-doped tellurite glasses for optical sensor," J. Lumin., vol. **208**, no. December 2018, pp. 342–349, doi: 10.1016/j.jlumin.2019.01.004.

[32] **M. R. Zaki, D. Hamani, M. Dutreilh-Colas, J. R. Duclère, O. Masson, and P. Thomas** (2018). "Synthesis, thermal, structural and linear optical properties of new glasses within the TeO2-TiO2-WO3 system," J. Non. Cryst. Solids, vol. **484**, no. January, pp. 139–148, doi: 10.1016/j.jnoncrysol.2018.01.034.

[33] **Grelowska, I. *et al.*** (2016). "Structural and optical study of tellurite–barium glasses," J. Mol. Struct., vol. **1126**, pp. 219–225, doi: 10.1016/j.molstruc.2016.01.034.

[34] **Doğan, A. and Erdem, M.** (2021). "Investigation of the optical temperature sensing properties of up-converting TeO_2-ZnO-BaO activated with Yb^{3+}/Tm^{3+} glasses," Sensors Actuators, A Phys., vol. **322**, pp. 2–9, doi: 10.1016/j.sna.2021.112645.

[35] **Li, L. *et al.*** (2018). "Enhancement of spectroscopic and luminescence properties of Er^{3+} doped tellurite glasses by adding P_2O_5 for lasing materials," J. Lumin., vol. **194**, no. 6, pp. 219–225, doi: 10.1016/j.jlumin.2019.01.004.

[36] **León-Luis, S.F. *et al.*** (2011). "Temperature sensor based on the Er^{3+} green upconverted emission in a fluorotellurite glass," Sensors Actuators, B Chem., vol. 158, no. 1, pp. 208–213, doi: 10.1016/j.snb.2011.06.005.

[37] **León-Luis, S.F. *et al*** (2013). "Effects of Er^{3+} concentration on thermal sensitivity in optical temperature fluorotellurite glass sensors," Sensors Actuators, B Chem., vol. **158**, no. 1, pp. 1167–1175, doi: 10.1016/j.snb.2012.09.067.

[38] **Pandey, A. *et al.*** (2014). "Enhanced upconversion and temperature sensing study of Er^{3+}-Yb^{3+} codoped tungsten-tellurite glass," *Sensors Actuators, B Chem.*, vol. **202**, pp. 1305–1312, doi: 10.1016/j.snb.2014.06.074.

[39] **Nian, S. *et al.*** (2018). "Optical properties of Er^{3+}/Yb^{3+} co-doped bismuth calcium borate glass system for NIR lasers and fiber amplifiers," J. Lumin., vol. **194**, no. July 2017, pp. 440–445, doi: 10.1016/j.jlumin.2017.10.036.

[40] **Kumar, M. and Ratnakaram, Y. C.** (2021). "Role of TeO_2 coordination with the BaF_2 and Bi_2O_3 on structural and emission properties in Nd^{3+} doped fluoro phosphate glasses for NIR 1.058 μm laser emission," Opt. Mater. (Amst)., vol. **112**, no. November 2020, doi: 10.1016/j.optmat.2020.110738.

[41] **Bachvarova-Nedelcheva, A., Iordanova,R., Ganev, S. and Dimitriev, Y.** (2019). "Glass formation and structural studies of glasses in the TeO_2 – ZnO – Bi_2O_3 – Nb_2O_5 system," J. Non. Cryst. Solids, vol. **503–504**, no. September, pp. 224–231, doi: 10.1016/j.jnoncrysol.2018.09.048.

[42] **Bao Lin, S. *et al.*** (2020). "Spectroscopic properties of Yb^{3+} doped TeO_2–TiO_2–Bi_2O_3 laser glasses," Results Phys., vol. **16**, no. October 2019, pp. 30–33, 2020, doi: 10.1016/j.rinp.2019.102852.

[43] **Manikandan, N., Ryasnyanskiy, A. and Toulouse, J.** (2012). "Thermal and optical properties of TeO_2-ZnO-BaO glasses," *J. Non. Cryst. Solids*, vol. **358**, no. 5, pp. 947–951, doi: 10.1016/j.jnoncrysol.2012.01.003.

[44] **Sugita, H., Honma, T., Benino, Y. and Komatsu**, **T.** (2007). "Formation of $LiNbO_3$ crystals at the surface of TeO_2-based glass by YAG laser-induced crystallization," Solid State Commun., vol. **143**, no. 6–7, pp. 280–284, doi: 10.1016/j.ssc.2007.06.002.

[45] **Komatsu, T., Tawarayama, H., Mohri, H. and Matusita**, **K.** (1991). "Properties and crystallization behaviors of TeO2LiNbO3 glasses," J. Non. Cryst. Solids, vol. **135**, no. 2–3, pp. 105–113, doi: 10.1016/0022-3093(91)90410-8.

[46] **Shirpay, A. and Bagheri-Mohagheghi, M. M.** (2019). "The precursor solution effect on the synthesis, structure, and optical properties of the WO_3–

TeO_2 binary compound," Appl. Phys. A Mater. Sci. Process., vol. **125**, no. 4, p. 0, 2019, doi: 10.1007/s00339-019-2557-1.

[47] **Suehara, S. *et al.*** (2004). "Localized hyperpolarizability approach to the origin of nonlinear optical properties in TeO_2-based materials," Phys. Rev. B –Condens. Matter Mater. Phys., vol. **70**, no. 20, pp. 1–7, doi: 10.1103/PhysRevB.70.205121.

[48] **Suehara, S. *et al.*** (2004). "Non-linear optical properties of TeO_2-based glasses: Ab initio static finite-field and time-dependent calculations," J. Non. Cryst. Solids, vol. **345–346**, pp. 730–733, doi: 10.1016/j.jnoncrysol.2004.08.191.

[49] **Jeansannetas, B. *et al.*** (1999). "Glass structure and optical nonlinearities in thallium(I) tellurium(IV) oxide glasses," J. Solid State Chem., vol. **146**, no. 2, pp. 329–335, 1999, doi: 10.1006/jssc.1999.8355.

[50] **Fargin, E. *et al.*** (1996). "Optical non-linearity in oxide glasses," J. Non. Cryst. Solids, vol. **203**, pp. 96–101, doi: 10.1016/0022-3093(96)00338-9.

[51] **Mirgorodsky, A. P., Soulis, M., Thomas, P., Merle-Méjean, T. and Smirnov, M.** (2006). "Ab initio study of the nonlinear optical susceptibility of TeO_2 -based glasses," Phys. Rev. B - Condens. Matter Mater. Phys., vol. **73**, no. 13, pp. 1–13, doi: 10.1103/PhysRevB.73.134206.

[52] **El-Mallawany, R. A. H.** (2012). "Tellurite Glasses Handbook Physical Properties and Data" Second Edition.

[53] **USGS** (2017). "Rare-Earth Elements Chapter," U.S. Geol. Surv., 2017 [Online]. Available: https://doi.org/10.3133/pp1802O.

[54] **Dramicanin, M.** (2018). "Luminescence Thermometry: Methods, Materials, and Applications (Woodhead Publishing Series in Electronic and Optical Materials)-1st Edition"

[55] **El-Mallawany, R.** (2018). "Tellurite glass smart materials: Applications in optics and beyond" Springer International Publishing.

[56] **Li, X., Yu, Y. and Zheng, Z.** (2016). "A temperature dependent investigation of upconversion emission in Er^{3+}:PLZT transparent ceramic," Ceram. Int., vol. **42**, no. 1, pp. 490–494, doi: 10.1016/j.ceramint.2015.08.135. [Online]. Available: http://dx.doi.org/10.1016/j.ceramint.2015.08.135

[57] **Manzani, D., Petruci, J. F. D. S., Nigoghossian, K., Cardoso, A. A. and Ribeiro, S. J. L.** (2017). "A portable luminescent thermometer based on green up-conversion emission of Er3+/Yb3+ co-doped tellurite glass," Sci. Rep., vol. **7**, no. June 2016, pp. 1–11, doi: 10.1038/srep41596. [Online]. Available: http://dx.doi.org/10.1038/srep41596

[58] **El-mallawany, R.** (2018). *Tellurite Glass Smart Materials.*

[59] **Bilir, G., Kaya, A., Cinkaya, H. and Eryürek, G.** (2016). "Spectroscopic investigation of zinc tellurite glasses doped with Yb^{3+} and Er^{3+} ions," Spectrochim. Acta - Part A Mol. Biomol. Spectrosc., vol. **165**, pp. 183–190, doi: 10.1016/j.saa.2016.04.042. [Online]. Available: http://dx.doi.org/10.1016/j.saa.2016.04.042

[60] **Malacara, D.** (2011). *Color Vision and Colorimetry: Theory and Applications, Second Edition*.

[61] **Choudhury, A.K.R.** (2014). *"Principles of colour appearance and measurement Volume 1: Object appearance, colour perception and instrumental measurement."* Woodhead Publishing Series in Textiles: Number 159.

[62] **Quintanilla, M., Benayas, A., Naccache, R., Vetrone, F., Quintanilla, M., Benayas, A., et al. (**2015). "Thermometry at the Nanoscale: Techniques and Selected Applications," *R. Soc. Chem. 2015. p. 124–66.*, vol. **1**, no. 69, pp. 5–24, 2015.

[63] **Wang, J. S., Vogel, E. M. and Snitzer, E.** (1994). "Tellurite glass: a new candidate for fiber devices," *Opt. Mater. (Amst).*, vol.**3**, no. 3, pp. 187–203, doi: 10.1016/0925-3467(94)90004-3.

[64] **Sahar, M.R., Jehbu, A.K. and Karim, M.M.** (1997). "TeO_2-ZnO-$ZnCl_2$ glasses for IR transmission," *J. Non. Cryst. Solids*, vol. **213–214**, pp. 164–167, doi: 10.1016/S0022-3093(97)00096-3.

[65] **Sajna, M.S. *et al.*** (2018). "NIR emission properties of RE^{3+} ions in multicomponent tellurite glasses," Tellurite Glas. Smart Mater. Appl. Opt. Beyond, pp. 203–224, doi: 10.1007/978-3-319-76568-6_9.

[66] **Dorofeev, V. V. *et al.*** (2011). "High-purity TeO_2-WO_3-(La_2O_3, Bi_2O_3) glasses for fiber-optics," Opt. Mater. (Amst)., vol. **33**, no. 12, pp. 1911–1915, doi: 10.1016/j.optmat.2011.03.032.

[67] **Dimitrov,V. and Sakka, S.** (1996). "Electronic oxide polarizability and optical basicity of simple oxides. I," *J. Appl. Phys.*, vol. **79**, no. 3, pp. 1736–1740, doi: 10.1063/1.360962.

[68] **Le Neindre, L., Jiang, S., Hwang, B. C., Luo, T., Watson, J. and Peyghambarian, N.** (1999). "Effect of relative alkali content on absorption linewidth in erbium-doped tellurite glasses," *J. Non. Cryst. Solids*, vol. **255**, no. 1, pp. 97–102, doi: 10.1016/S0022-3093(99)00428-7.

[69] **Shai, D. W. A.** (1986). "Inorganic Solid Flourides - Chemistry and Physics," *J. Fluor. Chem.*, vol. **31**, no. 4, p. 471, doi: 10.1016/s0022-1139(00)81273-7.

[70] **Carrasco, E. *et al*.** (2015). "Intratumoral thermal reading during photo-thermal therapy by multifunctional fluorescent nanoparticles," Advanced Functional Materials, vol. **25**, no. 4. pp. 615–626, 2015.

[71] **Wade, S. A., Collins, S. F. and Baxter, G. W.** (2003). "Fluorescence intensity ratio technique for optical fiber point temperature sensing," *J. Appl. Phys.*, vol. **94**, no. 8, pp. 4743–4756, doi: 10.1063/1.1606526.

[72] **F. Benayas, A. ,Rosal, B ,Perez-Delgado, A.,Santacruz-Gomez, K., Jaque, D., Hirata, G.A.,Vetrone** (2015). "Nd:YAG Near-Infrared Luminescent Nanothermometers."

[73] **Cerõn, E. N. *et al.***(2015). "Hybrid Nanostructures for High-Sensitivity Luminescence Nanothermometry in the Second Biological Window," Adv. Mater., vol. **27**, no. 32, pp. 4781–4787, doi: 10.1002/adma.201501014.

[74] **Goodwin, D. W.** (1979). "Optical Spectra of Transparent Rare Earth Compounds," *Phys. Bull.*, vol. **30**, no. 12, pp. 525–525, doi: 10.1088/0031-9112/30/12/040.

[75] **Zhao, Y., Wang, X., Zhang, Y., Li, Y. and Yao, X.** (2020). "Optical temperature sensing of up-conversion luminescent materials: Fundamentals and progress," J. Alloys Compd., vol. **817**, p. 152691, 2020, doi: 10.1016/j.jallcom.2019.152691. [Online]. Available: https://doi.org/10.1016/j.jallcom.2019.152691

[76] **Singh, B.P, Parchur, A.K, Singh, R.K., Ansari, A.A., Singh, P. and Rai, S.B.** (2013). "Structural and up-conversion properties of Er^{3+} and Yb^{3+} co-doped $Y_2Ti_2O_7$ phosphors," Phys. Chem. Chem. Phys., vol. **15**, no. 10, pp. 3480–3489, 2013, doi: 10.1039/c2cp44195k.

[77] **Goodwin, D.W.** (1969). "Spectra and Energy Levels of Rare Earth Ions in Crystals," Physics Bulletin, vol. **20**, no. 12. pp. 525–525, 1969.

[78] **Pandey, A. and Rai, V. K**. (2014). "Pr^{3+}-Yb^{3+} codoped Y_2O_3 phosphor for display devices," Mater. Res. Bull., vol. **57**, pp. 156–161, doi: 10.1016/j.materresbull.2014.04.071. [Online]. Available: http://dx.doi.org/10.1016/j.materresbull.2014.04.071.

[79] **Singh, S.K., Kumar, K. and Rai, S. B.** (2009). "Multifunctional Er^{3+}-Yb^{3+} codoped Gd_2O_3 nanocrystalline phosphor synthesized through

optimized combustion route," Appl. Phys. B Lasers Opt., vol. **94**, no. 1, pp. 165–173, doi: 10.1007/s00340-008-3261-6.

[80] **Mohanty, D.K., Rai, V. K., Dwivedi, Y. and Rai, S. B.** (2011). "Enhancement of upconversion intensity in Er^{3+} doped tellurite glass in presence of Yb^{3+}," Appl. Phys. B Lasers Opt., vol. **104**, no. 1, pp. 233–236, doi: 10.1007/s00340-011-4422-6.

[81] **Yeh, M. J. S. D. C. , Petrin, R. R. and Sibley, W. A., Madigou, V. and Adam, J. L.** (1989). "Energy transfer between Er and Tm ions in a barium fluoride glass," vol. **39**, no. 1, 1989.

[82] **Walsh, B. M., Barnes, N. P. and Di Bartolo, B.** (1997). "On the distribution of energy between the Tm $^3F_4$ and Ho $^5I_7$ manifolds in Tm-sensitized Ho luminescence," *J. Lumin.*, vol. **75**, no. 2, pp. 89–98, doi: 10.1016/S0022-2313(97)00110-5.

[83] **Richardson, L. J., Bonner, C. E., Lewis, J., Loutts, G. B., Rodriguez, W. J. and Walsh, B. M.** (2004). "Temperature dependence on the cross-relaxation rates in Tm^{3+} doped strontium fluorapatite," *J. Lumin.*, vol. **109**, no. 3–4, pp. 129–133, doi: 10.1016/j.jlumin.2004.02.002.

[84] **De Camargo, A. S. S., De Oliveira, S. L., De Sousa, D. F., Nunes, L. A. O. and Hewak, D. W.** (2002). "Spectroscopic properties and energy transfer parameters of Tm^{3+} ions in gallium lanthanum sulfide glass," *J. Phys. Condens. Matter*, vol. **14**, no. 41, pp. 9495–9505, 2002, doi: 10.1088/0953-8984/14/41/307.

[85] **Sreekanth Chakradhar, R. P., Ramesh, K. P., Rao, J. L. and Ramakrishna, J.** (2003). "Mixed alkali effect in borate glasses-EPR and optical absorption studies in xNa_2O-$(30 - x)K_2O$-$70B_2O_3$ glasses doped with Mn^{2+}," *J. Phys. Chem. Solids*, vol. **64**, no. 4, pp. 641–650, doi: 10.1016/S0022-3697(02)00365-7.

[86] **Vijaya Prakash, G., Narayana Rao, D. and Bhatnagar, A. K.** (2001). "Linear optical properties of niobium-based tellurite glasses," Solid State Commun., vol. **119**, no. 1, pp. 39–44, doi: 10.1016/S0038-1098(01)00195-8.

[87] **Mott, N. F. and Davis, E. A.** (1970). "Conduction in non-crystalline systems V. Conductivity, optical absorption and photoconductivity in amorphous semiconductors," Philos. Mag., vol. **22**, no. 179, pp. 903–922, 1970 [Online]. Available: https://doi.org/10.1080/14786437008221061

[88] **Seop, Y. and Heo, J.** (2003). "Cross relaxation mechanism among Tm^{3+} ions in $Ge_{30}Ga_2As_6S_{62}$ glass" vol. **316**, pp. 302–308, 2003.

[89] **Golubov S., Konobeev Y.** (1967). "Effects of Diffusion on Energy Transfer by Resonance in Solids," Physica Status Solidi (B), vol. **56**, no. 1. pp. 69–77, 1967.

[90] **Sennaroglu, A. , Kurt, A. and Özen, G.** (2004). "Effect of cross relaxation on the 1470 and 1800 nm emissions in Tm^{3+}:TeO_2-$CdCl_2$ glass," J. Phys. Condens. Matter, vol. **16**, no. 15, pp. 2471–2478, doi: 10.1088/0953-8984/16/15/001.

[91] **Halimah, M.K., Daud, W. M., Sidek, H. A. A., Zaidan, A. W. and Zainal, A. S.** (2010). "Optical properties of ternary tellurite glasses," Mater. Sci. Pol., vol. **28**, no. 1, pp. 173–180, 2010.

[92] **Tauc, J. and Menth, A.** (1972). "States in the gap," J. Non. Cryst. Solids, vol. **8–10**, no. C, pp. 569–585, doi: 10.1016/0022-3093(72)90194-9.

[93] **Fritzsche, H.** (1984). Noncrystalline semiconductors, vol. **37**, no. 10. 1984.

[94] **Azam, M., Rai, V. K. and Mohanty, D. K.** (2017). "Spectroscopy and enhanced frequency upconversion in Nd^{3+}-Yb^{3+} codoped TPO glasses: energy transfer and NIR to visible upconverter," Methods Appl. Fluoresc., vol. **5**, no. 3, p. 035005, 2017, doi: 10.1088/2050-6120/aa7ac1.

[95] **Pandey, A. and Rai, V. K.** (2014). "Rare Earth Doped Materials for Temperature Sensors," *Spectrosc. Tech. Secur. Forensic Environ. Appl.*, no. June, pp. 279–292, 2014.

CURRİCULUM VITAE

Name Surname **:Güliz KONCA**

EDUCATION **:**

- **B.Sc.** **:** 2018, Marmara University, Atatürk Faculty of Education , Department of Physics Teacher Education
- **M.Sc.** **:** 2022, Istanbul Technical University, Faculty of Science and Letters, Department of Physics Engineering